ABSTRACT

Title of dissertation: EXPLORATION OF LITHIUM ION BINDING TO MAGNESIUM BOUND ADENOSINE TRIPHOSPHATE AND ITS IMPLICATIONS FOR BIPOLAR DISORDER

Katharine Therese Briggs,
Doctor of Philosophy, 2015

Dissertation directed by: John P. Marino, Ph.D.
Department of Chemistry & Biochemistry

Lithium carbonate, a drug for the treatment of Bipolar Disorder, provides mood stability to treat an illness that causes recurrent episodes of mania and/or depression. The mechanism by which lithium acts to elicit these psychological changes remains unknown. Interestingly, this small bio-active salt has been shown to reduce the risk of suicide, and appears to lower the incidence of Alzheimer's disease. It has been proposed that lithium inhibits magnesium-dependent enzymes; however, there is no consensus as to how this occurs. Based on high resolution ^{7}Li, ^{23}Na, and ^{31}P T1 and Paramagnetic Relaxation Enhancement (PRE) Nuclear Magnetic Resonance (NMR) methods, which can be used to characterize the association of lithium (Li^{+}) at magnesium (Mg^{2+})-phosphorus chelation sites, we have identified a ATP·Mg·Li complex. The lithium binding affinity to form this complex is relatively high compared to other monovalent cations, with a $K_d < 1$ mM, and biologically relevant considering that at the typical dosing of Li^{+}, physiological concentrations of Mg and ATP are in the 0.6 – 2.5 mM range. This has led us to propose a mechanism of action for lithium based on the formation of Mg·Li-complexes at

dehydrated magnesium-phosphate sites and perhaps a role for ATP·Mg as a physiological carrier for Li^+. To test this model experimentally in the context of relevant ATP-protein binding sites, we have used NMR methods to characterize the formation of the complex at ATP binding sites on albumin. Similarly, we initiated studies investigating the relevance of the ATP·Mg·Li complex to a class of purinergic receptor proteins (P2XR), since they are stimulated by purine agonists and have been implicated in Bipolar Disorder.

EXPLORATION OF LITHIUM ION BINDING TO MAGNESIUM BOUND ADENOSINE TRIPHOSPHATE AND ITS IMPLICATIONS FOR BIPOLAR DISORDER

By

Katharine Therese Briggs

Dissertation submitted to the Faculty of the Graduate School of the
University of Maryland, College Park, in partial fulfillment
of the requirements for the degree of
Doctor of Philosophy
2015

Advisory Committee:

Professor Zvi Kelman, Chair
Adjunct Professor John Marino, Advisor, Co-chair
Associate Professor Jason Kahn, Dean's Representative
Professor John Orban
Dr. David Vanderah

Dedication

This dissertation research is dedicated to my parents, Nancy and Joseph, brother, Justin, and sister, Alyssa, and in loving memory of T.L.G. and F.G.Z.

Acknowledgements

Earning a Ph.D. has been compared to running a marathon, except without a map of the route, or a clear finish line. Now at the finish line, there are many people whom I would like to thank.

Dr. John Marino, my mentor and advisor, has always had an open door and been eager to talk science with me. His persistent optimism, when helping me to troubleshoot experiments, and constant encouragement were invaluable to me. It has been a privilege to be his student. I hold him in high esteem and am very grateful for the gift of his mentorship over these past several years.

Dr. Gary Giulian has a passion and enthusiasm for discovering lithium's mechanism of action and was instrumental in early discussions that shaped the foundation of this research. He brought his medical expertise and scientific curiosity to the discussions, which broadened the scope and understanding of the lithium project.

Dr. Zvi Kelman has helped me to see the lighter side of graduate life with his sense of humor, which has diffused stressful moments on some occasions. He has been a valuable consultant, for designing experiments, and career advisor, for which I am sincerely grateful.

I would like to thank the rest of my advisory committee, Drs. David Vanderah, John Orban, and Jason Kahn. They have been supportive throughout. I appreciate their advice and investment in my growth as a scientist.

I am grateful for our collaboration with Dr. Joseph Kao and Dr. Gong Li, at the University of Maryland School of Medicine in Baltimore, MD, who provided the rat neuronal data in Chapter 3 and valuable discussions towards the beginning of this research. An additional collaboration with Dr. David Mosser, at the University of Maryland College Park and his graduate student at the time, now Dr. Heather Cohen, gave me the opportunity to learn about inflammatory responses in macrophages (see Appendix). It was a pleasure to work with these researchers.

There are many people at IBBR who have shaped my experience as a graduate student. I would like to specifically acknowledge a few of them. Dr. Nese Sari willingly assisted me with troubleshooting any NMR problem. I appreciated her patience and calmness under pressure. Dr. Yili Li, in the lab of Dr. Roy Mariuzza, and Dr. Lori Kelman taught me aseptic techniques for maintaining Sf9 cell cultures. Yili provided initial guidance with baculovirus expression as well. Dr. James Todd Hoopes oriented me to the new FPLC and was a helpful resource for my Equilibrium Gel Filtration experiments (Chapter 4). Dr. Debbie Weinstein, Adobe Illustrator aficionado, gave me pointers for my illustrations.

Former and current lab mates, have all contributed to the positive, collaborative atmosphere at IBBR and made it a genuinely enjoyable work place. Dr. Andrea Szakal has been a supportive and encouraging friend to me. Her meticulous reading of my dissertation provided helpful feedback during my revision process, for which I am very grateful. Lunch conversations with friends, especially Dr. Raviprasad Aduri, Dr. Justyna Msyliwy, Tana Smith, and Dr. Cassiah Cox, were treasured breaks during the day.

Fellow graduate students, both past and present, have been good friends and I am grateful for their camaraderie. Miao Pan and Zhuo Li were especially helpful in assisting me with the initial Western blot and PCR experiments, too.

Outside of lab and school, I would like to thank my parents, who have emphasized the importance of a good education and gave me a strong foundation from my early years. They continue to be my steady and constant cheerleaders. I could not ask for more loving and generous parents. They inspire me to strive for greatness. I am grateful for my siblings who have been huge supporters, rooting me on all along the way. Their respective career successes are an inspiration to me as I embark on my career as a newly minted Ph.D. I would like to thank my wonderful friends who have seen me through highs and lows of life and school. I am so very grateful for you.

Finally, I would like to thank God that I made it to this finish line, and I look forward to crossing new finish lines in the next chapters of my life.

Table of Contents

List of Tables

List of Figures

List of Abbreviations

α	lower energy state
ADHD	Attention Deficit Hyperactivity Disorder
ADP	adenosine 5’-diphosphate
ATP	adenosine 5’-triphosphate
β	higher energy state
BD	Bipolar Disorder
BSA	bovine serum albumin
Ca^{2+}	calcium
^{13}C	Carbon
CDC	Centers for Disease Control
DPG	2,3-diphosphoglycerate
DSM-5	Diagnostic and Statistical Manual, 5^{th} Edition
eATP	extracellular adenosine 5’-triphosphate
E.coli	Escherichia coli
EDTA	ethylenediaminetetraacetic acid
FDA	U.S. Food and Drug Administration
FID	free induction decay
FPLC	Fast Protein Liquid Chromatography
GABA	gamma-aminobutyric acid
GDP	guanosine 5’-diphosphate
GPCR	G-protein coupled receptor
GSK-3β	Glycogen Synthase Kinase 3β
GTP	guanosine 5’-triphosphate
GWAS	Genome-Wide Association Studies

^{1}H	hydrogen
HSA	human serum albumin
IMPase	Inositol monophosphatase
ITC	Isothermal Titration Calorimetry
IMAC	Immobilized metal ion affinity chromatography
^{7}Li; Li^{+}	Lithium
Mg^{2+}	Magnesium
Mn^{2+}	Manganese
^{23}Na	Sodium
NDI	Nephrogenic diabetes insipidus
NMDA	N-methyl-D-aspartate receptor
NMR	Nuclear Magnetic Resonance
NIMH	National Institute of Mental Health
NOE	Nuclear overhauser effect
^{31}P	Phosphorus
P2	purinergic receptor protein
P2X	eATP activated ligand-gated ion channel
P2Y	eATP activated G-protein coupled receptor
PGM	phosphoglucomutase
PRE	Paramagnetic Relaxation Enhancement
RCT	randomized controlled trial
Sf9	Spodoptera frugiperda 9
SMIT	sodium myo-inositol transporter
SNP	single nucleotide polymorphism
USA	United States of America

US	Ultrashield
UV	Ultraviolet
VDAC	Voltage-dependent anion channel
WaterLOGSY	Water-ligand observed via gradient spectroscopy
WTCCC	Wellcome Trust Case-control Consortium

Chapter 1

Introduction: Lithium as a Treatment for Bipolar Disorder

To establish the background and significance of my thesis work, this chapter provides a comprehensive description of affective disorders, also called mood disorders, with a focus on Bipolar Disorder, and provides a history of the adoption of lithium as a treatment of these mental health diseases.

Bipolar Disorder

Bipolar Disorder, classically known as manic-depressive illness, is a disorder primarily of mood instability whereby an individual experiences intense and severe depression and/or mania (Table 1-1). The majority of individuals afflicted with this affective disorder usually have symptoms that classify them as having either Bipolar I or Bipolar II Disorder. Bipolar I and Bipolar II are delineated by the nature of the episodes experienced, manic or depressive, and the severity of the episode. Primarily, Bipolar I patients experience manic episodes more severely, and Bipolar II patients experience depressive episodes more severely. Bipolar Disorders are different from depressive disorders; depressive disorders include symptoms of depressive episodes that occur once, twice or several times throughout the life of a person without regularity [1], whereas Bipolar Disorders occur in a periodic fashion and are cyclical in nature. A small subset of Bipolar patients experience only mania or depression (unipolar), but are still classified as having Bipolar Disorder because of the cyclical nature of the disorder. It has been argued that manic-depressive illness would be a more accurate term for the disorder because it is broader and allows for the emphasis on the cyclical nature of the episodes, rather than the polarity. Some have argued that rather than two poles, mania is a more

Bipolar Spectrum Disorder	DSM-5[a] Definition
Bipolar I Disorder	For a diagnosis of Bipolar I Disorder, it is necessary to meet the criteria for a manic episode. The manic episode may have been preceded by and may be followed by hypomanic or major depressive episodes.
Bipolar II Disorder	For a diagnosis of Bipolar II Disorder, it is necessary to meet the criteria for a current or past hypomanic episode and the criteria for a current or past major depressive episode. There has never been a manic episode.

Table 1-1. DSM-5 criteria for the diagnosis of Bipolar I Disorder, and Bipolar II Disorder, two of several bipolar spectrum disorders. Defined in the Diagnostic and Statistical Manual, 5th Edition (DSM-5) [1].

severe form of depression, reinforcing the sometimes misleading term, ‘Bipolar Disorder’ [2]. However, the current accepted term for this disorder by the American Psychiatric Association is ‘Bipolar Disorder’ [1].

Procedure for Diagnosis

There is currently no blood test or brain scan that can quickly lead to the diagnosis of Bipolar Disorder (BD). The process of diagnosing a person with BD begins with a physical examination, consultation and laboratory tests to rule out other possible causes for changes in mood, such as a thyroid condition, stroke, or brain tumor. The patient may be referred to a psychiatrist, psychologist or other mental health professional once other ailments have been ruled out [3].

Psychiatrists use the diagnostic criteria found in the *Diagnostic and Statistical Manual (DSM)*, published by the American Psychiatric Association, to gather the necessary information and correctly diagnose patients [1]. Important information for clinicians includes the type, length, and severity of emotions and other symptoms in the life of the patient, as well as a full family history of mental illness. The specific diagnosis of the spectrum of BDs may include: Bipolar I, Bipolar II, Cyclothymia, Substance/Medication-Induced BD, and Bipolar and Related Disorder Due to Another Medical Condition [1]. While the latter two disorders are self-evident, briefly, cyclothymic disorder is when the patient experiences several periods of hypomanic symptoms without a full manic episode and several periods of depressive symptoms without a major depressive episode within a span of two years, does not meet the criteria

for a psychotic disorder, and cannot attribute the symptoms to another medical condition or drug. Bipolar I and Bipolar II Disorders are diagnosed according to the DSM criteria. For Bipolar I, a person must have at least one manic episode (Table 1-2). For Bipolar II, a person must have at least one hypomanic episode and one major depressive episode without having a manic episode. For the proper diagnosis of BD, the symptoms cannot be better explained by another disorder, such as schizoaffective disorder, schizophrenia, delusional disorder, or other psychotic disorder [1].

By way of further explaining/describing/defining the symptoms associated with BD, a manic episode can be distinguished from a hypomanic episode by the severity of the symptoms. If there are psychotic features, or the mood disturbance is enough to cause impaired functioning in social or occupational settings, or hospitalization is required, it is a manic episode. A hypomanic episode must present an uncharacteristic change in behavior and mood that is noticeable by others, but it is not severe enough to disrupt social or occupational functions or require hospitalization [1]. 'Mixed features' is a term that refers to a patient experiencing aspects of mania and depression within the same episode. For example, patients may experience manic symptoms of irritability and decreased need for sleep along with depressive symptoms of anxiety, excessive guilt, and suicidality [4]. 'Rapid cycling' is when four or more episodes of mania, hypomania, major depression, or mixed symptoms occur within one year. Sometimes rapid cycling can be so severe that multiple episodes occur within a week or even within a day [3].

Manic Episode	Major Depressive Episode
A distinct period of abnormally and persistently increased goal-directed activity or energy, lasting at least 1 week and present most of the day, nearly every day (or duration if hospitalization is necessary). Three (or more) of the following symptoms (four if the mood is only irritable) are present to a significant degree and represent a noticeable change from usual behavior: A. Inflated self-esteem or grandiosity. B. Decreased need for sleep. C. More talkative than usual or pressure to keep talking. D. Flight of ideas or subjective experience that thoughts are racing. E. Distractibility (i.e., attention too easily drawn to unimportant or irrelevant external stimuli), as reported or observed. F. Increase in goal-directed activity (either socially, at work or school, or sexually) or psychomotor agitation (i.e., purposeless non-goal-directed activity). The mood disturbance is sufficiently severe to cause marked impairment in social or occupational functioning or to necessitate hospitalization to prevent harm to self or others, or there are psychotic features.	Five (or more) of the following symptoms have been present during the same 2-week period and represent a change from previous functioning. A. Depressed mood most of the day, nearly every day, as indicated by either subjective report or observation made by others. B. Markedly diminished interest or pleasure in all, or almost all, activities most of the day, nearly every day. C. Significant weight loss when not dieting or weight gain; or decrease or increase in appetite nearly every day. D. Insomnia or hypersomnia nearly every day. E. Psychomotor agitation or retardation nearly every day (observable by others; not merely subjective feelings of restlessness or being slowed down). F. Fatigue or loss of energy nearly every day. G. Feelings of worthlessness or excessive or inappropriate guilt. H. Diminished ability to think or concentrate, or indecisiveness. I. Recurrent thoughts of death (not just fear of dying), recurrent suicidal ideation, or a suicide attempt. The symptoms cause clinically significant distress or impairment in social, occupational, or other important areas of functioning.

Table 1-2. Diagnostic and Statistical Manual, 5th edition (DSM-5) criteria for a full manic episode and a major depressive episode. Symptoms must not be attributable to another medical condition or to the effects of a substance. Refer to the DSM-5 for more extensive criteria [1].

Prevalence and Cost to Society

The World Health Organization collected World Mental Health surveys to assess disability caused by physical versus mental disorders in 15 countries. The World Bank classified these countries as either high-income (Belgium, France, Germany, Italy, Japan, The Netherlands, New Zealand, Spain, and the USA), or middle- and low-income (Colombia, Lebanon, Mexico, Peoples' Republic of China, South Africa, and Ukraine). The study found that in both high- and low-income countries, mental disorders were more disabling than physical disorders. Mental illnesses caused more disability than physical illnesses in social and personal areas, whereas their impact on work and productivity was equal. Also, this study found that BD was more prevalent in high-income than middle- and low-income countries (1.4 percent and 0.7 percent, respectively) [5].

In the United States of America, approximately 6.1 million, or 2.6 percent, of adults have BD [6]. In addition, the third most common reason for hospitalization of individuals between the ages of 18 and 44 is mood disorders, such as BD [7]. Bipolar illness affects all social classes and costs the U.S. economy billions of dollars each year [8].

Gender

Equal numbers of men and women have Bipolar I Disorder. However, for Bipolar II Disorder the data is inconclusive, as some studies show the gender ratio to be one while others suggest the condition is more common in females [1]. A larger proportion of women have symptoms of depression compared to males [9, 10]. Also, episodes of rapid cycling and mixed states are more likely to occur in women than in

men. Men and women have different patterns of co-morbidity as well [11]. Females with BD are at a higher risk for alcohol use disorder than both males with BD and females in the general population without BD [12].

Risks

Suicide Risk

In 2012, the Centers for Disease Control (CDC) released the 2010 statistics on causes of death in the United States. Suicide was the second leading cause of death in young people (age 15-34), with the leading cause being unintentional injury; in adults (age 35-44), suicide was the fourth leading cause of death. Over all ages, suicide was the tenth leading cause of death [13] .

The suicide rate in people with an affective disorder, or mood disorder, is 30 times greater than the general population [14]. Specifically, for BD, the suicide rate is estimated to be 10 to 20 times higher than the general population [15, 16]. People with BD have a 25 – 50 percent lifetime risk of attempting suicide, and a 6 - 15 percent lifetime risk of completing suicide [15-19]. Some strong predictors of BD patients who will attempt suicide are: younger age, long periods of depression, personality disorder, and having attempted suicide in the past [20]. In children and adolescents with BD, suicide attempt has been correlated with earlier onset of illness, more severe or mixed episodes, comorbid disorders, physical/sexual abuse, parental depression, and family history of suicide [21].

There are currently no FDA-approved drugs in the clinic that can be given to prevent suicide specifically in patients with BD. However, lithium carbonate (Li_2CO_3) is an FDA-approved mood stabilizer for BD, and a recent meta-analysis confirmed additional anti-suicidal properties of lithium. Although the analysis did not differentiate between unipolar and bipolar depressive disorders, the 48 randomized controlled trials (RCTs) including 6,674 participants showed lithium to be more effective than placebo in lowering the number of suicides and deaths for any reason, reducing the risk of suicide by more than 60 percent compared with placebo [14]. In addition, a retrospective study, including military veterans (who account for approximately 20 percent of suicides nationally [22]) with Bipolar I Disorder and Bipolar II Disorder, similarly concluded that patients taking lithium had a lower percentage of suicide attempts compared with those treated with divalproex and atypical antipsychotics [23].

Co-Morbidity

Of the mental disorders that often accompany BD, anxiety disorder is the most common and found in 75 percent of people with BD. Half of people with Bipolar I Disorder also have Attention Deficit Hyperactivity Disorder (ADHD) or a substance use disorder [1, 24]. People with BD are more likely to have a metabolic syndrome and migraines than the general population [1, 25-27]. Eating disorders, such as binge-eating disorder, co-occur in about 14 percent of patients with Bipolar II disorder [11]. Over half of individuals with Bipolar II Disorder experience three or more co-occurring mental disorders [1].

Prognosis

While there is no current cure for BD, it can be effectively managed with treatment. The most effective treatment involves open communication between the patient and doctor(s) and medication (i.e. lithium, carbamazepine, valproic acid) without abrupt changes (see subsequent section). Patients who follow this regimen may experience fewer symptoms of the disorder over time. Psychotherapy may also be helpful for preventing relapses of bipolar episodes [3].

Creativity

Despite the hardships of living with BD, one positive effect that can present with the disorder is increased creativity. With the unique blend of character traits, temperament, and circumstances, BD may enhance creative ability, even in some cases while the patient is concurrently taking mood-stabilizing medication. While the extreme lows of depression are traumatic, the highs of mania can be addicting, when high creativity, energy, elation, and thoughts flow with ease. The fears of losing creativity or losing the euphoric feelings of manic episodes are major reasons for low patient compliance with mood-stabilizing mediation, such as lithium. Studies have shown, however, that nearly 60 percent of creative people with BD who take lithium are more productive when treated with lithium than not. And, 20 percent reported no change to their productivity. There is an undeniable association between the creativity of some individuals and BD. Although not causative or maybe even directly related, BD has had a role in the creative works produced by writers, artists, poets, and scientists who have lived with the disease. Further research is necessary to clarify the spectrum of mania and

the specific impact of BD on the creativity of the individual [2]. As evidenced by the great number of talented and creative persons who have lived with bipolar illness, such as Ernest Hemingway, Virginia Woolf, Vincent Van Gogh, Richard Schumann, and Edgar Allen Poe, the great difficulties posed by affliction of this disease often paradoxically come with enormous potential for contributing to society in a unique way [28-34].

Etiology of Bipolar Disorder

While its exact nature is unknown, the underlying cause of BD appears to be multifaceted. There is strong evidence that BD is hereditary [35], however, the genetics of the disease are also not understood. Children of parents with BD are 2.7 times more at risk for developing a mental disorder and four times more at risk for developing an affective disorder, such as BD, compared with children of parents with no mental illness [36].

Few clinical studies have followed the offspring of parents with BD for more than a decade. One recent study reported a 12-year follow-up of 108 children of parents with BD. At the initiation of the study, the offspring ranged from 12 to 21 years of age. After twelve years, and at a mean age of 28, more than half of the participants developed a mood disorder, of which 13 percent were bipolar spectrum disorders. The study was in agreement with other studies in reporting that there was a higher percentage of offspring with Bipolar II disorder (8 percent) than with Bipolar I disorder (3 percent). Nearly all of the participants who were diagnosed with a bipolar spectrum disorder experienced a

depressive episode as their first affective episode. Also, most of the participants who developed a mood disorder had their first episode by 25 years of age [37].

Genetics

Inheritance studies, such as family, twin, and adoption studies, suggest that BD is hereditary [35]. The genetic linkage in families was established nearly 30 years ago and yet the process of pinpointing the specific genes responsible for BD only began to be fruitful in 2007 with the advent of Genome-Wide Association Studies (GWAS) and the initial publications of large sample sizes of clinical genomic data, such as those by the Wellcome Trust Case-control Consortium (WTCCC), and the National Institute of Mental Health (NIMH) [38, 39]. These and several subsequent studies discovered a selection of genes with genome-wide significant association, meaning genetic variation of these genes occurs more frequently in people with BD than the control group representing the non-disease general population. The main genetic variants that were identified from these studies occurred in the following genes: *ANK3*, *CACNA1C*, *SYNE1*, *ODZ4*, and *TRANK1* (Table 1-3) [40-42]. *ANK3* codes for a protein, Ankyrin G, which serves as an anchor for neuronal potassium and sodium channels. The protein product of the gene *CACNA1C* is a subunit of the L-type calcium channel. The phenotypes of the other genes have yet to be elucidated. These genes are now considered susceptibility genes in BD [43].

There are other genes that have been implicated in BD, but do not appear as significant using current statistical methods or were discovered in smaller sample sizes

Genetic Variant in Bipolar Disorder	Protein Encoded by Gene	Function of Protein
ANK3	Ankyrin G	An anchor for neuronal sodium and potassium channels
CACNA1C	Subunit of L-type voltage dependent calcium channel	Respond to changes in gene regulation inducing neuronal plasticity, possibly by direct effect on transcription[a].
SYNE1	Nesprin-1	1 out of 4 parts that form LINC (link nucleoskeleton to cytoskeleton)[b].
ODZ4	Teneurins	Cell surface protein involved in signaling and neuronal pathfinding[a]. Potential role in neuronal development and axonal myelination
TRANK1	(unknown)	Unknown but found to respond to valproic acid

Table 1-3. Genome-wide significant genetic variants and their phenotype in the BD population were revealed by Genome-Wide Association Studies [41-43].

and found to be not as significant in larger cohorts. Nonetheless, these genes are worth mentioning as they may also play a role in this polygenic disease. Other implicated genes are: *DGKH*, which codes for diacylglycerol kinase [39]; *ADCY2*, coding for a cyclic AMP (cAMP) dependent G-protein coupled receptor (GPCR) involved in neurotransmission [43]; *NCAN*, coding for neurocan, a glycoprotein in the extracellular matrix possibly involved in cell migration and adhesion [44]; *ACP1*, coding for acid phosphatase-1, which is found to be elevated in BD patients who complete suicide [43]; *P2RX7*, coding for P2X7 purinergic ligand-gated ion channel [45-47]; and *ABCA13*, coding for an ATP-binding cassette (ABC) superfamily responsible for transport across the cell membrane [48].

The current field of BD genetics is expanding GWAS sample sizes and population types, mainly headed by the Psychiatric GWAS consortium (PGC) BD Working Group, which includes large data sets from populations around the world. This group has also funded the development of a "PsychChip" for single nucleotide polymorphism (SNP) array analysis of DNA markers associated with psychiatric illness. In addition, subsets of BD population who take lithium are being analyzed for pharmacogenetic analysis. The Consortium for Lithium Genetics and Pharmacogenomics of Bipolar Disorder (PGBD) groups primarily spearhead understanding the genetic make-up of the population of lithium responders [43].

The field of BD genomics is developing the capacity to analyze exome, which focuses only on the exons of the genome, and whole genome sequencing of BD patients. The Bipolar Sequencing Consortium consists of approximately 13 groups dedicated to further understanding the genetic etiology of BD through sequencing exomes and whole

genomes of BD patients and controls. They have already collected ~3,500 BD and ~5,000 control exomes. Finally, gene-mapping studies hope to link genes with their function and provide key insights into the pathophysiology of BD [43].

Treatment for Bipolar Disorder

Treatment involves a combination of different medications for patients with BD. The process of determining the best medicine for treatment can be difficult to navigate for both patients and psychiatrists, especially in the initial stages of treatment. At first, treatment involves patients frequently meeting with a psychiatrist or clinical psychologist to closely monitor the changes in mood and to gauge the effectiveness of the drugs. The goal is to find the best cocktail of drugs and dosage quantity to maximize mood stability and minimize side effects [3]. In the future, the 'trial and error' of prescribing drugs for mental illness may be eliminated with the advent of personalized medicine and establishment of a genetic basis for the efficacy of one drug over another for a particular individual [49]. In addition to medication, some form of therapy is often suggested for patients [3].

There are five main drugs that are prescribed for mood stabilization: lithium, carbemazepine, valproic acid, lamotrigine, and quetiapine (Table 1-4). The mechanisms of action of all of these drugs are unknown. In addition to the mood-stabilizing drugs, depending on the symptoms of the patient, antidepressants or antipsychotics may also be prescribed. The effectiveness of all of these drugs varies between individuals and cases.

Drug Name	Drug Class	Indication for Use	Mechanism of Action
Lithium (Lithobid®)	Mood Stabilizer	• Bipolar Disorder: manic episodes • Bipolar Disorder: maintenance therapy	Unknown; proposed to alter sodium transport in nerve and muscle cells and shift the intraneuronal metabolism of catecholamines.
Quetiapine (Seroquel®)	Atypical Antipsychotic	• Schizophrenia • Bipolar I Disorder, manic or mixed episodes • Bipolar Disorder, depressive episodes • Major depressive disorder, adjunctive therapy with antidepressants	Unknown; proposed to act as an antagonist at dopamine type 2 (D_2) and serotonin type 2 ($5HT_2$) receptors.
Lamotrigine (Lamictal®)	Mood stabilizer; anti-epileptic agent	• Epilepsy • Bipolar Disorder in patients over 18 years of age: maintenance treatment of Bipolar I Disorder.	Unknown; anticonvulsant action proposed to inhibit neuronal voltage-sensitive sodium channels effectively modulating excitatory neurotransmitter release
Valproic Acid (Depakene®)	Mood stabilizer; anti-epileptic agent	• Monotherapy and adjunctive therapy of complex partial seizures	Unknown; valproate ion proposed to increase gamma-aminobutyric acid (GABA) in the brain.
Carbamazepine (Tegretol®)	Mood stabilizer, carboxamide, anti-epileptic agent	• Epilepsy • Trigeminal neuralgia	Unknown; proposed to produce anticonvulsant activity by lowering the polysynaptic responses and preventing the post-tetanic potentiation.

Table 1-4. Prescription drugs for the indication of Bipolar Disorder [50].

Nonetheless, lithium is one of the most effective drugs for on-going mood stability in a person with BD.

Lithium Treatment and Clinical Use

The use of lithium as a drug dates back almost two centuries. Physicians used lithium salts to treat everything from gout to epilepsy in the mid to late 1800s. However, by the early 1900s, hopes for a cure-all tablet of lithium were dashed by the real dangers presented as patients experienced cardiac depression, intoxication, and death. The efficacy of lithium to remedy 'psychotic disorders' or mood disorders, such as manic-depressive illness, was discovered rather serendipitously by an Australian scientist, John Cade, in 1949, when he first noticed the lethargic effects of lithium carbonate on guinea pigs and his curiosity led to the case study of 10 men who were either manic (i.e., highly excited) or epileptic [51]. The results of this study spurred a renewed interest in lithium, this time in the field of psychiatry. In particular, a Danish psychiatrist, Mogens Schou, spearheaded both non-blind and then ground-breaking double-blind clinical trials proving the efficacy of lithium treatment for both acute and prophylactic care in manic-depressive patients [52]. In 1970, lithium carbonate was approved by the FDA for the indication of manic depression in the U.S. and lithium, in the form of citrate or carbonate salts, became the standard drug treatment for this disorder [53].

During the 1980s and 1990s, the quality of the clinical trials that established lithium as an effective mood stabilizer were criticized and questioned, especially as new drugs came to the marketplace. These lithium trials were conducted when uniform criteria for diagnosing BD were either shifting or had not been firmly established, records

were not clear about reasons for patient withdrawal, and the diagnosis of depression was often not distinguished as unipolar or bipolar depression. In addition, in trials where the same patients switched from lithium to placebo during the study, called 'cross-over' trials, the patients were abruptly, rather than gradually, removed from lithium. It is now known that abrupt changes in medication, especially lithium, often result in relapses. Placebo patient relapses in a cross-over clinical trial could have biased the control data, falsely boosting the effectiveness of lithium [49].

Since the validity of the clinical trials was questioned, lithium use declined during the 1990s and the use of newer drugs, such as valproate, lamotrigine, and atypical antipsychotics, increased. At the same time, the pharmaceutical industry was not interested in funding additional clinical trials of lithium because, as an element, lithium cannot be patented, and so no profit motive existed to pursue lithium as a therapy. In addition, the evolution of criteria for diagnosis from a basic understanding of manic-depression to the currently accepted full range of BDs, called 'bipolar spectrum disorders', may have made lithium appear less effective due to a wider range of patients with atypical symptoms who may not respond to lithium treatment [1, 49].

More recent clinical trials, over the last 20 years, using standardized and clearly delineated criteria for diagnosis have reestablished lithium as a very effective drug treatment. This reestablished lithium as the gold standard comparator for new drugs. There is strong evidence for lithium efficacy in the treatment of acute manic episodes over placebo [49], although one study reported that haloperidol, an antipsychotic drug, was more effective than lithium in the treatment of acute manic episodes [54]. Another study showed that both valproate and lithium were effective treatments for mania or

mixed episodes over placebo [55]. It should be noted that lithium has a slow onset of action, approximately 6-10 days, and, therefore, it may not be ideal for treating acute mania. For comparison, risperidone and olanzapine, two atypical antipsychotics, take effect approximately 2-6 days after treatment initiation [49].

Fewer clinical trials have focused on lithium efficacy in the treatment of bipolar depression episodes specifically. Research shows that lithium is effective in treating bipolar depression, but more studies with a focus on bipolar depression or BDII depressive episodes may reinforce these findings. Some clinical trials compared lithium to other antidepressants in the treatment of acute BDII depression, but there is not enough evidence to conclude that lithium is more effective than antidepressants. In addition, few clinical trials have researched the effectiveness of lithium combined with other drugs, although initial studies have suggested certain combinations of drugs to be more effective than one drug alone [49].

Aside from acute episodes, lithium is used in preventative care. During this maintenance phase, lithium is the agent of choice for BD, as it is highly effective. Lithium is found to be superior to placebo, carbamazepine, and valproate for maintenance therapy. It is more robust in preventing mania than in preventing depression, but effective in both nonetheless. Combination drug therapy for the maintenance phase has not been tested extensively, but some trials show superior preventative care with combinations of lithium and quetiapine, or lithium and valproate [49].

Lithium is not a perfect drug

One aforementioned drawback to lithium treatment is the 6-10 day lag time between treatment initiation and therapeutic effectiveness. Lithium intoxication is one danger for patients taking lithium. Lithium levels in serum above 1.5 mM can be toxic, leaving a very narrow therapeutic window (0.6- 1.2 mM) [2]. Any loss of fluid (i.e., diarrhea, vomiting, diuretics, or volume depletion) puts the patient at risk for lithium intoxication. Drug combinations, such as lithium with certain nonsteroidal anti-inflammatory drugs (NSAIDs) or angiotensin converting enzyme (ACE) inhibitors, place a patient at greater risk for lithium intoxication. Patients must be carefully monitored by their physician for signs of lithium intoxication, including confusion, tremors, speech, uncoordinated movement, uncontrollable eye movement, seizures, and impaired consciousness. Lithium intoxication can lead to death so medical intervention for detoxification may be critical. Lithium detoxification includes replenishing fluids with isotonic saline, monitoring for hypernatremia, whole bowel irrigation with polyethylene glycol to coat the intestines and prevent further lithium absorption, and, finally, lithium removal by hemodialysis [56].

In addition to overall toxicity, lithium can cause specific problems with kidney function. Two very common side effects of lithium treatment are thirst and increased urine output. Lithium causes a decreased reaction to the antidiuretic hormone (ADH) in the renal tubule, which can lead to nephrogenic diabetes insipidus [57]. The onset of nephrogenic diabetes occurs in nearly 40 percent of lithium patients [49]. Increased urination due to decreased ability to concentrate urine puts patients at risk for sodium depletion and excessive fluid loss, risk factors for lithium intoxication. Lithium-induced

changes occur in the collecting tubule function [57]. Patients who take lithium for longer durations (in excess of 10-20 years), who are older, or who experience lithium intoxication episodes are at risk for two nephropathies, chronic and end-stage renal disease (ESRD), although they are uncommon [49].

Another difficulty with lithium treatment is for women who are or become pregnant, as lithium may have teratogenic effects on an embryo. During the first trimester of development, lithium may cause Ebstein's anomaly, a heart malformation [58]. However, lithium has not been firmly established as a teratogen. A meta-analysis of RCTs found little evidence for congenital malformations caused by lithium treatment [59]. Clinically, lithium is taken with caution during a pregnancy. A planned pregnancy can be carefully monitored by decreasing dosage of lithium or slowly discontinuing the mood stabilizer for at least the first trimester, whereas unplanned pregnancies may have already exposed the fetus to harm. As mentioned earlier, abrupt discontinuation of lithium has been shown to cause relapse episodes, which may cause further harm to the fetus. So, pregnant woman with BD must carefully weigh the decision to stop treatment, as untreated manic and depressive episodes put both the fetus and mother at risk [58].

Lithium treatment is linked to several other conditions as well. For one, approximately 25 percent of patients who receive lithium treatment develop thyroid or parathyroid maladies. A meta-analysis of RCTs concluded that there was a higher prevalence of hypothyroidism in patients taking lithium compared with placebo. The findings also indicated an increase in the thyroid stimulating hormone (TSH), blood calcium, and parathyroid hormone [59]. Lithium treatment was also associated with more weight gain compared to placebo [59]. Additional adverse effects of lithium

treatment include experiencing tremors, nausea, diarrhea, lethargy, reduced self-perceived creativity, and gastric discomfort [49].

Lithium benefit in neurodegenerative diseases

Lithium is a mood-stabilizing drug and has displayed anti-suicidal benefits, but it has also been shown to impart neuroprotective properties. Lithium slows disease progression and increases neuronal growth and protection in animal models of neurodegenerative diseases. These animal models represented: stroke, Amyotrophic Lateral Sclerosis (ALS), Fragile X syndrome, Down syndrome, Huntington's disease, Alzheimer's disease, Parkinson's disease, retinal degeneration, spinal cord injury, and human immunodeficiency virus (HIV) infection, among others [60-64]. Some of these findings supported the advancement to human clinical trials for lithium treatment in diseases such as ALS, for which there is presently no effective treatment. Daily lithium doses during a 15-month observation period resulted in delayed disease progression. Correlation of delayed ALS in humans and an ALS mouse model points towards a lithium effect on increasing mitochondria in motor neurons, activated autophagy, and increased number of neurons [63]. Another clinical trial tested the cognitive and biological effects of lithium on people with amnestic mild cognitive impairment. This study showed improvements such as better attention and decreased phosphorylated tau, a microtubule-associated protein that aggregates into neurofibrillary tangles, seen in Alzheimer's disease, upon hyperphosphorylation. These results propose lithium as a potential early drug intervention for the prevention of Alzheimer's disease, which may be

a safer and more feasible use of lithium than in the elderly with late stage Alzheimer's [65-67]. Further evidence of neuroprotective effects of lithium comes from a study of elderly bipolar patients who have had chronic lithium treatment compared with elderly bipolar patients who have not. The prevalence of dementia in the lithium treated group matched the prevalence of the general population, which was significantly lower than the prevalence among non-lithium-treated BD elderly patients [68].

Lithium's Mechanism of Action

Although the effectiveness of lithium in treating mood disorders has been known for over 60 years, it is remarkable that today there is still no known mechanism of action for either lithium's therapeutic efficacy or side effects. The following research addresses the pharmacology of lithium as a drug treatment for BD and may serve to provide a guiding fundamental model for elucidating the pathophysiology of BD, the cause of adverse side effects of lithium ingestion and of lithium toxicity, and reasons for its attributed neuroprotective nature.

The significant shortcoming of current lithium and BD research is the lack of a molecular mechanism of action that is supported by direct measurements under physiologically relevant conditions. Previously published reports show *competition* of lithium with magnesium under non-physiological concentration ratios of lithium to magnesium, or otherwise lack sufficient consideration of alternate interpretations of complex data [69, 70]. These have been widely referenced and taken as lithium's most likely physiological mechanism of action at metal binding sites, whether on enzymes, ATP, or ATP-bound-enzymes (see Chapter 3).

In an attempt to address this problem, this project sought to provide a unifying physiologically relevant model for how lithium works at the molecular level that could be tested through biochemical and biophysical experiments. The results have led to a paradigm shifting hypothesis for lithium's mechanism of action in the treatment of mood disorders.

Chapter 2

Probing Lithium's Mechanism of Action: From Animal Models to Biophysical Approaches

Numerous methods have been used to try to understand how lithium acts as a mood stabilizer, from human clinical trials and disease models in animals to cellular assays. Molecular studies of lithium, however, have been challenging and limited due to the small size of the element (7 Daltons) which poses challenges in experimental design and signal detection. This chapter describes the different approaches that have been used previously to study lithium molecular and biological mechanisms, as well as those employed primarily in this thesis research. The theory and practical aspects of each approach are outlined along with the strengths and limitations of each technique.

Challenges in Lithium Research

Animal Model Research

Animal models have been used to mimic certain aspects of Bipolar Disorder (BD). However, the subjective nature of neuropsychiatric symptoms makes modeling mental illnesses in animals very challenging. Instead, animal models are used to model specific symptoms or aspects of the illness, rather than the entire illness in one animal. In some ways, mental illness seems uniquely human. Cognitive symptoms like hallucinations, delusions, sadness, and guilt cannot be easily described in a mouse model system. Until the physiological basis for these symptoms is better understood, animal models will not be able to test these cognitive symptoms. Instead, more measurable symptoms, like changes in social behavior and motivation, can be used to mimic aspects of mental illness in animal models. Currently, no BD animal model exists that is capable of spontaneously cycling through episodes of mania and depression [71]. Therefore, researchers using animal models as a neurobiological tool or disease model use a range of

methods to simulate the disease. Animal models of mental illness symptoms are generated by means of genetic, pharmacological, environmental, or electrical stimulant manipulations. For example, mania is modeled in rodents that are administered psychostimulants, like cocaine or amphetamine. Overexpression of glycogen synthase kinase-3β (GSK-3β), known to be inhibited by lithium, is also used to produce transgenic mice with some manic-like behaviors [72]. These mice exhibit lower 'anxiety-like' behavior in risk-taking assessments, and increased mobility and locomotion. Another transgenic mania model is a loss-of-function mouse with a mutation in the *Clock* gene. These mice have altered circadian rhythms, similar to changes in sleep patterns of BD patients [71, 72]. There are also mouse models of depression, which are normal mice exposed to repeated stresses, like physical manipulations or social agitations [72]. Again, cognitive symptoms, such as suicidality and emotions, cannot be objectively measured, but changes in behavior due to stress can be similar to depression. The rodent response to stress can cause changes in pleasurable activities, weight gain, and insulin levels. These models are validated by the reversal of symptoms by administration of antidepressants [72]. Taken together, these models can be somewhat useful for validating targets and predicting behavioral outcomes of medications [73]. However, a more fundamental understanding of BD is necessary to develop a more robust model of the disease in animals.

Lithium Research in the Laboratory

With a molecular weight of 7 Daltons, the small size of lithium poses a significant challenge for direct detection and purification by many commonly used biochemical

methods. There is no filter or membrane small enough to trap lithium. There is no radioisotope of lithium that can be used for detection, and no intrinsic fluorescence or fluorescent lithium-binding dye available. In structure determination, X-ray diffraction cannot 'see' lithium ions since it is not large enough to cause a detectable signal.

Two methods that have been used for the direct detection of lithium in biological research are flame Atomic Emission spectrophotometry and flame Atomic Absorption spectrophotometry. Atomic Absorption or Atomic Emission are reasonable methods for quantifying the lithium concentration in histological slices. Yet, only a qualitative assessment of the distribution and localization of lithium can be obtained by these methods. In addition, the delicate process of slicing, freezing, and thawing tissue samples is time consuming, labor intensive and complicated. Lithium specific microelectrodes were developed in the late 1970s and can detect the transport of lithium in living cells; however, they have not been used extensively, possibly because of the interference by other biological ions in the cellular milieu. Mass spectrometry can easily distinguish between the ^{6}Li and ^{7}Li isotopes. Secondary ion mass spectrometry (SIMS) measures the mass to charge ratio of ions in a thin solid sample such as biological tissues by projecting a beam of primary ions onto the sample. This technique is mostly qualitative because of the difficulty in setting standards of tissue samples, but in some cases quantitative measurements have been attained [74]. Nuclear magnetic resonance (NMR) can be used to directly detect lithium in solution in the presence of several different molecules. Both ^{6}Li and ^{7}Li are detectable by NMR, but ^{7}Li has a much higher sensitivity as it is found at higher natural abundance.

Lithium activity *in vivo* has been detected by assays with secondary reporters or readouts. For example, lithium inhibition of inositol monophosphatase (IMPase) was discovered by the buildup of the reactant, inositol monophosphate, and the decrease in the product, inositol, in the IMPase-catalyzed dephosphorylation reaction [75] (see Chapters 3 and 6 for hypotheses of lithium's mechanism of action). The many possible molecular targets of lithium can be tested at the organismal and cellular levels, but to elucidate the most fundamental mode of lithium action, clarity must be gained at the molecular level.

Methods for Measuring Weak Binding

In addition to its small size, lithium binds weakly (μM to mM) to biological molecules, making it difficult to measure binding and affinity of lithium for its target. There are a number of biophysical methods that can measure weak binding (Table 2-1). Isothermal Titration Calorimetry (ITC) is a thermodynamic-based method where endothermic and exothermic biochemical reactions are characterized by change in heat capacity as a function of the ligand or molecule titrated [76, 77]. In this project, lithium was not found to cause a detectable change in heat capacity upon binding, thus making this approach impractical. Another method to measure weak binding interactions is equilibrium dialysis. Equilibrium dialysis allows a system divided into two compartments by a partition to reach equilibrium. A filter membrane partition between the two chambers is permeable to the ligand, but not to the protein. The binding affinity can be

Method	Practical Limitations
NMR	Requires concentrated samples (typically near mM) due to low sensitivity
Isothermal Titration Calorimetry (ITC)	Requires a change in heat capacity
Fluorescence	Requires intrinsic fluorescence or design of reporter
Equilibrium Dialysis	Requires availability of membrane pore size smaller than the ligand
Equilibrium Gel Filtration	Requires dynamic range of UV detection

Table 2-1. Measurement challenges of molecules with weak binding affinity.

calculated from the concentration of protein on one side, and the equilibrium concentrations of ligand in each chamber. The concentration of the protein-ligand complex is calculated by obtaining the difference in equilibrium ligand concentration of the two chambers. The unbound protein concentration is equal to the starting protein concentration minus the protein-ligand complex concentration calculated above. This method requires a detectable signal to quantify the concentrations. In theory, this method is simple and straightforward. In practice, the system used in this work either did not reach equilibrium or did not come to equilibrium within a reasonable time frame, and the measured concentrations were not reproducible.

Another method to measure binding interactions of low affinity is by Equilibrium Gel Filtration, which was used to measure the binding of lithium and ATP to albumin and is described further towards the end of this Chapter and in detail in Chapter 4 [78-80].

NMR Methods for Measuring Lithium

This doctoral research primarily employed methods in NMR spectroscopy for lithium detection. Aside from Atomic Absorption, NMR is the most common method utilized to directly detect the lithium ion. In addition, the natural abundance of the ^{7}Li isotope is quite high (92.5%) so detecting the lithium NMR signal is practical in short time periods (minutes to hours). NMR is well suited to measure weak binding interactions and to answer biochemical questions about the atomic interactions of lithium. The methods detailed below offer new applications of NMR for the advancement of lithium research.

NMR Theory

NMR is a phenomenon affecting particular nuclei placed in a static magnetic field and exposed to electromagnetic radiation in the form of radio waves. Nuclei that are observable by NMR spectroscopy have a quantum property called spin. Spin is a characteristic possessed by unpaired electrons, protons, and neutrons. Any atom with an odd number of protons or an odd number of neutrons has a net nuclear spin and is considered an NMR active nucleus. The odd number indicates net spin property, while the spins of an even number of nucleons pair up and cancel each other. ^{7}Li has 3 protons and 4 neutrons, rendering it an NMR active nucleus, directly detectable by NMR. Nuclei that do not possess net spin are not detectable in NMR, but can gain a spin characteristic by changing the number of neutrons, as in a different isotope. One detection limitation may be the natural abundance of the isotope. ^{7}Li has a high natural abundance so this was not a limiting factor for this research (Table 2-2.).

Nuclear spin is a constant quantum mechanical attribute of the nucleus; it never stops or changes speed. The spinning positive charge creates a constant magnetic field that aligns with its axis of spinning. The strength of the magnetic moment that the atom produces is the gyromagnetic ratio (γ), which is unique to the nuclear spin of each atom and does not change. When nuclei with net spin experience an external magnetic field, the nuclear magnet aligns with or against the external magnet in a lower energy (α) or higher energy (β) state, respectively (Figure 2-1).

The distribution of spinning nuclei aligning with and against the magnet is nearly equal at thermal equilibrium, but there is a slight excess of spins residing in the α state. The Boltzmann distribution further correlates the two populations of spins with

NMR Nucleus	Natural Abundance (%)	Spin
^{7}Li	92.5	3/2*
^{31}P	100	1/2
^{23}Na	100	3/2*
^{1}H	99.985	1/2

Table 2-2. Properties of NMR nuclei used in this research project. Asterisk (*) denotes spins with a quadrupolar moment.

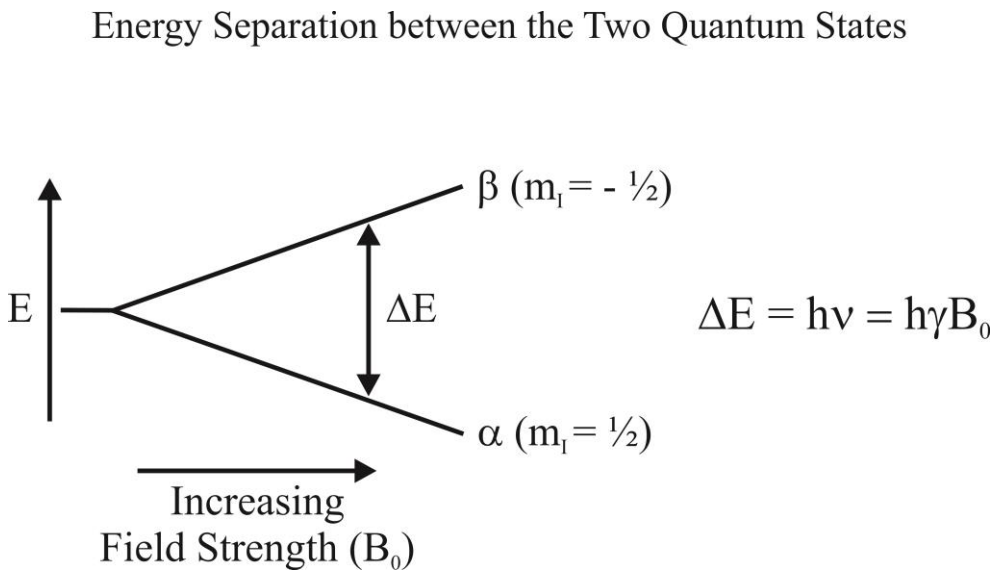

Figure 2-1. Energy states of an NMR-active nucleus.

temperature. The ratio of β spins to α spins decreases below room temperature, increasing the difference in the number of spins between the two states. Conversely, the ratio approaches 1 at temperatures higher than room temperature, effectively decreasing the difference in the number of spins between the two states. The majority of spins have no measurable magnetization, or signal, because for every matched spin, high and low energy, their emitted photons cancel each other out resulting in zero net magnetization. A rough estimation is that only 1 in 10^6 spins have a detectable net magnetization upon absorption of a photon that can be measured. This is the reason that NMR is an insensitive method and requires micrograms to milligrams of material to detect a signal. The NMR signal is proportional to the difference in spin population between the two states, or the excess of spins in one state.

The alignment of nuclei in these two spin states is not static but rotates in a circular motion around the z-axis in the x-y plane as a result of the angular momentum of the nuclear spin and the torque exerted by the external magnetic field. This motion, similar to a spinning top, is called precession (Figure 2-2). The precession rate (ν), also known as the resonant frequency or Larmor frequency, is proportional to the atomic gyromagnetic ratio (γ), and the external magnetic field strength (B_0) (Eq. 1).

$$\nu = \gamma B_0 / 2\pi \qquad \textbf{Eq. 1}$$

The units of precession rate are cycles per second, or hertz. While the gyromagnetic ratio is constant, the external magnetic field depends on the NMR instrument and hardware, as well as the chemical environment.

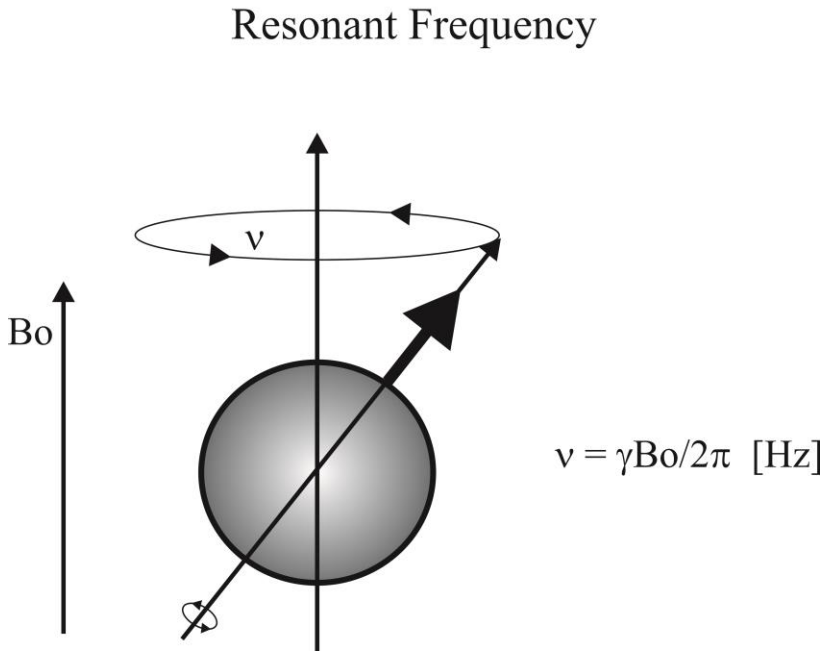

Figure 2-2. Resonant frequency.

The energy separation of spin populations by the external magnetic field is the key to NMR. Like tuning a radio to a particular frequency to hear a radio station, the frequency of the radiofrequency pulse tunes to match the resonant frequency of the nucleus-of-interest. When resonance of the two frequencies occurs, those specific nuclei absorb the energy input and jump to the higher energy state. Their emission of this photon can be detected and gives rise to a signal. The quantum nature of these two states requires that the radiofrequency energy input must exactly match the energy gap in order for the energy of the photon to be absorbed. This energy gap (ΔE) is related to the resonant frequency (ν) by Plank's constant ($h= 6.626 \times 10^{-34}$ J s), where

$$\Delta E = h \nu \qquad \textbf{Eq. 2}$$

The energy difference between the two quantum states of aligned precessing spins is also proportional to the field strength (B_0) (Eq. 3).

$$\Delta E = h \gamma B_0 \qquad \textbf{Eq. 3}$$

A stronger, higher field magnet causes a larger gap between these two quantum states. Stronger magnets are more sensitive because a higher signal-to-noise ratio can be achieved from a larger gap in energy states, which results in better separation between frequencies.

In addition to the opposite vectors of the two spin states canceling each other out, the excess spins in the lower energy state have random phase at equilibrium. While all the excess spins possess the same resonant frequency, the directions of the axes of these precessing spins are not uniform, and lack coherence. Therefore, at equilibrium, the x and y components of the vector also cancel each other because all the vector directions are represented in the population. The only remaining magnitude is the positive z

component of the spin vector. The sum of z components results in the net magnetization vector, M. The magnitude of this vector, M_0, is proportional to the spin population difference, or number of excess spins, and the gyromagnetic ratio of the spins. This z component is used in measuring relaxation detailed below.

Coherence of the ensemble of excess spins can be achieved by applying a radiofrequency pulse. The spins then precess in a uniform manner and the sum of the magnetization in the x-y dimensions yields a magnetization vector in the x-y dimension that can be detected as an NMR signal.

The NMR signal is relayed as a measureable voltage produced by the coherent, precessing ensemble of spins. The instrument that facilitates nuclei to experience the NMR phenomenon by providing a magnetic field is the NMR Spectrometer (Figure 2-3). It is a superconducting magnet produced by circulating electric current through highly specialized coils made of a copper alloy. The superconducting wires operate at cryogenic temperatures, thus the coils are in a compartment filled with liquid helium that is surrounded by a secondary compartment of liquid nitrogen. The NMR magnet has a specialized and removable probe that is inserted into the central bore of the magnet. The probe can tune the radiofrequency input to match the resonant frequency of an NMR active atomic nucleus. The NMR sample is in a 5 millimeter glass tube and rests just inside the top of the probe inside the magnet. Inside the probe are shim coils that compensate for inhomogeneity of the static magnetic field and create a homogeneous

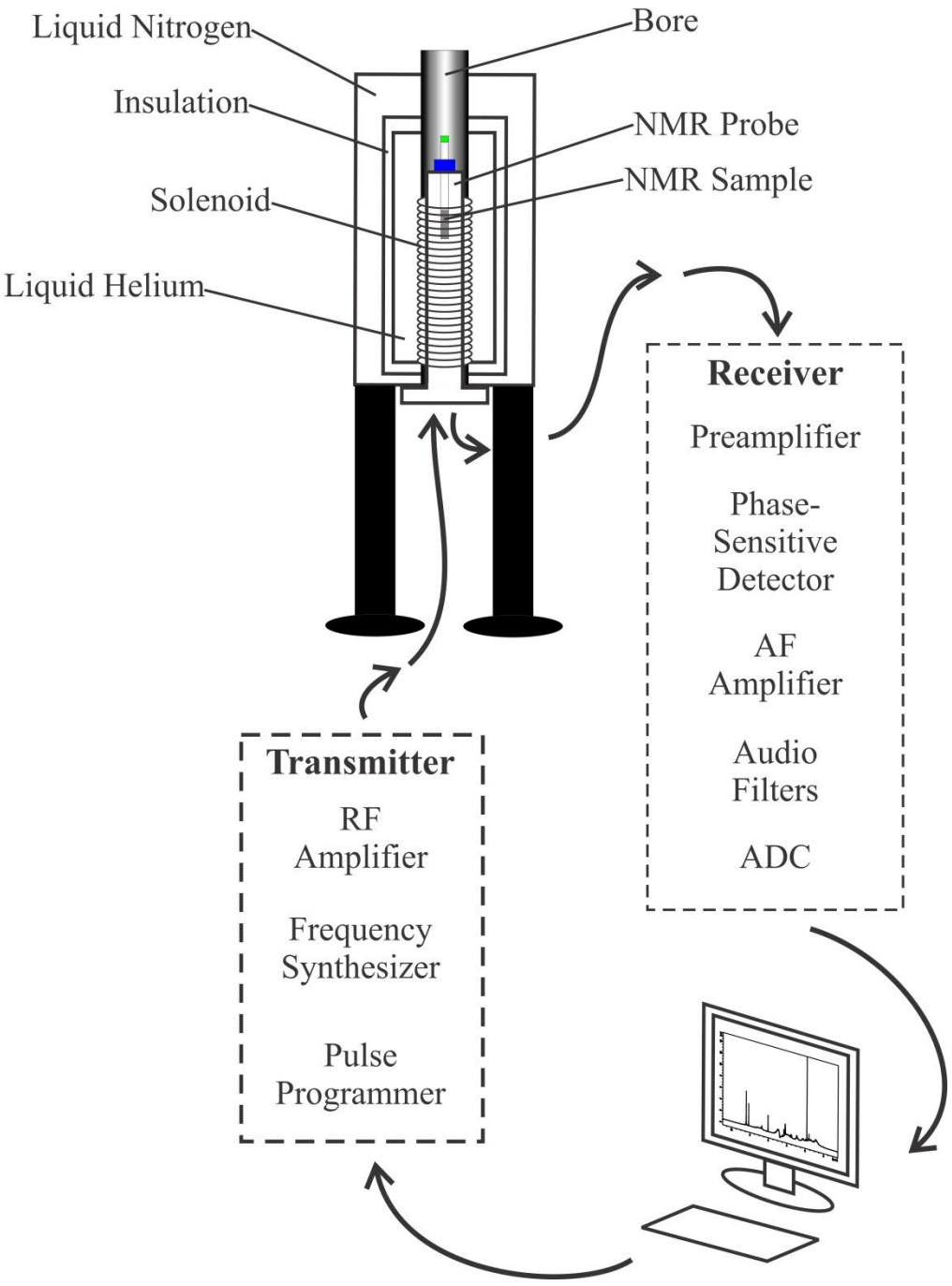

Figure 2-3. Nuclear Magnetic Resonance spectrometer hardware.

field in the x-y-z dimensions immediately surrounding the sample. The NMR sample rests inside the top of the probe containing a coil that is sensitive to changes in voltage produced by the perturbation of the nuclei after a receiving a radiofrequency pulse. The voltage produced by the magnetized nuclei is a time-dependent signal called the free induction decay (FID) which decays over time as the nuclei return to their equilibrium state and coherence is lost. The signal which is detected as a voltage is amplified and sent to the computer for processing and analysis.

Taking a reductionist's approach, the research in this thesis project sought to resolve fundamental questions about lithium's atomic interactions by using NMR as the primary method. The results of the NMR experiments, which are described in the subsequent chapters, yielded a simple biophysical model that can be built upon to test in the more complex cellular stage. These are the experimental methods for this research:

^{31}P Chemical Shift Perturbation

Chemical shift is a measurement of the change in the resonant frequency of an atom, characteristic of the atom's nucleus, but also influenced by the atom's specific position, or chemical environment, within a molecule; a given nucleus will experience slightly different magnetic fields depending on the magnetic influence of nearby nuclei, due either to covalent or through-space interactions. This is why the resonant frequency may vary slightly from one nucleus to the next. The chemical shift of nuclei is like a chemical fingerprint giving evidence of the local environment of each individual nuclei [81]. NMR chemical shift perturbation was measured for the phosphorus atoms of the phosphates of ATP in the presence and absence of lithium and magnesium ions to gain

information about the binding interactions of the metal ions with the phosphate groups (see Chapter 3).

^{7}*Li T1 Relaxation*

Nuclear spins at equilibrium have a random phase (lack coherence), as discussed above. This equilibrium state is disturbed by an energy input in the form of a radiofrequency pulse. The consequence of this radiofrequency pulse at the resonant frequency of a particular nucleus is the absorption of a photon of energy and the movement from the α state to the β state. Following the absorption of energy is the phenomenon of relaxation. Spin nuclei that have absorbed energy release this photon and 'relax' back to the equilibrium spin state.

In practical terms, relaxation gives information about molecular motion and binding of the atomic nuclei. There are two types of relaxation and both occur simultaneously, but NMR pulse sequences can used to distinguish between the two modes of relaxation. The first is T1 relaxation, also called spin-lattice or longitudinal relaxation, and is the type of relaxation in the z-dimension that was primarily measured in the research in this thesis; T1 varies depending on the quantity, proximity, and types of neighboring nuclear magnets [81]. The second is T2 relaxation, also called transverse or spin-spin relaxation. T2 measures the loss of coherence during the return to equilibrium in the x-y dimensions and involves the interaction of spins with each other. T2 is always faster than T1: i.e., the recovery to equilibrium in the x-y dimension is always faster than in the z dimension. Atomic nuclei can relay information about the molecule to which they are bound by their rate of relaxation. Although the nuclei are not themselves

involved in bonding, like their electrons, they experience the changes in magnetic field due to the nearby nuclear magnets. The dynamics of the molecule, such as their tumbling in solution, or correlation time, can be inferred by rate of relaxation of the nuclei that receive a radiofrequency pulse.

T1 relaxation is the time constant for the recovery of the z component of the nuclear spin magnetization, M_z, to return to its equilibrium magnitude, M_0. Inversion-recovery experiments were conducted to measure the T1 relaxation of lithium nuclei (Figure 2-4). In these experiments, the spins at equilibrium receive a radiofrequency pulse to invert them to the higher energy state. Relaxation of the nuclei occurs for some time (τ). Lastly, the remaining magnetization is observed as the nuclei relax along the z axis. We used ^{7}Li T1 to detect whether or not lithium bound to ATP (see Chapter 3).

Specifically, a 180˚ pulse was applied to the ^{7}Li nuclear spins to invert the energy state of the nuclear spins. This was followed by a recovery period where the nuclei relax along the z-axis. Finally, a 90˚ pulse was applied in order to collect the z magnetization in the x-y dimension. This experiment was repeated several times, varying the recovery time, τ, or mixing time. The signal intensities of each experiment were plotted as a function of τ, and the T1 value was obtained by fitting the points to a single-exponential equation (Eq. 4), where *I* is the signal intensity.

$$I_\tau = I_0\left(1 - 2e^{(-\tau/\mathrm{T1})}\right) \qquad \textbf{Eq. 4}$$

Paramagnetic Relaxation Enhancement (PRE)

Paramagnetic Relaxation Enhancement (PRE) experiments were used to test the hypothesis that lithium's mode of action is mediated molecularly through interactions with phosphate group-containing small molecular cofactors, particularly ATP, and to

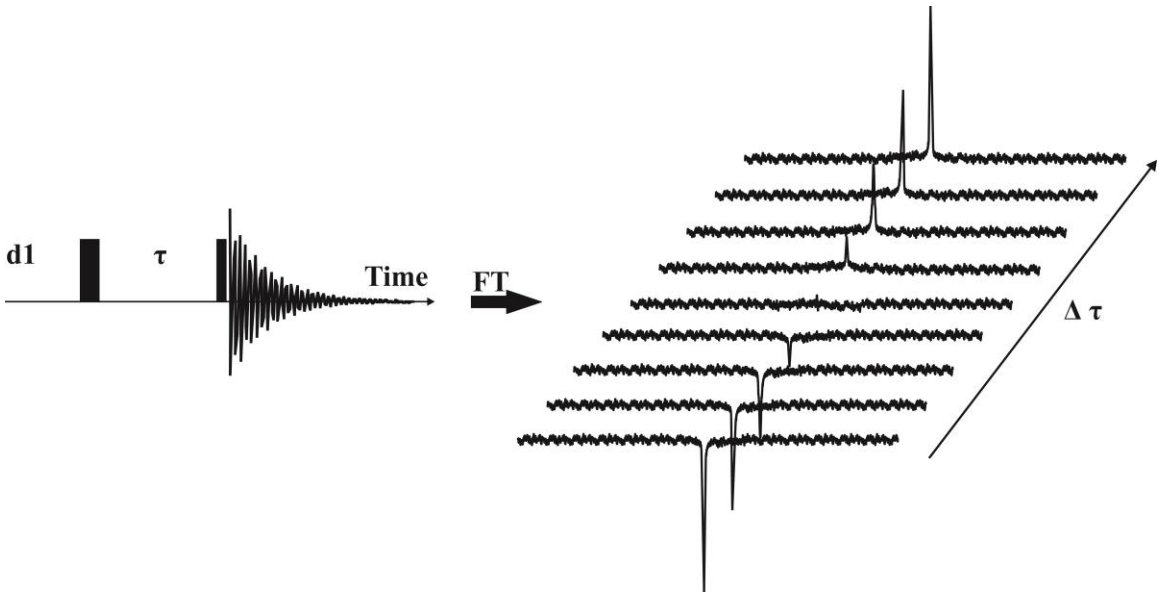

Figure 2-4. Schematic representation of NMR method, Inversion Recovery, to measure the T1 relaxation of nuclei. T1 is time constant for the recovery of the z component of the nuclear spin magnetization to return to its equilibrium magnitude. The free induction decay (FID) is detected over time and is Fourier transformed (FT) into the frequency domain. d1 is the relaxation delay, or recycle delay; τ is the recovery time, or mixing time.

determine whether lithium is competitive with respect to magnesium (see Chapter 3). This experiment employs the use of a paramagnetic atom to cause a PRE [82]. A paramagnetic atom has an unpaired electron. The electron spin of the paramagnetic atom produces a strong magnetic field and greatly increases relaxation. The paramagnetic atom will decrease T1 values of non-paramagnetic atoms within 20 - 30 Å distance of itself. A decrease in T1 value is shorter time for relaxation and is therefore described as a relaxation enhancement that is caused by the paramagnetic atom. The paramagnetic atom can serve as a probe of surrounding non-paramagnetic nuclei measured by T1 relaxation [81]. In the case of ionic interactions, a paramagnetic ion that is in fast exchange with another ion, particularly an ion that is not observable by NMR, can give insight into a non-observable ion by a PRE.

Briefly, chemical exchange refers to the process in which atomic nuclei exchange between two or more environments. These may be intramolecular exchanges, such as motion in protein side chains or conformational change in a molecule, or intermolecular exchanges, such as a ligand binding to a macromolecule. Differences in certain NMR parameters, such as chemical shift or relaxation time, may indicate changes in the nuclear environment. The NMR time-scale refers to how fast an event happens relative to the difference in frequency of the NMR observables, such as chemical shift or relaxation. A slow exchange allows for two separate species of atomic nuclei to be observed, whereas a fast exchange observes the average of these two exchanges [83].

In PRE experiments, the paramagnetic ion, manganese (Mn^{2+}), was used to exchange with magnesium (Mg^{2+}), an atom that is not directly observed by the NMR experiment. Mn^{2+}, while not chemically identical to Mg^{2+}, has been used in studies as an

interchangeable reporter for Mg^{2+} sites in protein and nucleic acids [84]. Manganese was added in very small concentrations to the samples, with a ratio of 0.5 % Mn^{2+} to 99.5 % Mg^{2+}. It was verified that manganese is in fast exchange with magnesium in binding to the triphosphates of ATP as it rapidly sampled, on the NMR time-scale, all of the available ATP-magnesium binding sites and caused all the other detectable nuclei (^{31}P, ^{1}H) in ATP to experience a PRE.

Apparent Lithium Binding Affinity

There are two primary ways to measure the binding affinity of receptor-ligand interactions at equilibrium. The first method detects the saturation of the target receptor as the ligand is titrated. The second detects the association and dissociation rates of the ligand receptor complex as a function of ligand or receptor concentration. We detected the saturation of the receptor site, ATP, by measuring the T1 relaxation of free lithium ligand as it shifts to bound lithium population. Lithium is in fast exchange with ATP so the average of the free and bound population of lithium is represented in the data points. The T1 relaxation of a nucleus adopts the relaxation property of the molecule to which it is bound and is distinct from the T1 relaxation of an atomic nucleus not bound to the molecule. As the ATP is titrated, the population of lithium nuclei shifts from the free to the bound state and the T1 relaxation becomes faster until it reaches saturation. The binding isotherm is an inversion of a typical hyperbolic binding isotherm because the method of detection for binding is a reduction in the T1 relaxation. The T1 relaxation is expected to be inversely proportional to the concentration of ligand bound to substrate and the data can be fit as follows.

The equilibrium dissociation constant (K_d) is defined as:

$$K_d = \frac{[A][B]}{[AB]} \qquad \textbf{Eq. 5}$$

where A + B ⇆ AB. The observed ^{7}Li T1 signal (T_{obs}) was interpreted using a two-state model- where the two states refer to free and ATP•Mg bound Li, and treated as the population-weighted average of the signals from the two states:

$$T_{obs} = T_0 f_0 + T_f f_f \qquad \textbf{Eq. 6}$$

where T_0 represents the free Li signal, f_0 represents the fraction of free Li, T_f represents the ATP•Mg bound Li signal, and f_f represents the fraction of ATP•Mg bound Li.

$$T_{obs} = T_0 - \frac{(T_0 - T_f)x}{[Li_0]} \qquad \textbf{Eq. 7}$$

where,

$$x = \frac{(K_D + [Li_0] + [ATP_0]) - \sqrt{(K_D + [Li_0] + [ATP_0])^2 - 4([Li_0][ATP_0])}}{2}$$

where $[Li_0]$ is the total lithium concentration and $[ATP_0]$ is the total concentration of ATP.

Model Tested on Cells

Fluorescence Microscopy

The model for the interaction of lithium with ATP in the presence of magnesium that developed as a result of the aforementioned experiments led to a hypothesis that lithium actions might be affected through modulation of the interactions of extracellular ATP (eATP) with cellular receptors (Chapter 3). To test this hypothesis, *in vivo* experiments were designed and carried out. The cellular response to ATP, or ATP in the presence of metals, was characterized by measuring the calcium influx facilitated by

ligand-gated ion channels in neuronal cells. P2X receptors are ligand-gated ion channels activated by ATP, and are described in more detail in Chapters 5 and 6. In these experiments, changes in calcium concentration were detected in real time using fluorescence microscopy (Figure 2-5). An intracellular calcium-binding fluorescent reporter, Fluo-3, indicated calcium influx observed by the fluorescence emission intensity of Fluo-3 [85]. This experiment explored whether the presence of lithium in the hypothesized ATP·Mg·Li model could disrupt or modulate the normal activity of the P2X receptor since the ATP-activated P2X receptor regulates Ca^{2+} flow into the cell.

Model Tested on Protein

Protein Expression of P2X Receptor

Results from the cellular studies on the modulation of the P2X receptor in neuronal cells (see Chapter 3) inspired the further elucidation of this effect at the isolated protein receptor level. Studies were initiated to determine if lithium acts as Li-Mg-ATP moieties through modulation of the activity of ligand-gated ion channels such as the membrane purinergic receptor proteins, P2X, whose specific agonist is ATP. These data were sought to provide a direct molecular linkage between the ATP-lithium model and the observed neuronal response (see Chapter 5 for more detailed explanation of experimental methods).

Human Serum Albumin

The ATP-lithium model also led to a study of a possible mechanism for lithium transport on proteins and more generally of modeling lithium association with proteins

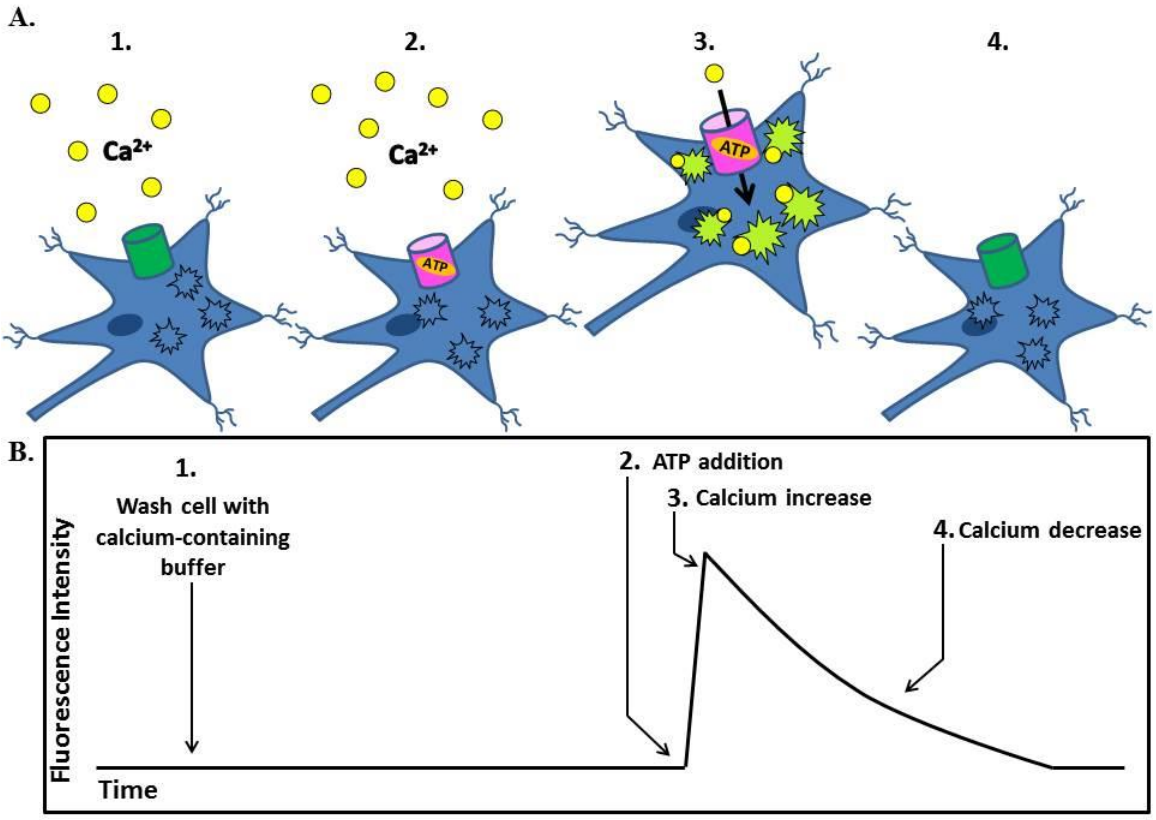

Figure 2-5. Calcium binding reporter, fluo-3, visualized by fluorescence microscopy. Cartoon shows the neuronal assay in four steps, detecting fluo-3 fluorescence upon ATP addition (A). Expected fluorescence response at the four steps displayed in panel A (B).

through ATP cofactors. Human serum albumin (HSA) was used as a model protein for this work (see Chapter 4). HSA is a well-characterized blood serum protein, containing ATP binding site(s), which acts as a carrier of small molecules.

HSA was chosen as a model protein because it is biologically relevant, as the most abundant protein found in the blood plasma, has a known ATP-binding site, and is generally well characterized by NMR and other methods. It is also known as a "carrier" for many drugs, such as the commonly known pain medication, ibuprofen, and blood anti-coagulant, warfarin. Its high solubility and stability also makes it easy to work in the NMR [86, 87]. In combination with the aforementioned NMR methods, the following experimental methods aided in the characterization of Li-Mg-ATP binding to HSA:

WaterLOGSY by NMR

Water-ligand observed via gradient spectroscopy (WaterLOGSY) is an NMR method that indicates the binding of a small molecule (< 750 Da) to a macromolecule (>30 kDa). It is useful in drug discovery efforts to screen libraries of small molecules for drug targets, and in fragment-based drug discovery for the rational development of high affinity binding molecules. In NMR, the small ligand has a shorter correlation time and diffusion rate when it is bound to the macromolecule than when it is free in solution. If the ligand is not bound, it will have a longer correlation time, which will match the correlation time of the free ligand in solution. The mechanics of the experiment involve the saturation transfer of magnetization from bulk water to the ligand via the water directly and via labile protons and bound water on the protein near and far from the

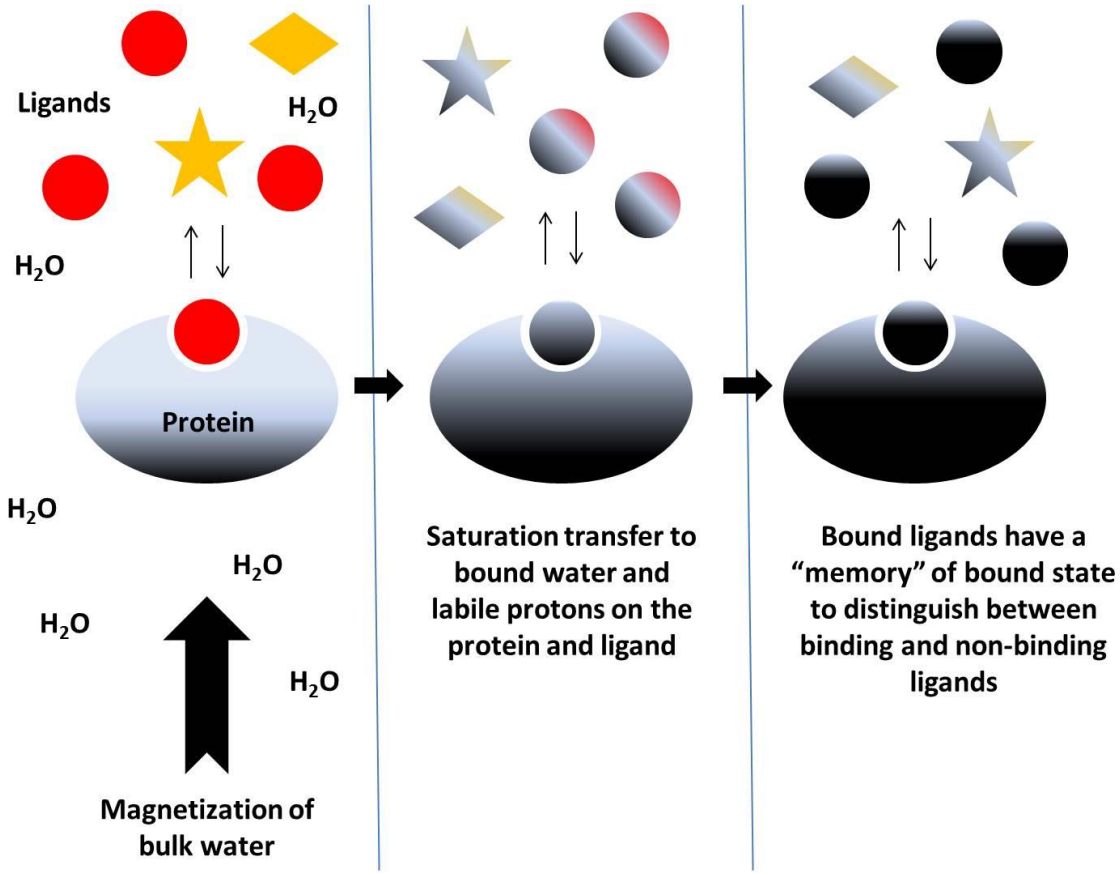

Figure 2-6. Illustration of water-ligand observed via gradient spectroscopy (WaterLOGSY) method for detection of ligands binding to protein (larger oval). Saturation transfer of bulk water and bound proton magnetization. Bound ligands (circles), adopt a correlation time of larger protein, while free ligands (stars, diamonds) have a correlation time distinctive of free ligands.

binding pocket (Figure 2-6). The ligand that binds to the macromolecule, experiencing the magnetization, cross-relaxes with the labile protons and water molecules bound to the protein. As the ligand dissociates from the macromolecule, it carries a changed relaxation due to magnetization transfer from the protein bound water. Meanwhile, more of the population of ligands bind and experience the cross relaxation from the protein bound waters, thereby increasing the detectable signal of bound ligand. The intermolecular nuclear overhauser effect (NOE) from bulk water to the non-binding ligand would not experience the additional cross-relaxation effects of the labile protons and bound water on the protein and therefore exhibit a characteristic small NOE due to the fast molecular tumbling.

The experiment involves taking the difference between a spectrum taken with water saturation and that with the saturating pulse set far away from the resonance signals to match any heating effects of the pulse on the sample without directly perturbing the actual signals. In the difference spectrum, ligands that are bound have a negative sign and appear positive in the spectra, and ligands that are unbound have a positive sign and appear negative in the spectra [88-90]. Clearly distinguishable peaks of ligands bound versus unbound make this a very useful tool for determining whether a ligand is bound to a protein.

Equilibrium Gel Filtration

It was not possible to determine the apparent affinity of Li to ATP when bound to HSA by ^{7}Li *T*1 Relaxation NMR. The protein concentrations necessary to conduct the titration experiment exceeded what was practical. Equilibrium Gel Filtration

chromatography was therefore used to measure the binding affinity of ATP to HSA (see Chapter 4). Equilibrium Gel Filtration chromatography is a method by which a ligand-protein binding affinity can be determined, and is particularly useful for weak binding affinities. Gel filtration, or size-exclusion chromatography, separates biomolecules on the basis of the Stokes radius of the protein or molecules flowing through the column. The method of equilibrium gel filtration uses a gel filtration column that is equilibrated with an elution buffer containing a constant concentration of the ligand (Figure 2-7). When the protein is injected and eluted from the column, the ligand from the buffer binds to the protein. The composition of the column resin allows large molecules to elute first, followed by smaller molecules. The UV absorbance of molecules through the flow cell of the FPLC indicates the elution of the protein-ligand complex. This is followed by a drop in UV absorbance below the baseline indicating the depletion of ligand from the elution buffer by the faster moving protein [80, 91-93].

Applications to other Enzyme and Receptor Studies

Measurements in the context of this biophysical model, by the methods above, offer new avenues for examining the enzyme inhibition of lithium in the literature and its possible other roles in biological processes, such as in receptor-ligand binding, and transport.

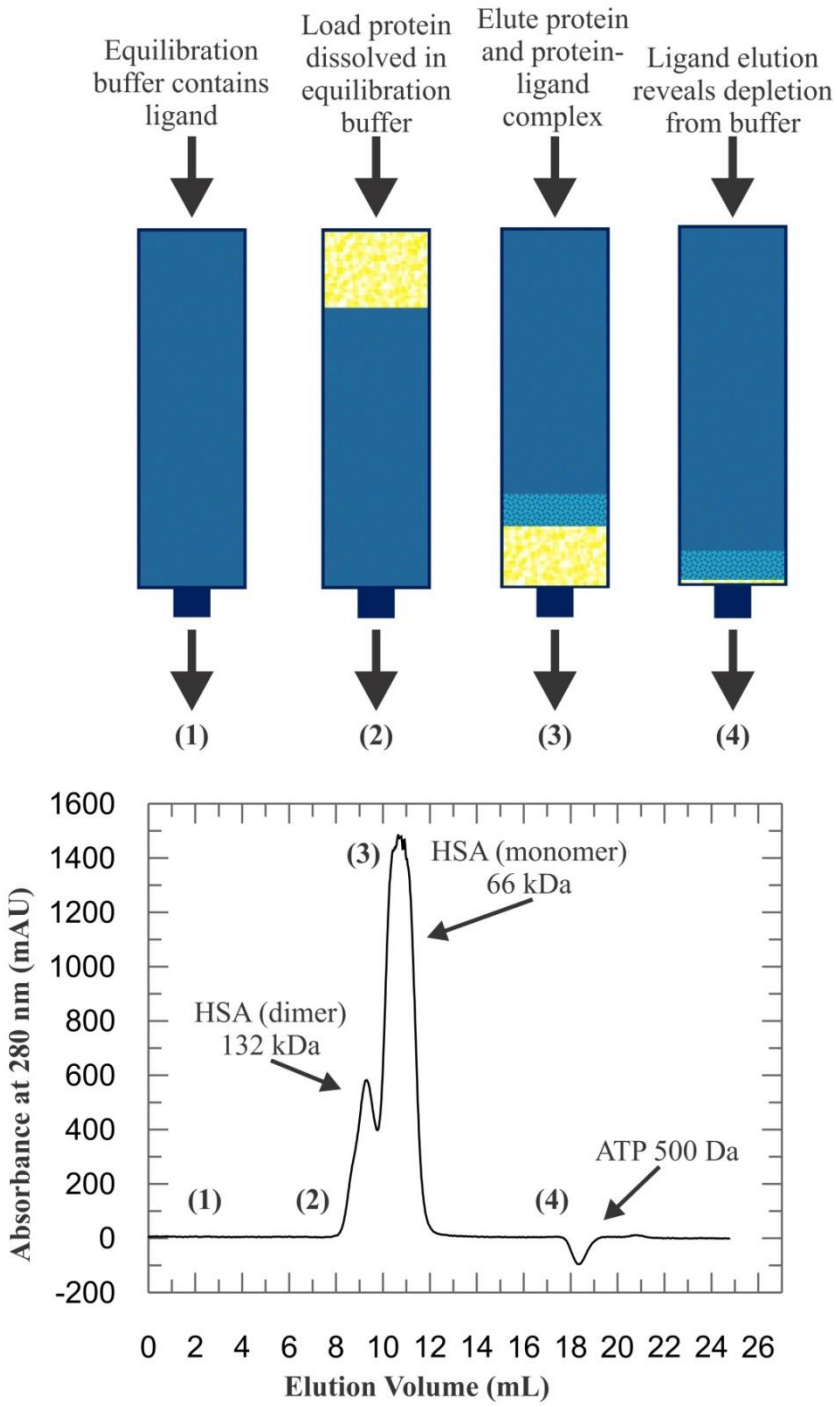

Figure 2-7. Equilibrium Gel Filtration for detecting ligand-protein complexes. Buffer (blue) contains free ligand (1). Protein (yellow) is loaded (2) and eluted (3) from the column with protein-ligand complex. Lower concentration of free ligand (light blue) is eluted (4).

Chapter 3

A General Molecular Model for Lithium's Biological Interactions

Introduction

Lithium has been used in 'treatments' of various ailments since the 1850s, was repurposed to treat 'psychotic excitement' by Australian scientist, John Cade, in 1949, and was officially approved by the U.S. Food and Drug Administration (FDA) for the treatment of Bipolar Disorder(BD) (manic-depressive illness) in 1970. Today, despite advances in modern medicine and drug development, lithium is still prescribed as the standard treatment for mitigating and preventing damaging/detrimental mood swings. Aside from a small subset of patients with BD, most patients find this treatment to be extremely effective, despite the negative side effects and other downsides. Despite over 60 years of lithium research, the mechanism of action of lithium therapy remains unknown.

Biochemical Mechanism of Action- Original Focus on Magnesium

At first pass, it seems unlikely that lithium carbonate would cause any noticeable effect on a person. Despite its small 7 Dalton size, lithium (Li^+) salts have an outsized effect on mood stability in people with BD. Li^+ provides a treatment for many patients through prophylaxis of mood swings, stabilization of acute manic episodes and lower incidences of suicide where other drugs have failed [52]. Magnesium (Mg^{2+}), a Group 2A alkaline earth metal, has a diagonal relationship with Li^+ on the periodic table, indicating certain similarities between the two elements [94]. The ionic radii of Li^+ and Mg^{2+} are quite close to each other at 0.60 Å and 0.65 Å, respectively, and to other neighboring atoms on the periodic table [95]. Li^+ and calcium (Ca^{2+}) also have similar chemical characteristics such as their hydrated radii, electronegativity, and polarizability [95]. Interestingly, Li^+ and Mg^{2+} ions are more strongly hydrated than the other ions of

their respective groups [96]. Mg^{2+} is hexahydrated, coordinating with 6 water molecules when it is not bound by other ligands, and Li^{+} is tetrahydrated, organizing 4 water molecules around itself [97, 98]. Since Mg^{2+} and Ca^{2+} are intricately involved in numerous biological processes, the introduction of exogenous lithium into humans may act through interference with these biological processes due to the similarity of the Li^{+} ion to Mg^{2+} and Ca^{2+}.

Historical Perspective for Current Theory of Lithium's Mechanism of Action

Hypotheses for the molecular mechanism of lithium's action were first proposed in the years after the FDA approved lithium carbonate as a drug for manic episodes in 1970. In a brief exposé in 1976, inorganic chemists Dr. J.J.R. Frausto Da Silva and R.J. P. Williams proposed that lithium may act through a "challenge" to other biological cations, e.g., Na^{+} (sodium), K^{+} (potassium), Ca^{2+} (calcium), Mg^{2+} (magnesium), and thereby cause a biological effect [99]. The diagonal relationship between lithium and magnesium developed into a theory of lithium substituting for magnesium *in vivo* due to their physical similarities. Da Silva and Williams stressed the importance of considering the experimental conditions, e.g., media in which the measured reaction takes place, and emphasized that an absolute stability (affinity) constant may be misleading in a biological system. Rather, they reported 'conditional' stability constants using adenosine 5'-triphosphate (ATP) as a sequestering agent for divalent cations, and then in the same mixture measured stability of the cations bound to a uric acid derivative. They reported that in favorable conditions, lithium could "compete with magnesium to some 20-30 percent for its binding sites." Based on the chemical structure of this uric acid derivative,

Da Silva showed that lithium preferred chelating sites and this lead him to propose that lithium challenged magnesium in key enzymes [100]. This elicited a response from lithium pharmacologist Nicholas J. Birch, who in 1975 published gel filtration data that probed lithium and nucleotide interactions. Birch presented a revised interpretation of DaSilva's data that pointed out that Da Silvia did not consider that lithium may bind to the ATP as well. Birch even speculated on the possibility of lithium binding in a complex with nucleotide and magnesium [101]. He proposed that lithium may actually have its therapeutic effect by interrupting ATP-ADP equilibria in key enzymes such as ATPases. Of special note was the statement in the report that they had "concluded that there is preliminary evidence for a ternary complex of the Li^{+}-Mg^{2+}-ADP type though this awaits confirmation by physical methods [102]."

Although there is no consensus in the literature on hypotheses for the mechanism of action for lithium, most reports suggest the likelihood of a mechanism involving competition between Li^{+} and Mg^{2+}. According to ^{1}H (hydrogen), ^{13}C (carbon), and ^{31}P (phosphorus) Nuclear Magnetic Resonance (NMR) chemical shift perturbations of ATP, which give information about the chemical environment of the selected nuclei, and ^{7}Li T1 relaxation times, which can offer information about binding events, ATP and ADP have been reported as sites where competition between Li^{+} and Mg^{2+} could occur. As such, this early NMR data did not support Birch's proposed ternary nucleotide complex. In many of these ^{31}P NMR studies, however, the lithium concentration was two orders of magnitude higher than Mg^{2+} (e.g., 300:1) because of its lower affinity for ATP or ADP than Mg^{2+}, and also to observe a significant chemical shift [69]. The observed ^{31}P chemical shifts reported in these studies revealed that there is competition between Mg^{2+}

and Li^+; however, the result of using such a high lithium concentration (150 mM LiCl) relative to magnesium more than likely represents a non-physiological 'salting' effect, and so the interpretation of these results in the context of the *in vivo* mechanism of lithium action must be carefully considered. Despite the fact that the conclusions from these studies are misleading, competition of Li^+ at lower affinity Mg^{2+} sites *in vivo* is the most widely presumed underlying chemical mechanism of action reported in the literature today [70]. In another study, temperature was used to vary the exchange regime of the Li^+, Mg^{2+}, and ATP. In a slow exchange regime at low temperatures, it is possible to see signals for the free and bound positions of ATP. Using ^{31}P chemical shift perturbation, it was shown that Li^+ preferentially displaced Na^+ rather than Mg^{2+}, in the ATP·Na versus the ATP·Mg metal complexes. The authors, however, did not discount the possibility of Li^+ displacing Mg^{2+} in biological systems given the most favorable conditions [103].

Results and Discussion

To test whether Li^+ binds in a competitive manner with respect to Mg^{2+}, we used a simplified model of Mg^{2+} binding to ATP (Figure 3-1), whose beta (β) and gamma (γ) phosphates are chelated by Mg^{2+} with an affinity of roughly 100 μM [104]. To determine a saturating amount of Mg^{2+} that was also stoichiometric with ATP, phosphorus chemical shift was measured at increasing Mg^{2+} concentrations (Figure 3-2). Each phosphate peak in the presence of Mg^{2+} represents an averaging of the free and bound states because Mg^{2+} is in fast exchange with ATP. The titration of Mg^{2+} into a sample of ATP caused a chemical shift, particularly in the β and γ phosphates where Mg^{2+} is chelated.

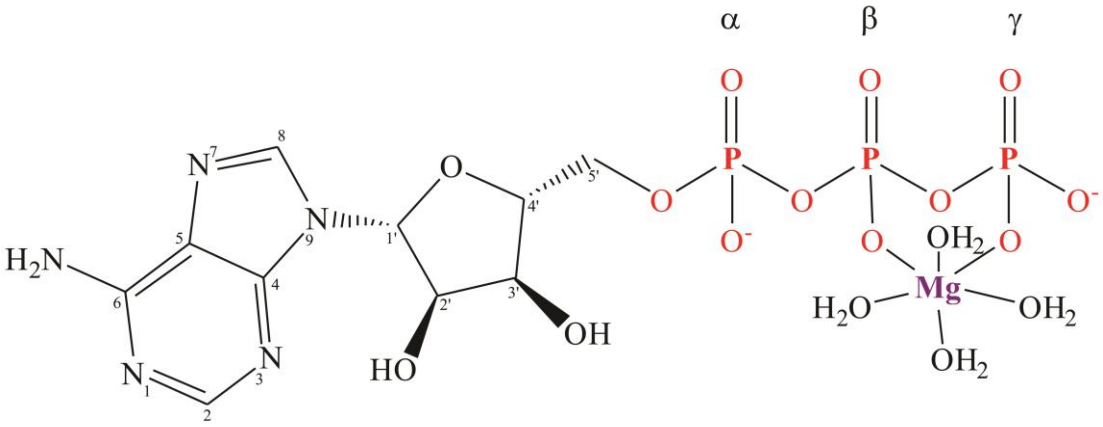

Figure 3-1. Line-angle formula of Adenosine 5'-Triphosphate (ATP) with Mg^{2+} bound at the β and γ phosphate positions.

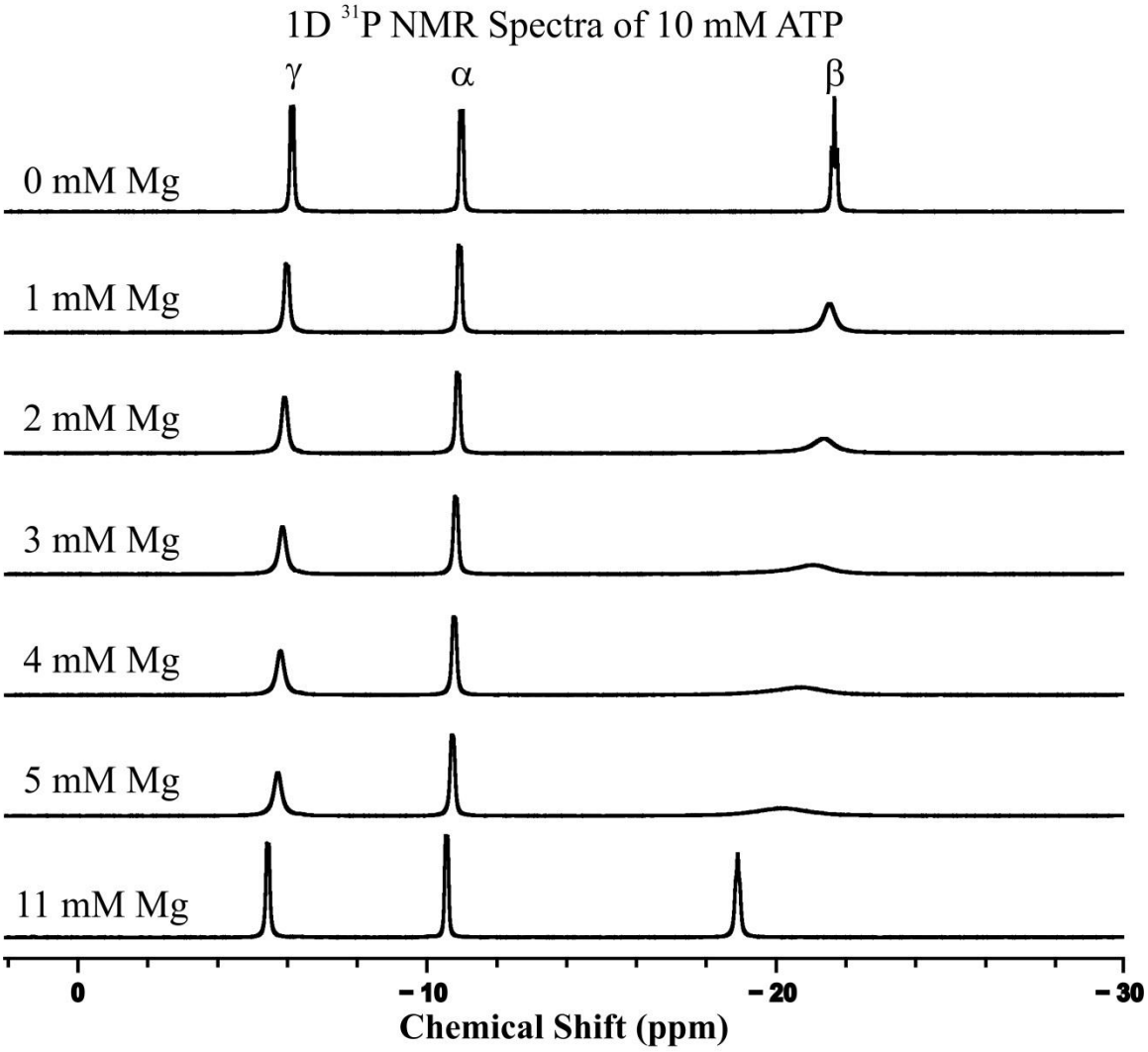

Figure 3-2. 1D ^{31}P of magnesium titrated in to a sample of 10 mM ATP. The α, β, and γ phosphates of ATP are labeled in the top NMR spectrum and shift slightly with the addition of $MgCl_2$. The total $MgCl_2$ concentration is indicated at the left of each spectrum. Data collected on 600 MHz NMR Spectrometer at 310 K.

Additionally, significant line broadening is evident in the intermediate exchange regime, where the free phosphate population is shifting to Mg^{2+}-bound. Saturation of the ATP phosphates by Mg^{2+} is shown by the shifted peak sharpening, or having a more narrow line width, with increasing concentration of Mg^{2+}, representing a shift in the average population of phosphorus to the fully bound state. At 11 mM $MgCl_2$ concentration, the 10 mM ATP was fully saturated as seen in the bottom spectra of Figure 3-2. The influence of Li^+ on a fully saturated Mg^{2+}-binding site, ATP, was initially assessed by ^{31}P 1D NMR under stoichiometric conditions of Li^+ (10 mM added) (Figure 3-3). The top two ^{31}P spectra represent the ATP free (purple) and ATP·Mg bound (green). The addition of 10 mM LiCl (red) does not cause an appreciable change in chemical shift for any of the phosphorus nuclei. This spectrum therefore does not show any evidence that Li^+ competes with Mg^{2+} for binding to ATP, but also does not provide an indication of any Li^+ binding to ATP·Mg. The bottom spectrum (blue) shows a very slight chemical shift in the phosphates of ATP due to Li^+ alone, showing that in this instance the binding of Li^+ to ATP can be detected through chemical shift perturbation.

Using lithium (^7Li) as the nucleus for detection, we measured the binding behavior of lithium by observation of the ^7Li T1 relaxation, a nuclear spin phenomenon that is measurable by NMR through an inversion recovery experiment using a radiofrequency pulse in the context of an external magnetic field. Unlike many methods which detect secondary effects upon lithium addition, NMR spectroscopy is able to directly detect lithium, and is able to distinguish between the free and bound states of lithium. As Li binds to a larger substrate and the population shifts from ‘free’ ion to bound, the relaxation increases and the correlation time decreases (see Chapter 2).

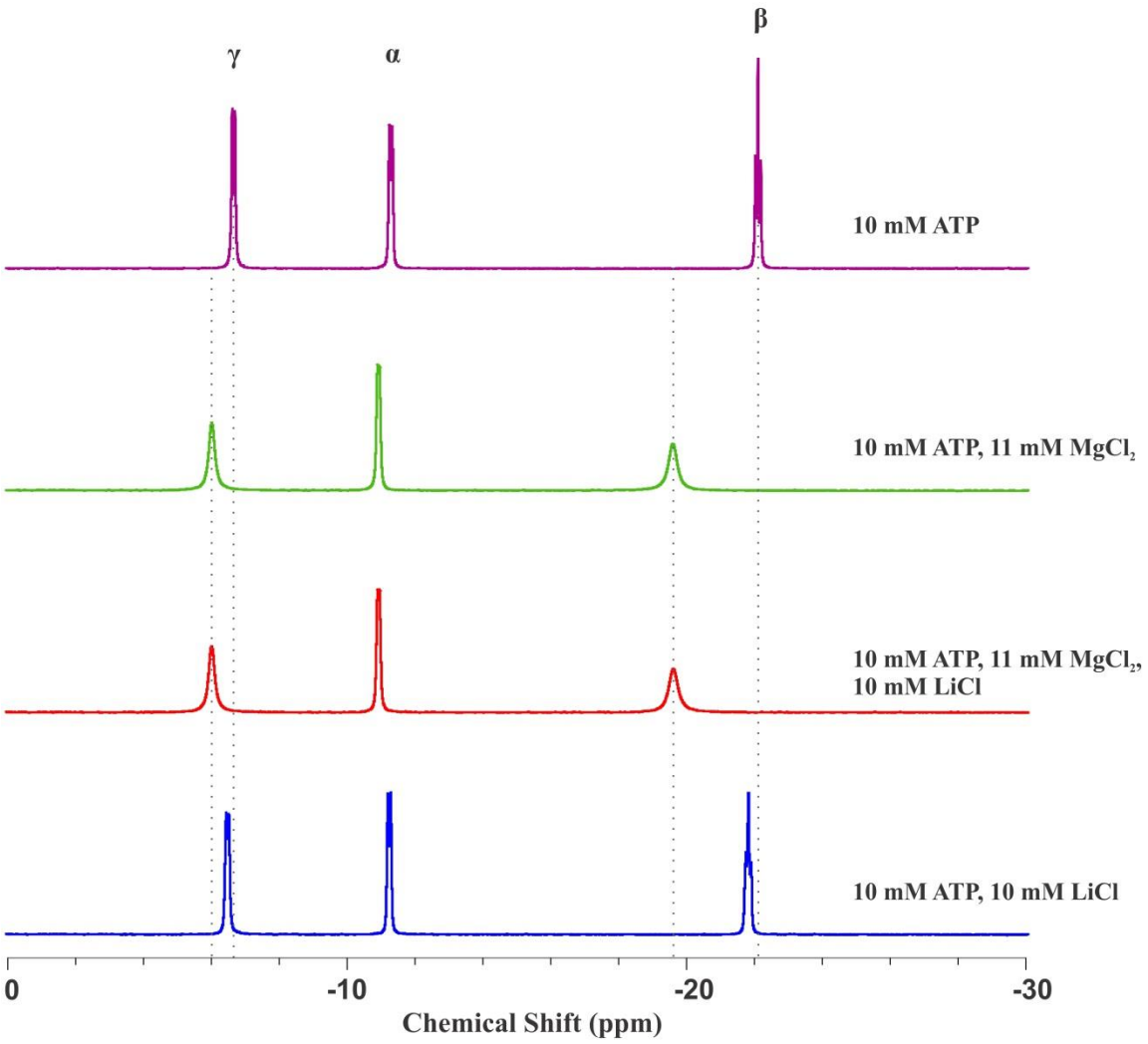

Figure 3-3. 1D ^{31}P Chemical shift perturbation of the phosphates of ATP with the addition of $MgCl_2$ and LiCl. The α, β, and γ phosphates of ATP are labeled in the top NMR spectrum. The sample composition is indicated at the right of each spectrum. Data collected on 600 MHz NMR Spectrometer at 283 K.

Representative ^{7}Li T1 relaxation data (open circles) displays a plot of the peak intensities as a function of relaxation delay (D1) in seconds (Figure 3-4). These points are fit to a single exponential yielding an overall T1 relaxation time constant. The ^{7}Li T1 relaxation for 10 mM LiCl and 11mM $MgCl_2$ in the absence of ATP was determined to be 12.8 s at 283 K (10°C), as a measure of the unbound free Li^+ ion in solution (Table 3-1). The ^{7}Li T1 relaxation of 10 mM LiCl in the presence of 10 mM ATP and 11mM $MgCl_2$ was determined to be 6.7 s, which is about two-fold faster than the T1 of Li^+ free in solution, signifying that Li^+ is binding ATP in a measureable way.

Unlike the ^{31}P chemical shift, which is insensitive to lithium binding, the ^{7}Li T1 relaxation clearly indicates that Li^+ binds to ATP in the presence of Mg^{2+}, but this measurement alone does not provide information about the location and/or possible displacement of the Mg^{2+} upon Li^+ binding. To address these questions, we employed the use of a paramagnetic nucleus, manganese (Mn^{2+}), to detect whether Li^+ is displacing the Mg^{2+} from ATP prior to binding. The electron magnetic dipole moment of Mn^{2+} causes a relaxation enhancement to all nuclei within an approximate distance of 30 Å. The paramagnetic relaxation enhancement (PRE), effectively an increase in nuclear T1 relaxation (i.e. a shorter correlation time) is measurable by NMR inversion recovery (refer to Chapter 2). A ratio of Mn^{2+} to Mg^{2+} of 1: 220 was used and, due to the fast exchange at the Mg^{2+} site (> 1000 s^{-1}), Mn^{2+} rapidly samples all available Mg^{2+} binding sites on ATP in the sample giving insight into the local environment of Mg^{2+}. Fast exchange and sampling of all the ATP substrates between the two divalent ions (Mg^{2+}/Mn^{2+}) of similar ionic radii are observed by the broadening of ^{1}H and ^{31}P 1D spectra of 10 mM ATP, 11 mM $MgCl_2$, 10 mM LiCl in the presence (red) and absence

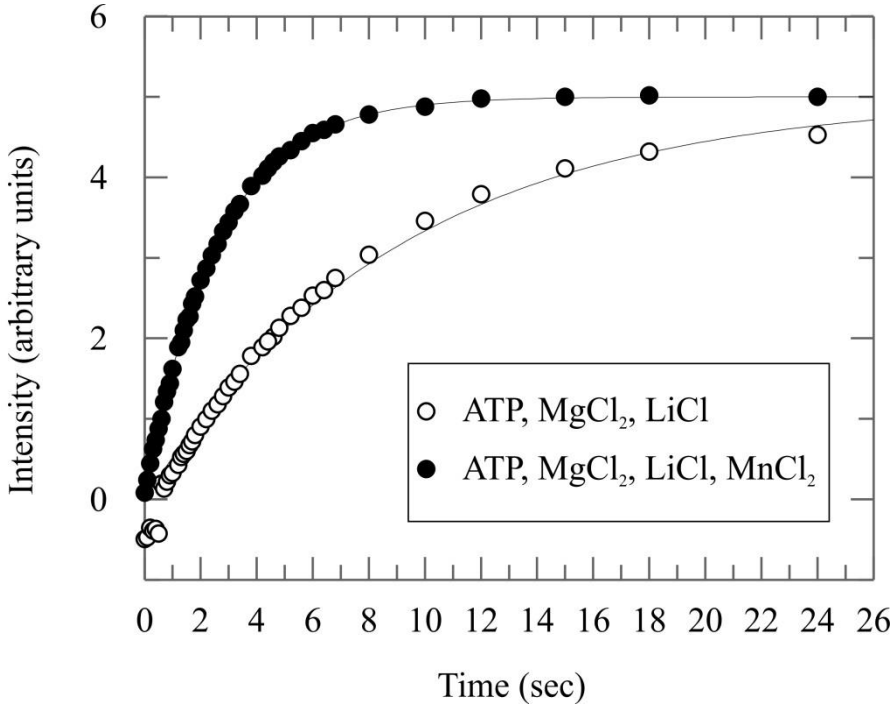

Figure 3-4. Representative ^{7}Li T1 relaxation data in the absence of $MnCl_2$ (open circles) and presence of 50 μM $MnCl_2$ (closed circles). Line fits to a simple exponential are shown.

NMR Experiments on 600 MHz NMR Spectrometer at 283 K

ATP	Mg	Li	^{7}Li T1 (s)	^{7}Li T1 (s) (+ 50 μM Mn)	Relaxation Enhancement (%)
-	+	+	12.80	12.10	5.5
+	+	+	6.70	2.62	60.9
			^{23}Na T1 (ms)	^{23}Na T1 (ms) (+ 50 μM Mn)	Relaxation Enhancement (%)
+	+	+	34.2	34.0	0.6
10 mM	**11 mM**	**10 mM**			

Table 3-1. ^{7}Li T1 relaxation time constants are given for 11 mM $MgCl_2$ and 10 mM LiCl in solution and with the addition of 50 μM $MnCl_2$. ^{7}Li T1 relaxation time constants are given for 10 mM ATP, 11 mM $MgCl_2$, 10 mM LiCl in solution and with the addition of 50 μM $MnCl_2$. ^{23}Na T1 relaxation time constants are given in the presence and absence of 50 μM $MnCl_2$. Relaxation Enhancement (%) was calculated by subtracting the PRE (+ $MnCl_2$) T1 value from the initial T1, dividing the difference by the initial T1, and multiplying by 100. Experiments collected on a 600 MHz NMR spectrometer at 283 K.

(blue) of 50 μM $MnCl_2$ (Figure 3-5). Non-uniform broadening is observed due to the distance dependence of the Mn^{2+} electron magnetic moment. For example, the H8 is broader than the H2 proton due its closer proximity to the Mn^{2+} and also indicates the adenosine and phosphate tail of ATP are in the 'anti' conformation.

PRE on ^7Li T1 was used to probe Li^+ binding to ATP·Mg. There are three theoretical outcomes of adding a stoichiometric amount of Li^+ to ATP·Mg: Li^+ could 1) not bind to ATP·Mg, 2) bind to ATP by displacing the Mg^{2+}, or 3) bind to ATP·Mg without displacing the Mg^{2+} (Figure 3-6). Through direct detection of the Li^+ by NMR, a ^7Li T1 PRE would indicate that the sites being sampled by Mn^{2+} are located in proximity (< 30 Å) to the Li^+. Conversely, a ^7Li T1 PRE would not be observed if Mg^{2+}, or its paramagnetic sampler, is displaced by Li^+. Additionally, no PRE would be observed if Li^+ does not bind to ATP·Mg. Representative ^7Li T1 relaxation data, mentioned earlier, showing the plot of ^7Li peak intensities as a function of relaxation delay clearly shows a PRE of the ^7Li T1 relaxation with the addition of 50 μM $MnCl_2$ (closed circles) to the sample of 10 mM ATP, 11 mM $MgCl_2$, and 10 mM LiCl compared to the sample without Mn^{2+} (open circles) (Figure 3-4). The PRE experiment resulted in a T1 relaxation enhancement from 6.70 seconds to 2.62 seconds (Table 3-1). This finding is direct evidence that under stoichiometric conditions, Li^+ does not displace the Mg^{2+} on ATP, but rather binds within 30 Å to the Mg^{2+} on ATP·Mg.

As a control, the addition of Mn^{2+} to a sample of Li^+ and Mg^{2+} alone in buffer yielded a ^7Li T1 relaxation of 12.1 s, which is very close to the rate of Li^+ and Mg^{2+} in the absence of Mn^{2+}, 12.8 ms. No PRE was observed in this control, lending confidence that the T1 measurements with ATP·Mg are not due to random collisions between free

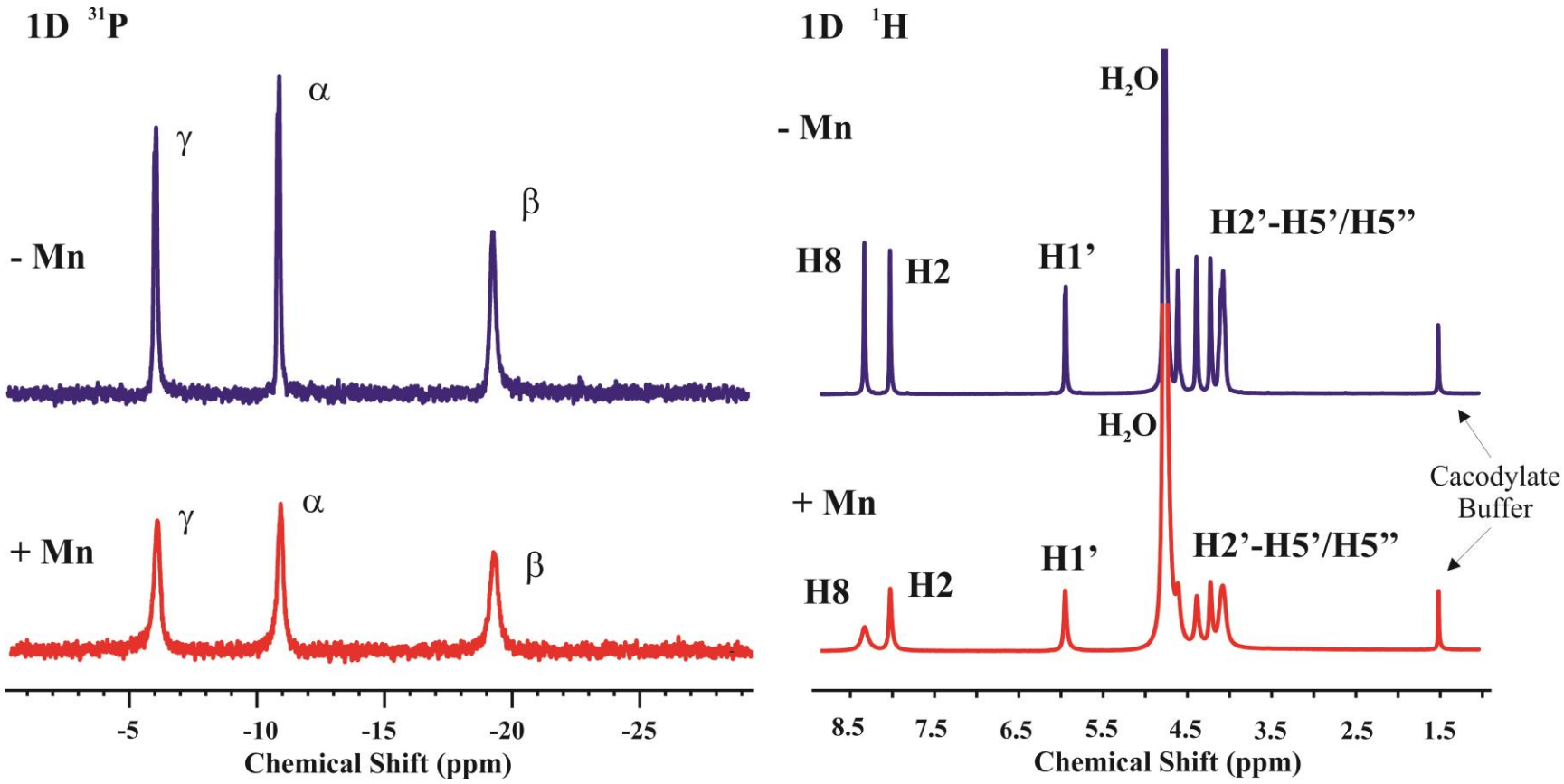

Figure 3-5. ^{31}P NMR Spectra of ATP with (bottom) and without (top) 50 μM $MnCl_2$ (left). ^{1}H NMR Spectra of ATP with (bottom) and without (top) 50 μM $MnCl_2$ (right).

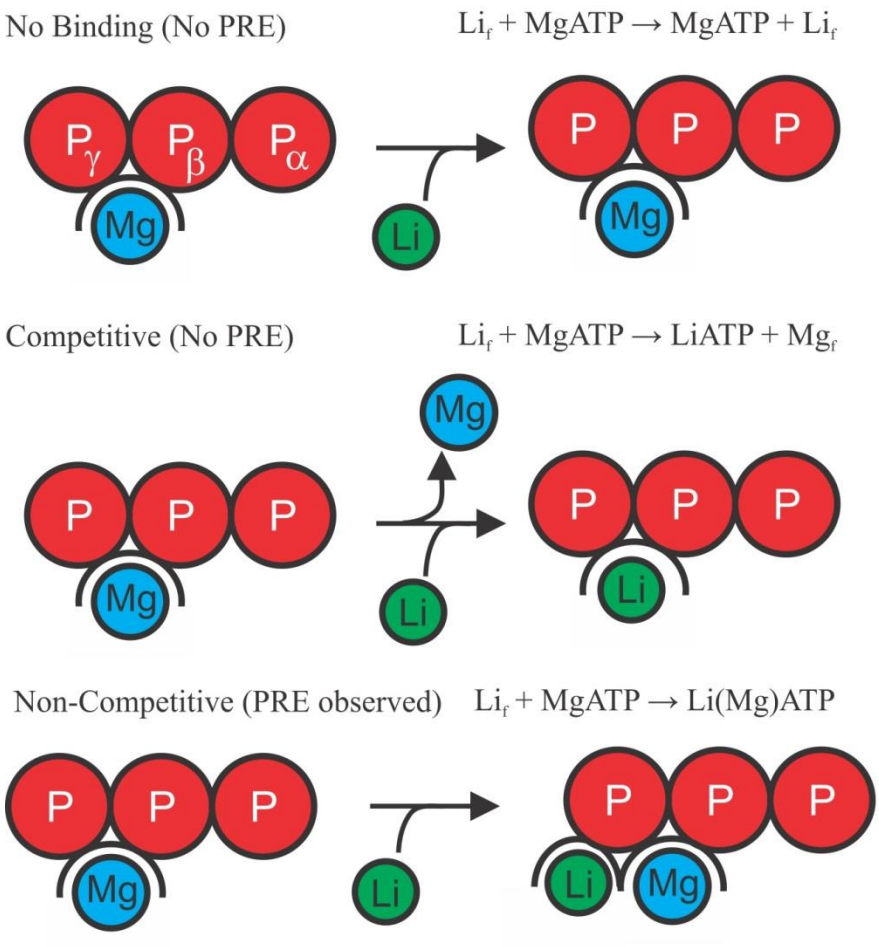

Figure 3-6. Possible binding modes of lithium are illustrated with ATP phosphates (red spheres), Mg^{2+} (blue sphere), and Li^{+} (green sphere).

Mn^{2+} and Li^{+} in solution. Rather, the observation of PRE indicates that Mg^{2+} is present upon Li^{+} binding to ATP. Furthermore, since all samples contain sodium (Na) in the buffer solution, we measured the ^{23}Na T1 relaxation for a sample containing ATP, $MgCl_2$, and LiCl and found it to be 34.2 ms in the absence of Mn^{2+}, and 34.0 ms in the presence of Mn^{2+}. Na^{+} has no significant PRE in the presence of the paramagnetic ion at these concentrations. However, Na^{+} has a larger quadrupole than Li and relaxes an order of magnitude faster. Although this is not a perfect control, the Na^{+} concentration is 5 times higher than the concentration of Li^{+} in the sample and a PRE is still not observed. This may be an indication that Na^{+} does not bind appreciably to ATP·Mg.

The observation of Li^{+} binding to ATP·Mg led to the question of whether other nucleotides exhibited a similar Li^{+} binding behavior. ^{7}Li T1 relaxation PRE experiments were collected with nucleoside di- and tri- phosphates (Table 3-2). Guanosine 5'-triphosphate (GTP), adenosine 5'-diphosphate (ADP) and guanosine 5'-diphosphate (GDP), whose phosphates are known to chelate Mg^{2+} with varying affinities [105, 106], were all observed to interact with lithium in the presence of Mg^{2+} and each exhibited a PRE when the ^{7}Li T1 relaxation was measured in the presence of Mn^{2+}. This again shows that Li^{+} is binding in proximity to Mg^{2+}. ADP and GDP exhibit a relaxation enhancement of 77 percent and 55 percent, respectively, which is in the range of ATP at 61 percent, while GTP appears to have slightly smaller enhancement of 26 percent. One could speculate that the amino group at position 2 of GTP may interact with the triphosphate tail and destabilize Li^{+} binding leading to the observed variation in T1. Similar to the ^{23}Na T1 control experiments for ATP discussed above, a PRE of the ^{23}Na T1 relaxation is not observed with Mn^{2+} addition and serves as an internal control for the

NMR Experiments on 600 MHz NMR Spectrometer at 283 K

ADP	Mg	Li	Mn	^{7}Li T1 (s)	^{23}Na T1 (ms)
+	+	+	-	5.94	31.4
+	+	+	+	1.36	36.4
10 mM	**11 mM**	**10 mM**	**50 μM**		
			Relaxation Enhancement (%):	77.1	-15.9

GTP	Mg	Li	Mn	^{7}Li T1 (s)	^{23}Na T1 (ms)
+	+	+	-	5.98	31.3
+	+	+	+	4.44	37.10
10 mM	**11 mM**	**10 mM**	**50 μM**		
			Relaxation Enhancement (%):	25.8	-18.5

GDP	Mg	Li	Mn	^{7}Li T1 (s)	^{23}Na T1 (ms)
+	+	+	-	9.47	36.9
+	+	+	+	4.23	36.6
10 mM	**11 mM**	**10 mM**	**50 μM**		
			Relaxation Enhancement (%):	55.3	0.8

Table 3-2. ^{7}Li T1 relaxation and PRE compared to control of ^{23}Na T1 relaxation and no PRE observed for ADP, GTP, and GDP. Relaxation Enhancement (%) was calculated by subtracting the PRE (+ $MnCl_2$) T1 value from the initial T1, dividing the difference by the initial T1, and multiplying by 100. Experiments were collected on a 600 MHz spectrometer at 283 K.

ADP, GTP, and GDP measurements. In fact, a negative percentage for relaxation enhancement was observed for ADP and GTP, indicating that the T1 relaxation slowed with the addition of Mn^{2+}, although it is not clear why this would occur. The ^{7}Li T1 relaxation data provides clear evidence that Li^{+} binds to ATP·Mg, ADP·Mg, GDP·Mg, and GTP·Mg under stoichiometric binding conditions.

The next consideration is whether the nucleoside base and ribose sugar are necessary for Li^{+} binding close to the Mg^{2+} site. ^{7}Li T1 experiments were applied to test Li^{+} binding to triphosphate·Mg. The ^{7}Li T1 of a sample of 10 mM triphosphate, 11 mM $MgCl_2$, and 10 mM LiCl measured 1.39 seconds. This T1, which is faster than the free Li^{+} ion, indicates that Li^{+} is bound to the triphosphate. Apparently, Li^{+} binding does not require the nucleoside base and ribose sugar moiety nor does it displace the Mg^{2+} ion, as observed through ^{31}P chemical shifts (data not shown).

This finding led to the question of whether other molecules with phosphates would bind to Li^{+} in a similar way. 2,3-diphosphoglycerate (DPG), also known as 2,3-bisphosphosglycerate, a small molecule found in erythrocytes, is known to chelate Mg^{2+} (Figure 3-7) [107-109]. Initial ^{7}Li T1 PRE measurements were collected on a 500 MHz NMR (Table 3-3) and later repeated on a 600 MHz NMR (Table 3-4). At both the lower and higher magnetic field strengths, the results were expected to show the same trends. Indeed, a ^{7}Li PRE is observed in the presence of Mn^{2+} at both the higher and lower field strengths, and relaxation enhancements were approximately 60 percent. Again, ^{23}Na T1 control experiments did not show a PRE, indicating, to some degree, that Na^{+} does not bind appreciably with Mg^{2+} to DPG in the presence of Li^{+}. This data points towards Li^{+}

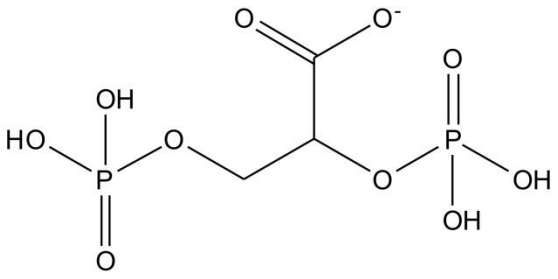

2,3-Diphosphoglycerate (DPG)

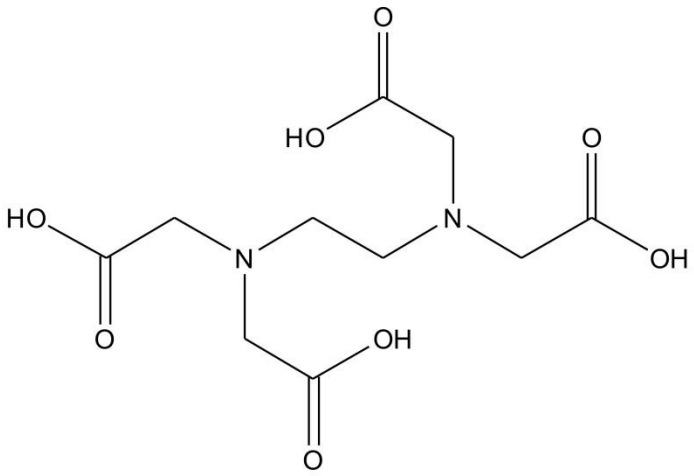

Ethylenediaminetetraacetic acid (EDTA)

Figure 3-7. Line-angle formula of 2,3-diphosphoglycerate (DPG) (top) and ethylenediaminetetraacetic acid (EDTA) (bottom).

^{7}Li T1 Relaxation Experiments on 500 MHz NMR at 283 K

DPG	Mg	Li	Mn	^{7}Li T1 Relaxation (s)
+	+	+	-	7.65
+	+	+	+	2.92
10 mM	**11 mM**	**10 mM**	**50 μM**	
		Relaxation Enhancement (%)		61.8

^{23}Na T1 Relaxation Experiments on 500 MHz NMR at 283 K

DPG	Mg	Li	Mn	^{23}Na T1 Relaxation (ms)
+	-	-	-	16.02
+	-	+	-	17.17
+	+	-	-	27.10
+	+	+	-	27.24
+	+	+	+	27.39
10 mM	**11 mM**	**10 mM**	**50 μM**	
		Relaxation Enhancement (%)		-0.6

Table 3-3. ^{7}Li T1 relaxation experiments showing lithium binding to 2, 3-diphosphoglycerate (DPG) and the ^{23}Na T1 relaxation controls showing sodium. Relaxation Enhancement (%) was calculated by subtracting the PRE (+ $MnCl_2$) T1 value from the initial T1, dividing the difference by the initial T1, and multiplying by 100. Experiments collected on a 500 MHz NMR spectrometer.

DPG Experiments at Different Temperatures - 600 MHz NMR

				^{7}Li T1 Relaxation (s)		
DPG	**Mg**	**Li**	**Mn**	**283K**	**298K**	**310K**
+	+	+	-	6.86	8.27	10.18
+	+	+	+	2.79	3.40	3.84
10 mM	**11 mM**	**10 mM**	**50 µM**			
			Relaxation Enhancement (%)	59.4	58.9	62.3

Table 3-4. ^{7}Li T1 relaxation data of lithium binding to DPG in the presence of magnesium at 283 K, 298 K, and 310 K. Relaxation Enhancement (%) was calculated by subtracting the PRE (+ $MnCl_2$) T1 value from the initial T1, dividing the difference by the initial T1, and multiplying by 100. Experiments collected on a 600 MHz NMR spectrometer.

binding at phosphate·Mg sites as this is a common feature between the nucleotides, triphosphates, and DPG.

Ethylenediaminetetraacetic Acid (EDTA) is known to chelate magnesium with its coordinating carboxyl groups (Figure 3-7) [110]. To determine if Li^+ specifically requires phosphates for its binding to Mg^{2+} sites, ^{7}Li T1 relaxation PRE experiments were measured on EDTA·Mg (Table 3-5). The ^{7}Li T1 is 22.58 seconds in the absence of Mn^{2+}, and 10.41 seconds in the presence of Mn^{2+}, indicating a PRE. The relaxation enhancement of 53.9 percent indicates that it is possible for Li^+ to bind to Mg-chelation sites comprised of coordination ligands other than phosphates. This suggests that, in addition to nucleotides and other phosphate-containing small molecules, there may be a role for Li^+ to act together with Mg^{2+} at Mg-sites on proteins, although that remains to be tested.

Returning to the nucleotide model for Mg^{2+} binding, and having established that Li^+ binds to ATP·Mg without displacing the Mg^{2+}, NMR was used to quantify the Li^+ affinity for ATP·Mg by direct detection of ^{7}Li. The ^{7}Li T1 relaxation was observed at 2 mM LiCl as a function of increasing ATP·Mg concentration. Non-linear least squares fitting to a quadratic function for the observed ^{7}Li T1 relaxation at different concentrations of ATP·Mg gave information about the binding affinity of Li^+ (see Chapter 2) (Figure 3-8). The plot shows the initial T1 relaxation of Li^+ in the absence of ATP·Mg (0 mM). As aliquots of ATP·Mg were titrated into a LiCl sample, faster relaxation was detected and over the course of the titration the T1 time constants capture the transition from free Li^+ (0 mM ATP·Mg) to fully bound ATP·Mg·Li. The change in

EDTA Experiments at 600 MHz

EDTA	Mg	Li	Mn	^{7}*Li T1 Relaxation (s)* **310 K**
+	+	+	-	22.58
+	+	+	+	10.41
10 mM	**11 mM**	**10 mM**	**50 µM**	
			Relaxation Enhancement (%)	53.9

Table 3-5. ^{7}Li T1 relaxation data of Li^{+} binding to EDTA in the presence of Mg. Relaxation Enhancement (%) was calculated by subtracting the PRE (+ $MnCl_2$) T1 value from the initial T1, dividing the difference by the initial T1, and multiplying by 100. Experiments were collected on a 600 MHz NMR spectrometer at 310 K.

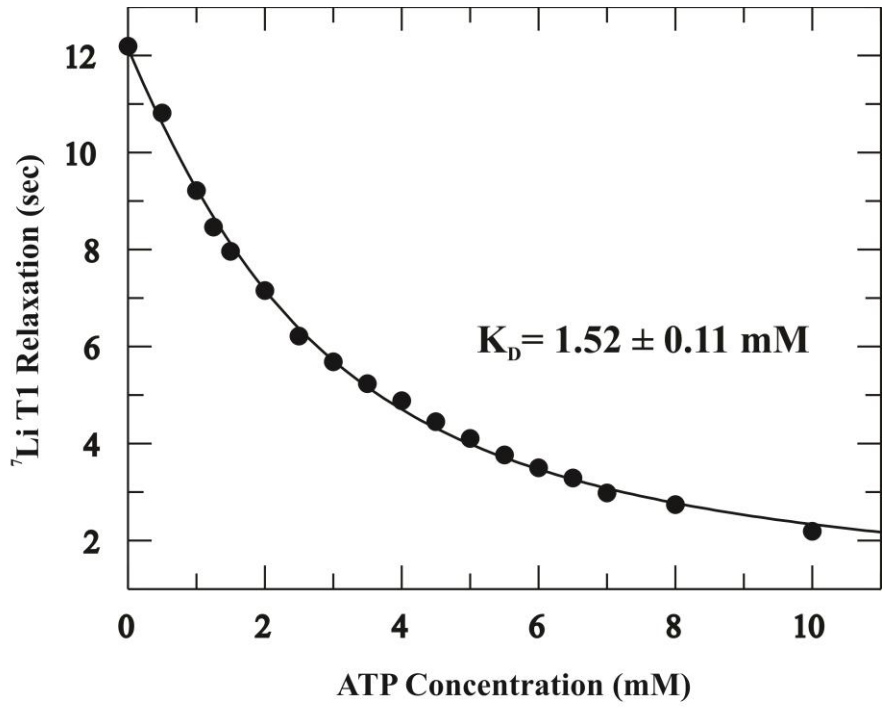

Figure 3-8. A plot of ^{7}Li T1 relaxation (black circles) at 283 K measured using 18 samples as a function of increasing concentrations of ATP and $MgCl_2$ and a constant concentration of 2 mM LiCl. Data was fit using equation 7 (Chapter 2) to yield a K_D of 1.52 mM. Data collected on 600 MHz NMR Spectrometer.

relaxation is directly correlated to the proportion of Li^+ bound to the ATP·Mg substrate at a given data point. The equilibrium dissociation constant (K_D) of Li^+ for ATP·Mg, which was measured in triplicate at 283 K, was found to be 1.52 with a standard deviation of ± 0.11 mM. Due to the nature of the long T1 experiments and the large number of samples, the ATP in each sample was checked by 1D ^{31}P NMR for degradation (Figure 3-9). Of the 17 samples, only 1, the sample with the lowest concentration of ATP·Mg (bottom spectra) showed any hydrolysis of ATP at the completion of the ^7Li T1 experiments. Overall, the integrity of ATP was confirmed in the samples, as ADP phosphate peaks would have otherwise appeared between the α and γ phosphate peaks of ATP.

The weak, but appreciable, binding of Li^+ to ATP·Mg raised the question as to the minimally required molecules for the lithium binding event to occur. The PRE data verified that Li^+ binds to Mg^{2+} sites on other nucleotides and small molecules. Variation in Li^+ affinity measurements may give clues as to a preferred Li^+ binding environment. Similar to the ATP·Mg titration, ADP·Mg, GTP·Mg, and GDP·Mg were titrated into 2 mM LiCl in separate experiments (Table 3-6). All the molecular entities tested exhibit Li^+ binding with equilibrium dissociation constants in the low millimolar range. The K_D of Li^+ to ADP·Mg is 3.24 mM with an uncertainty of ± 0.56 mM, for GTP·Mg is 4.81 mM with an uncertainty of ± 0.55 mM, and for GDP·Mg is 6.76 mM with an uncertainty of ± 1.21 mM. The results show that Li binds with relatively similar affinity, i.e., within ~1.5-2-fold, regardless of whether there are two or three phosphates on the nucleotide, or which purine base, adenine or guanine, is present. The Li^+ affinity to the triphosphate·Mg was also determined in a similar manner. At 283 K, the Li affinity to triphosphate·Mg was 0.71 mM with an uncertainty of ± 0.23 mM and at 310 K, it was

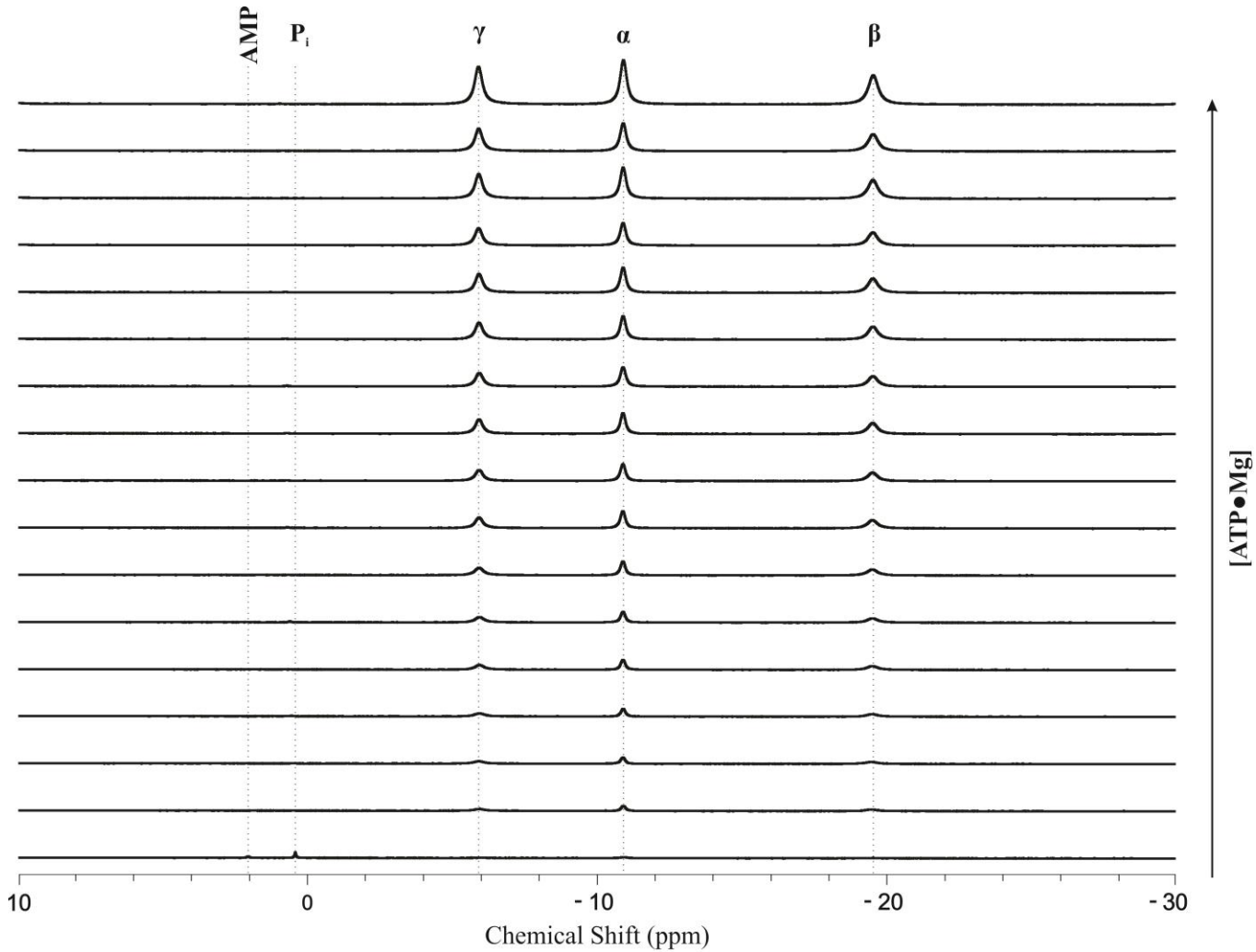

Figure 3-9. 1D ^{31}P of ATP in 17 NMR samples used to measure Li^+ binding affinity. The α, β, and γ phosphates of ATP are labeled in the top spectrum. The ATP·Mg concentration increases from the bottom to top spectrum. Collected on 600 MHz NMR at 283 K.

0.31 mM with an uncertainty of ± 0.16 mM. The K_D of Li^+ to triphosphate·Mg may be lower than that of Li^+ to nucleotide·Mg because the triphosphate is unrestrained by the nucleoside and has one extra negative charge on a terminal phosphate, which may increase the propensity for Mg^{2+} binding while still only binding to one Mg^{2+} ion at a time. The Li^+ may have a higher rate of association with triphosphate·Mg as a reflection of higher on rates of Mg^{2+} to triphosphate. This may be the reason for a lower dissociation constant. Taken together, this data indicates that, minimally, Li^+ associates with molecular entities other than ATP and suggests that the minimal requirement for binding is phosphate·Mg. However, the equilibrium dissociation constant of Li^+ to EDTA·Mg is 6.01 mM with an uncertainty of ± 2.72 mM, which is also in a similar binding range to the nucleotides and adds another possibility of Li binding at carboxylate·Mg^{2+} chelation sites (Table 3-6). The Li affinities measured for the nucleotides are physiologically relevant findings because they are on the order of magnitude with the serum concentration safely allowed for patients with BD (0.6-1.2 mM).

The PRE and binding affinity evidence for Li^+ binding to EDTA·Mg indicates that carboxylate·Mg·Li may be an alternate way for Li^+ to interact and other combinations may exist. However, the full range of biologically relevant Mg chelation sites that can form a Li^+ complex to explain the mechanism of Li^+ action was beyond the scope of this dissertation. The ATP·Mg·Li molecular entity was chosen as the focus for this dissertation as a possible mode for Li^+'s interaction in a biological context, and the PRE and binding affinity evidence led to the hypothesis that the pharmacological mechanism of action of Li^+ may involve modulation of normal ATP interactions, such as

Molecule	Temperature (K)	Lithium K_D (mM)
ADP·Mg	283	3.24 ± 0.56
GTP·Mg	283	4.81 ± 0.55
GDP·Mg	283	6.76 ± 1.21
DPG·Mg	283	0.89 ± 0.13
	310	0.71 ± 0.11
EDTA·Mg	310	6.01 ± 2.72

Table 3-6. Lithium equilibrium dissociation constants for ADP•Mg, GTP•Mg, GDP•Mg, DPG•Mg, and EDTA•Mg. The dissociation constant (K_D) was calculated from ^{7}Li T1 relaxation NMR measurements. Experiments were collected on two different 600 MHz NMR spectrometers.

those that occur in ATP-dependent enzymes and ATP-activated receptors. One example of ATP activated receptors are purinergic, or P2, receptors (see Chapter 5). There are two classes of ATP-activated P2 receptors, P2X and P2Y, which are responsible for calcium (Ca^{2+}) regulation, among other functions, and can be found in the cell membrane of many neurons, among other cells. P2X receptors are ion channels that regulate calcium uptake by the cell and P2Y receptors are G-protein coupled receptors that regulate intracellular Ca^{2+} concentrations through signaling cascades (see Chapter 5).

Fluorescence microscopy experiments were employed by our collaborator, Dr. Joseph Kao at the University of Maryland School of Medicine, to measure the neuronal response upon stimulation with ATP·Mg·Li. Nodose ganglion neurons, which express P2 receptors [85], were prepared by enzymatic dissociation of ganglia dissected from rats. The concentration of Ca^{2+} increase from basal level was measured upon activation of the P2 receptors a function of time using a Ca^{2+} binding fluorescent dye, Fluo-3, on a Laser Scanning Confocal Microscope. Initially, control experiments measured the variability of P2 response to repeated ATP stimuli within a single neuron (Figure 3-10). The paired t-test between the first and third application of ATP indicated that repeated responses in the same cell are not significantly different. After establishing that, the neuronal response to ATP·Mg was measured and compared to the response of ATP with no metals, and then to ATP·Li with no Mg^{2+} (Figure 3-11). The P2 receptors appear to be stimulated to a similar extent indicated by similar peak intensities, but the addition of ATP·Li into the extracellular buffer increases the length of time that P2X remains open compared to both ATP alone and ATP·Mg, by 39 percent. The addition of Li^{+} to ATP in the absence of Mg causes a cellular response that is significant. In another experiment, stimulation of P2

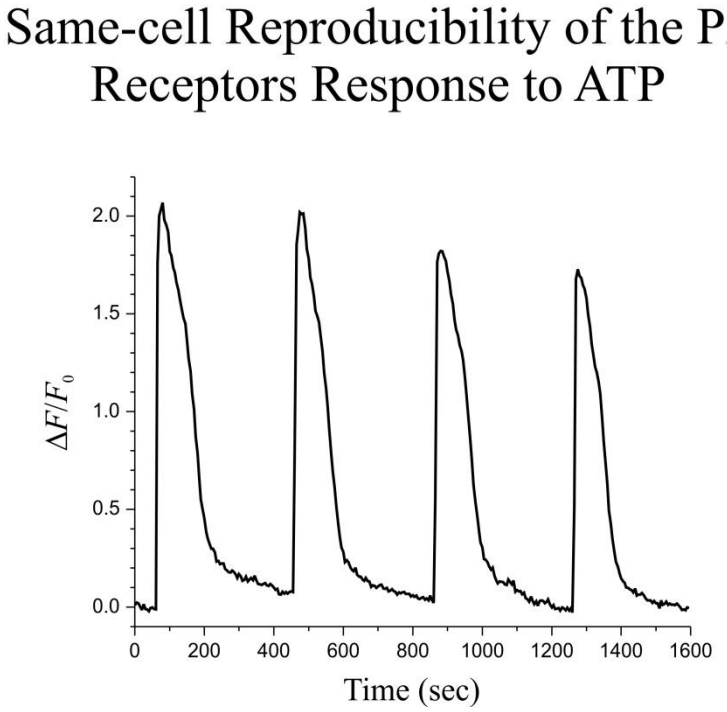

Figure 3-10. Fluorescence response after 4 separate 20-second applications of 100 μM ATP. Fluorescent calcium indicator is Fluo-3. Experiments were collected on a laser scanning confocal microscope. The paired t-test indicates that repeated responses in the same cell are not significantly different (compare 1st and 2nd response: n=9; $\langle t_{100\text{-}20} \rangle$ = 114, 112 sec, σ = 121, 121 sec; p= 0.83). Data was provided by Dr. Joseph Kao, University of Maryland School of Medicine.

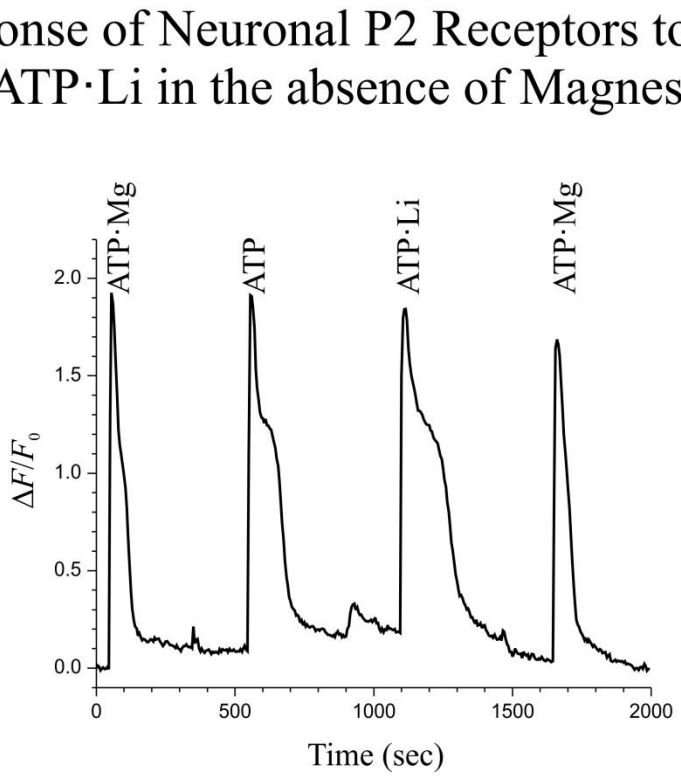

Figure 3-11. Fluorescence response after 4 separate 20-second applications of 100 μM ATP·Mg (first and fourth application), 100 μM ATP (second application), or 100 μM ATP·Li (third application). Fluorescent calcium indicator is Fluo-3. Experiments were collected on a laser scanning confocal microscope. The paired t-test indicates that $ATP{\cdot}Li^{+}$ without Mg^{2+} significantly lengthens the ATP response by 39% (compare 2nd and 3rd response (ATP vs. ATP·Li, $[Mg^{2+}]_0$= 0 mM) n=12; $\langle t_{100\text{-}20} \rangle$ = 139, 193 sec, σ = 102, 138 sec; p = 0.015). Data was provided by Dr. Joseph Kao, University of Maryland School of Medicine.

receptors by ATP·Mg was compared to ATP·Mg·Li (Figure 3-12). Again, the relative fluorescence intensities were approximately the same for both ATP·Mg and ATP·Mg·Li stimulation. However, the activation of the P2 receptor by the ternary complex of ATP·Mg·Li increases the length of time for Ca levels to return to baseline significantly more than ATP·Mg (2.2-fold) indicating a change in the deactivation of the P2 receptor due to Li^+ or slower Ca^{2+} reabsorption by internal Ca^{2+} stores. This suggests that the addition of Li^+ to ATP·Mg modulates the P2 receptors in some way to elicit a slower return to basal Ca^{2+} concentrations. As mentioned, there are two types of P2 receptors; P2Y, a GPCR, facilitates Ca^{2+} release from intracellular stores, whereas P2X, an ion channel, allows extracellular Ca^{2+} to flow into the cell. To distinguish whether the slower Ca^{2+} reuptake observed in the presence of ATP·Mg·Li ternary complex is due to P2X or P2Y, extracellular Ca^{2+} was removed from the buffer in the experimental conditions (Figure 3-13). This was to solely test the P2Y response to stimuli. The neuron was stimulated with ATP·Mg followed by ATP·Mg·Li. The result was that the Ca concentrations were the approximately the same upon stimulation with ATP·Mg versus ATP·Mg·Li, shown by the same fluorescence intensities between applications, which was consistent with the previous microscopy experiments. However, in the absence of extracellular Ca^{2+}, stimulation with ATP·Mg·Li did not cause a slower P2 receptor deactivation over stimulation with ATP·Mg. This result indicates that the P2Y component of the cellular response to ATP does not significantly change in the presence of Li^+. Thus, the slower deactivation or Ca^{2+} reuptake that the ATP·Mg·Li complex causes is likely through interaction with P2X receptors. The stimulation by this ternary complex presumably corresponds to a longer opening of the ion channel. This finding,

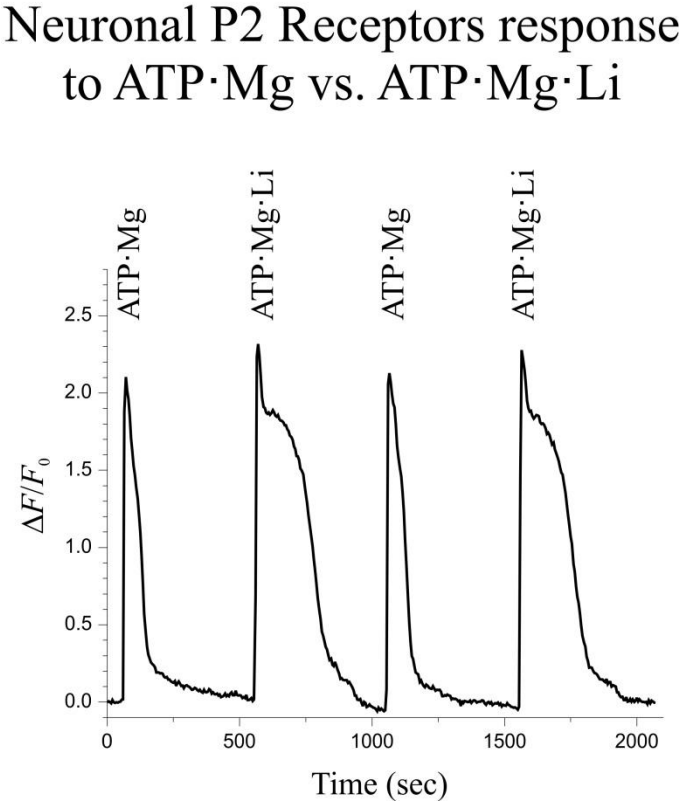

Figure 3-12. Fluorescence response after 4 separate 20-second applications of either 100 μM ATP·Mg (first and third application) or 100 μM ATP·Mg·Li (second and fourth application). Extracellular calcium was in the buffer at a concentration of 2.5 mM. Fluorescent calcium indicator is Fluo-3. Experiments were collected on a laser scanning confocal microscope. The paired t-test indicates that ATP·Mg·Li evokes a significantly longer response than ATP·Mg by 2.2-fold (compare 1st and 2nd response (ATP·Mg vs. ATP·Mg·Li): n = 20; $\langle t_{100\text{-}20} \rangle$ = 86, 191 sec, σ = 63, 113 sec; $p = 2.4 \times 10^{-5}$)(compare 1st and 3rd response (ATP·Mg vs. 2nd ATP·Mg; internal control): n = 20; $\langle t_{100\text{-}20} \rangle$ = 86, 88 sec, σ = 63, 54 sec; $p = 0.78$). Data was provided by Dr. Joseph Kao, University of Maryland School of Medicine.

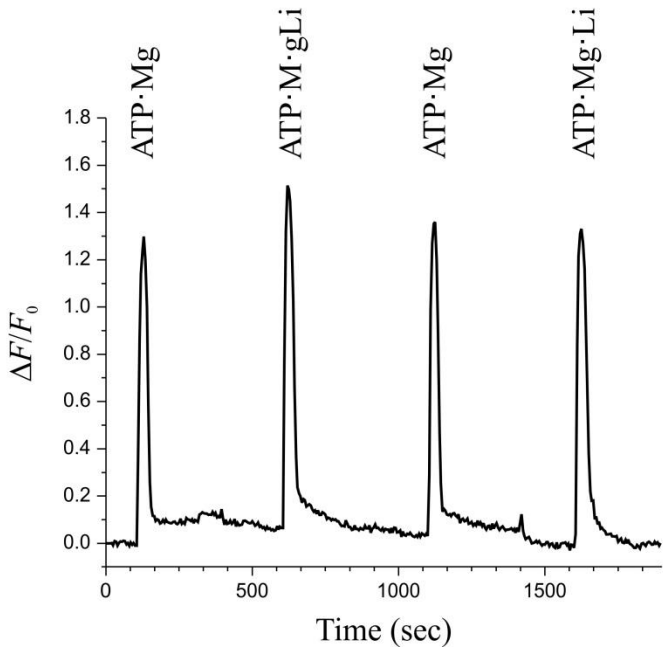

Figure 3-13. Fluorescence response after 4 separate 100-second applications of either 100 μM ATP·Mg (first and third application) or 100 μM ATP·Mg·Li (second and fourth application). No calcium was in the extracellular buffer. Fluorescent calcium indicator is Fluo-3 and represents intracellular calcium. Experiments were collected on a laser scanning confocal microscope. The P2Y component of ATP response does not depend significantly on Li^+ (compare the 1st and 2nd response (ATP·Mg vs. ATP·Mg·Li): n = 28; $\langle t_{100\text{-}20} \rangle$ = 41, 50 sec, σ = 33, 45 sec; p = 0.17338) (compare 1st and 3rd response (ATP·Mg vs. 2nd ATP·Mg; internal control): n = 28; $\langle t_{100\text{-}20} \rangle$ = 41, 38 sec, σ = 33, 35 sec; p = 0.73). Data provided by Dr. Joseph Kao, University of Maryland School of Medicine.

though preliminary, illustrates the need to explore the biological targets of Li^+ in light of a fundamental biophysical model, which this Chapter seeks to provide. The data presented herein supports an alternative and more plausible mechanism of action where Li^+ and Mg^{2+} coordinate and bind together (Figure 3-14). This paradigm-shifting hypothesis that Li^+ acts in a complex with magnesium at magnesium-binding sites allows one to reconsider the wealth of biological data that has been collected over the last several decades in a new light. For example, one can reconsider the many Mg-phosphates, such as on ATP cofactors, or even Mg-carboxylates involved in biological processes, which are the subject of much of the previously explored literature in Li^+ research, and re-interpret the data through this model to gain new insights. Many of the enzymes known to be inhibited by Li^+ at physiologically relevant concentrations, such as glycogen synthase kinase 3β (GSK3β) and inositol monophosphatase (IMPase), require both ATP and Mg^{2+} binding (often two or three metal binding) for critical for enzyme activity and could be sites where, instead of Mg^{2+} displacement, a ternary complex of ATP·Mg·Li acts (see Chapter 6).

In putting forth a new basic molecular hypothesis of Li^+'s action in biology, a foundation has been laid for guiding new directions in Li^+ research, which could uncover new potential drug targets, assist in better drug design, and possibly finally get to a fundamental understanding of the underlying causes of BD. The preliminary neuronal evidence leads to one such new target of Li^+ action, e.g., cellular membrane surface receptors, such as P2X receptors, which are involved in cellular stress and activated during inflammation. Ultimately, a clear understanding of the physicochemical

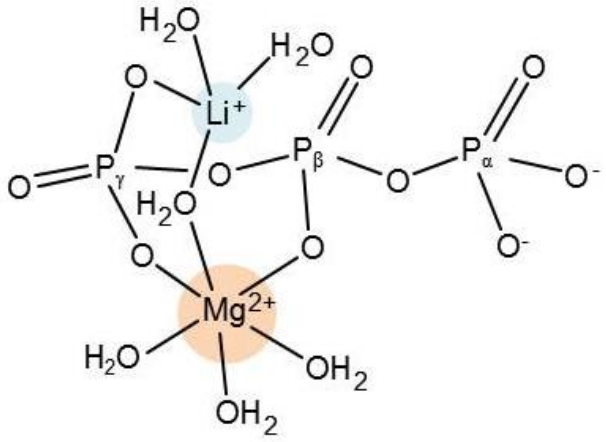

Figure 3-14. Possible model for the ternary complex of triphosphate, magnesium (peach) and lithium (blue). Mg^{2+} is hexacoordinated and shown to coordinate to the β and γ phosphates via dehydration of two water molecules. Li^{+}, which is tetracoordinated, is modeled to bind via a single dehydration to the γ phosphate and a shared water bridge with Mg^{2+}.

mechanism of lithium action is the best starting point for biological and, eventually, clinical studies.

Materials and Methods

NMR Sample Preparation

NMR samples were prepared in 5 mm NMR tubes (Wilmad Labglass) with a H_2O/ D_2O (90%/10%) mixture to a final volume of 500 µL (Deuterium Oxide from Cambridge Isotope Laboratories, Inc.). Dry stocks of ATP, adenosine diphosphate, guanosine triphosphate, and guanosine diphosphate as sodium salts (Sigma-Aldrich) were dissolved in water, adjusted to pH 8.0 with NaOH and stored at -20°C in 100 mM aliquots until ready for use. A standard pH Meter and probe were used from Beckman ϕpH Meter; Orion pH Electrode from Thermo Scientific. Samples were prepared in NMR Buffer (25 mM sodium chloride and 1 mM sodium cacodylate, pH 6.5) from a 10x stock. Sodium chloride, sodium cacodylate, lithium chloride solution (8M), magnesium chloride 6-hydrate, manganese chloride (II) tetrahydrate were purchased from Sigma-Aldrich. Unless otherwise stated, NMR samples contained 10 mM ATP (50 µL of 100 mM stock), 11 mM $MgCl_2$ (5.5 µL of 1M $MgCl_2$ stock), 10 mM LiCl (5 µL of 1M LiCl stock), with or without 50 µM $MnCl_2$ (2.5 µL from 10 mM $MnCl_2$ stock), 50 µL D_2O, and the remaining volume up to 500 µL was NMR Buffer.

NMR Data Collection

Data were collected on either a Bruker 600 MHz AVANCE spectrometer with a Broadband Observe (BBFO) probe located at the IBBR or a Bruker 600 MHz AVANCE

spectrometer equipped with a Broadband Inverse probe located at the NIST. Datasets were collected at 283K (9.85°C), 298K (24.85°C), 300K (26.85°C), 303K (29.85°C), or 310K (36.85°C) and data are presented in the text with specific temperatures of acquisition.

^{7}Li T1 Relaxation Measurements

One dimensional ^{7}Li NMR inversion recovery experiments to measure T1 relaxation used the following experimental acquisition parameters unless otherwise noted in the text: pre-delay (D1) of roughly 5 times the ^{7}Li T1, which was measured at each temperature and typically exceeded 100 sec. The total digitization (TD) was 4096 points, sweep width 699.63, dummy scans (DS) = 4, number of scans (NS) = 8, with a spectrometer frequency of 233.233 MHz for lithium at 14.4 Tesla (600 MHz proton frequency spectrometer). The variable delay list was kept constant for comparable sets of experiments but may otherwise be different depending on the expected relaxation rate (i.e. experiments at different temperatures). Spectra collected at different delay times were processed with the same zero filling to 2X the number of data points and apodized with experimental multiplication using 2.0 Hz line broadening and phase corrected based on the zero time delay of the variable delay. The lithium signal was peak picked, the peak height and integrated volume of the signal was then measured and plotted for each experiment at the different variable delays to allowing a fitting to a T1 relaxation rate using Topspin 1.3 with the following commands: ‘xf2’, ‘t1guide’, ‘extract slice’ from Fid number 32, ‘define ranges’ to obtain integral, export region to relaxation module, ‘relaxation window’ to plot data, fit the data.

Lithium Titration Binding Measurements by NMR

Li binding affinity to ATP was determined by a series of ^{7}Li inversion recovery experiments measuring the ^{7}Li T1 relaxation with increasing concentrations of ATP•Mg (Mn). The Bruker automation software, IconNMR, was used with the Bruker automation hardware, NMR Case, for acquisition of the multiple samples required in these experiments. The T1 relaxation was determined using the Topspin 'T1Guide' program, described above, and then plotted and fit using a non-linear equation in GraFit 5.

^{31}P-NMR Measurements

The ^{31}P 1D experiments used a zero go pulse program with the Broadband probe tuned to 242.93 MHz for phosphorus at 14.4 Tesla (600 MHz proton frequency spectrometer), number of scans (NS) = 1024, dummy scans (DS) = 4, and total digitization (TD) = 8192. Spectra were process with zero filling to 2X the number of data points and apodized with a cosine function over 512 points.

$[Ca^{2+}]_i$ Measurements on Rat Neurons

Male Sprague-Dawley rats, weighing 150-250 kg, were purchased from Harland Laboratories (Frederick, MD) and killed by CO_2 asphyxiation, as approved by the Institutional Animal Care and Use Committee of the University of Maryland Biotechnology Institute. Dissociation of nodose ganglion neurons (NGNs) was performed as described previously [111] with the exception that sterile technique was used and the final neuronal pellet was resuspended in Leibovitz L-15 medium (Gibco-

BRL, Grand Island, NY) containing 10% fetal bovine serum (FBS; JRH Bioscience, Lenexa, KS). The resulting cell suspension was plated as 0.2 mL aliquots onto 25-mm glass coverslips (Fisher Scientific, Newark, DE) coated with poly-D-lysine (0.1 mg/mL; Sigma, St. Louis, MO). NGNs were incubated at 37°C for 24 h, maintained at room temperature to prevent neurite outgrowth, and used for experiments for 72 h. NGNs were loaded with fluo-3 by incubation with the acetoxymethyl (AM) ester of fluo-3, as previously described [85]. During imaging experiments, the neurons were superfused with Locke solution containing the following (in mM): 120 NaCl, 3.0 KCl, 1.5 $MgCl_2$, 1.0 NaH_2PO_4, 25 $NaHCO_3$, 2.5 $CaCl_2$, and 10.0 dextrose; the solution was equilibrated with 95% O_2-5% CO_2 to reach a final pH of 7.4. Where nominally Ca^{2+}-free solution was required, $CaCl_2$ was replaced with an equivalent amount of $MgCl_2$. P2 receptor activation was induced by exposure to 100 μM ATP, 100 μM $MgCl_2$, and 1 mM LiCl in the superfusate as specified in the data. A laser scanning confocal microscope was used to image changes in fluo-3 fluorescence elicited by agonist challenges in the NGNs. Fluorescence excitation was at 490 nm and other experimental parameters with Fluo-3 detection were performed as described previously [85]. The fluorescence intensity was recorded relative to the baseline fluorescence ($\Delta F/F_0$). Student's *t*-test was applied to the data to determine significance between two means, as described in [85].

Structures

ATP, DPG, Triphosphate, and EDTA structures were built using ChemBioDraw (Perkin Elmer) and Microsoft Powerpoint. Figures were refined using CorelDraw X7 and GraFit5 (Erithacus Software).

Chapter 4

ATP·Mg·Li binds as a Ternary Complex to Serum Albumin

Introduction

As was introduced in Chapter 1, each year, BD affects approximately 6.1 million American adults, ages 18 and older [112, 113]. Li^+ was first introduced as a treatment for BD over 50 years ago and, despite advancements in pharmaceuticals, is still considered the 'gold standard' for effective treatment of this illness. Unfortunately, Li^+ also has a number of negative side effects, such as kidney and thyroid toxicity, which make it less than an ideal drug. Other drawbacks to Li^+ treatment include the challenge of non-compliance from patients, the narrow gap between efficacy and intoxication, and effects on unborn children and nursing infants [1, 52]. The molecular mechanism(s) of such a simple, yet effective, medication with such harmful side effects still needs to be understood in terms of both the cellular target(s) of Li^+, and the transport and distribution of Li^+ throughout the body. Today, there is no validated mechanism of action for Li^+'s pharmacology.

Lithium carbonate or lithium citrate is administered in the form of an oral tablet and the drug is absorbed in the small intestine for a standard formulation, or in the small or large intestine for a slow-release formulation. Experiments measuring gastrointestinal epithelial cells upon acute exposure to Li^+ confirmed cellular influx to be through passive diffusion down its electrochemical gradient [74]. Li^+ is filtered from the blood through the kidneys for either excretion from the body or reabsorption by the body. During fluid filtration in the lumen, about 60 percent of Li^+ is reabsorbed in the proximal tubule to circulate in the bloodstream, while about 25 percent is excreted in the urine [74, 114]. The transport and distribution of Li^+ are not well understood. Because Li^+ is absorbed

and circulates through the bloodstream, the following research considers the protein serum albumin as a protein with which Li^+ might interact in the blood plasma.

Human serum albumin (HSA) is the most abundant protein in the blood plasma at a concentration of approximately 0.6 mM [115]. Physiologically, HSA regulates plasma oncotic pressure (i.e., the osmotic pressure in a blood vessel's plasma that tends to pull water into the circulatory system) and assists in cellular repair at cell membranes by shuttling fatty acids to and from sites of cellular damage [116, 117]. In addition to fatty acids, HSA binds and transports hormones, bilirubin, heme, metal ions, and certain drugs, delivering these molecules through the bloodstream [118, 119]. Of particular interest and importance to the pharmacological community is understanding fatty acid binding and drug binding properties of HSA. It is known that there are two preferred binding sites for small molecule drugs on HSA, Site I and Site II, referred to as Sudlow Sites [86, 119] (Figure 4-1). While both sites bind to aromatic molecules, Site I has been observed to more specifically bind bulky molecules with a centralized negative charge, while Site II has been found to prefer binding to extended conformations of molecules with a negative charge at one end of the ligand [120, 121]. Furthermore, HSA has identified seven fatty acid sites [122]: sites 2, 4, and 5 bind to fatty acids with relatively higher affinity, while sites 1, 3, 6, and 7 bind fatty acids with a relatively lower affinity, thereby allowing for the possibility of competition with other ligands or drugs at these lower affinity binding sites [122].

Though not extensively reported in the literature, the binding of ATP to HSA, as well as bovine serum albumin (BSA), has been studied under various conditions using

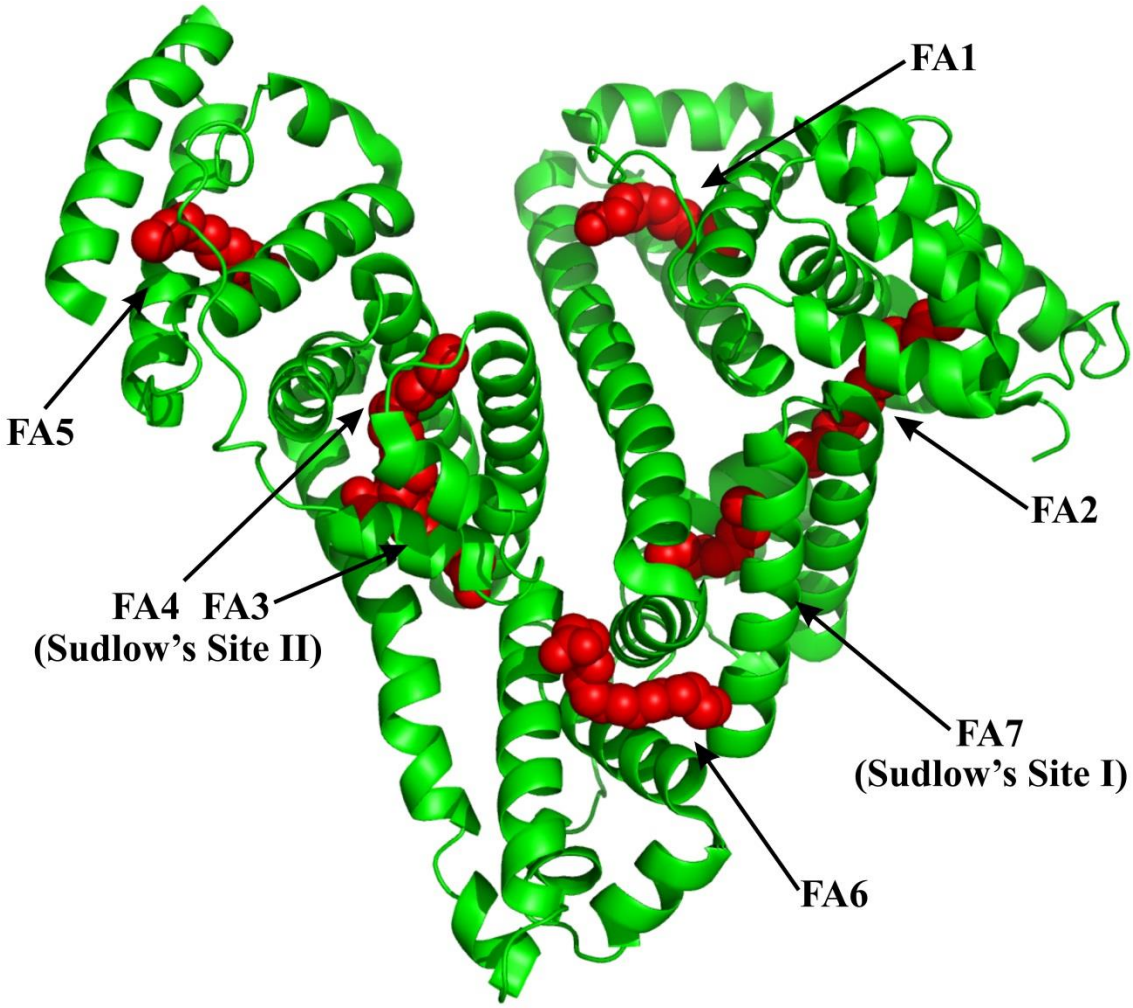

Figure 4-1. Human serum albumin (HSA) is shown as a ribbon diagram (green) with fatty acids (FA) (red) bound to seven fatty acid sites on HSA. Drug binding sites are labeled as Sudlow's Site I, occupied by FA7, and Sudlow's Site II bound to FA3 and FA4. The coordinates were retrieved from the PDB entry 1E7H. The image was rendered in PyMol.

several methods. Ultrafiltration and equilibrium dialysis experiments demonstrated that ATP binds to HSA, and that the binding affinity decreases with increasing pH [123]. Electron Spin Resonance (ESR) verified the specific binding of spin-labeled derivatives of ATP to BSA [124]. ATP binding to BSA was also studied by NMR and ultrafiltration, and was found to occur with a stoichiometry of 1:1, and a K_D of 40 μM at pH 6.4 and a K_D of 120 μM at pH 7.4 [125]; this interaction exhibits a similar pH dependence as the one discussed above for HSA. Furthermore, the structure that ATP·Mg adopts when bound to BSA was probed using ^{1}H-NMR TRNOESY and was found to be similar to the conformation it assumes when bound to several enzymes that bind ATP [126]. ^{31}P NMR diffusion studies have also shown that ATP in the absence of Mg^{2+} binds both HSA and BSA at low affinity binding sites [127]. Although crystal structures have been solved for HSA in the apo form [128] and with 5 fatty acids bound [129], and for BSA [130, 131], to date, no structure of HSA with ATP bound has been solved. Thus, it is not known whether ATP binding occurs at Site I, Site II and/or some other as yet identified site.

As described in Chapter 3, our work has shown that Li^{+} can form a ternary complex with Mg^{2+} and ATP. Taking a reductionist approach, and building on this basic finding, the research presented in this Chapter is aimed at exploring the integrity of this ternary complex in the presence of HSA and identifying any effect Li^{+} might have on the binding of ATP to HSA. In particular, we sought to determine if the ternary ATP·Mg·Li complex is maintained in the presence of HSA, how its structure might change in the presence of HSA and if/how the ternary complex might interact with HSA.

Results and Discussion

Although it has been suggested that Li^+ could bind directly to serum proteins, to date, no direct evidence of such an interaction has been measured. In light of our findings that Li^+ could form a complex with ATP·Mg, the possibility that Li^+ binding to proteins, like HSA, might be mediated through an intermediary, such as a nucleotide ligand, seemed quite plausible. Here, we used a number of techniques that could interrogate the binding of Li^+ to ATP·Mg in the presence of HSA to investigate the potential of the ternary complex further binding to HSA (Figure 4-2).

ATP Binds to Albumin in the Presence of Li^+ and Mg^{2+}

While ATP and ATP·Mg have been shown to bind to HSA, the effect of Li^+ on this binding interaction is unknown. Therefore, to first probe ATP binding to HSA in the presence of Mg^{2+} and Li^+, Water ligand-observed gradient spectroscopy (WaterLOGSY) NMR experiments were performed (see Chapter 2 for details). Briefly, in this experiment, which is commonly used to screen drug compounds for binding to a protein, magnetization of bulk water is transferred to the hydration shell of the ligands and bound protons of the protein and ligands. Since free ligands have a longer relaxation time than those that are bound to the protein, the two possibilities for the ligand (e.g. free versus bound) can be distinguished from each other.

A negative control experiment was first carried out to test the WaterLOGSY experimental set-up. A WaterLOGSY of HSA and the small molecule, DPG, which we have previously determined, through indirect measurements using ^{7}Li T1, to have no appreciable binding to BSA, was collected (Figure 4-3; Table 4-1). The reference

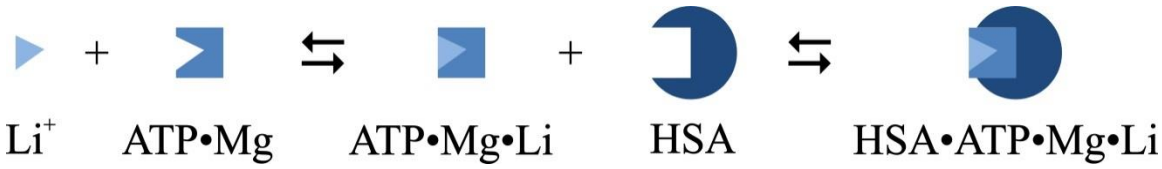

Figure 4-2. Scheme of Li^+ binding to ATP·Mg and ATP·Mg·Li binding to HSA.

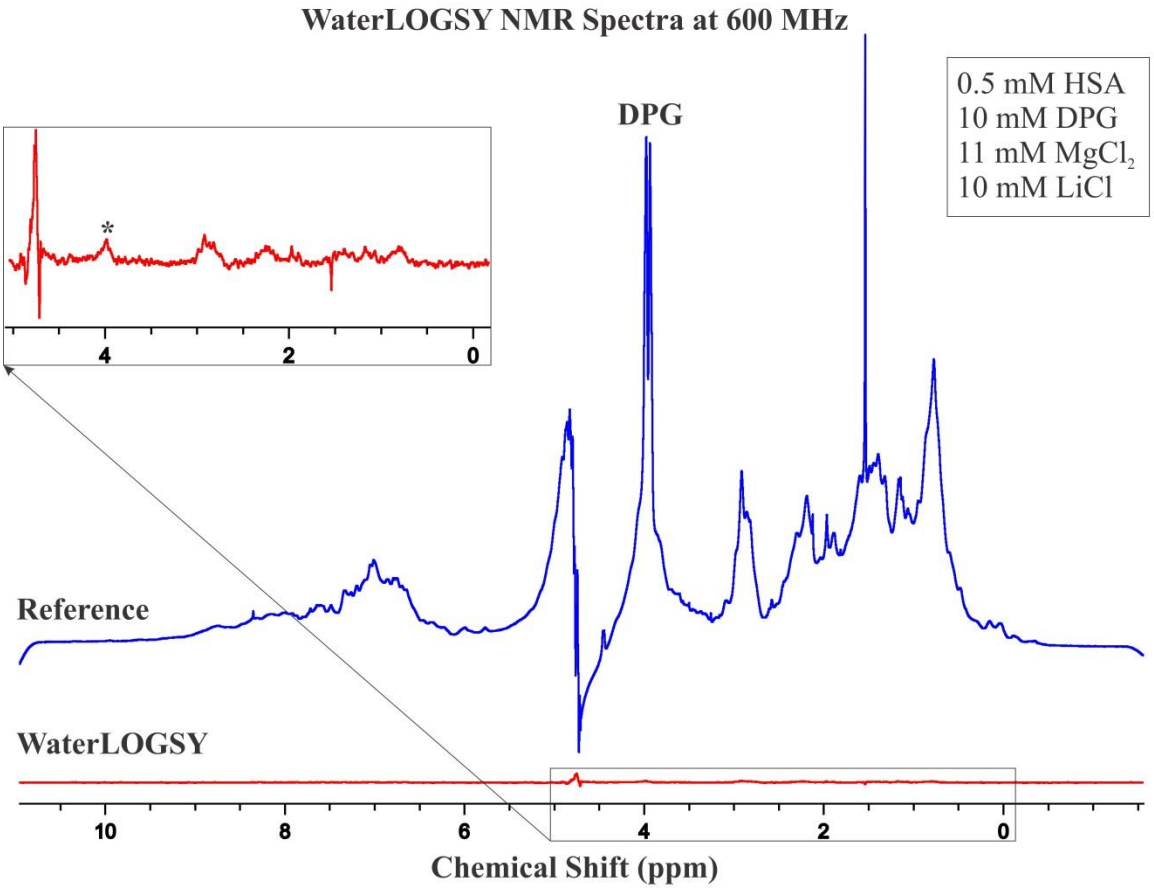

Figure 4-3. ^{1}H NMR Spectra of a 0.5 mM HSA sample with 10 mM DPG, 11 mM Mg, and 10 mM LiCl as reference (blue) and the WaterLOGSY (red). The chemical shift of the DPG is indicated with an asterisk in the inset spectrum. These spectra were collected on a 600 MHz NMR spectrometer.

DPG Experiments at 283 K on 500 MHz NMR

BSA	DPG	Mg	Li	Mn	^{7}Li T1 Relaxation (s)
+	+	+	+	-	6.97
-	+	+	+	-	7.65
+	+	+	+	+	6.07
0.5 mM	**10 mM**	**11 mM**	**10 mM**	**50 μM**	

Table 4-1. ^{7}Li T1 relaxation NMR experiment with 2,3- Diphosphoglycerate (DPG) and Bovine Serum Albumin (BSA). Experiments were collected on a 500 MHz NMR spectrometer at 283 K.

spectrum in blue shows a large ^{1}H signal for DPG at approximately 4.0 ppm. In the WaterLOGSY, the low positive signal at 4.0 ppm indicates there is very weak, if any, binding of DPG to the HSA (red spectrum). This result was also consistent with ^{7}Li T1 relaxation data (Table 4-1). The ^{7}Li relaxation in a sample of 10 mM DPG, 11 mM $MgCl_2$, and 10 mM LiCl was 7.65 seconds. The addition of 0.5 mM BSA decreases the ^{7}Li relaxation only slightly to 6.97 seconds. Similar ^{7}Li relaxation times in the presence and absence of BSA suggests that either the DPG·Mg·Li complex does not bind, or binds very weakly. The confirmation of weak or no binding of DPG to BSA supports the WaterLOGSY finding and verifies that the experimental parameters are correct.

A WaterLOGSY was next used to test whether ATP bound to HSA in the presence of Mg^{2+} and Li^{+} ions (Figure 4-4). A 1D ^{1}H reference spectrum of 0.5 mM HSA, 10 mM ATP, 11 mM $MgCl_2$, and 10 mM LiCl, for the WaterLOGSY, is shown in blue. The WaterLOGSY spectrum shows the positively phased signals of the protons of ATP in the red spectrum, indicating that ATP binds to HSA in the presence of both Mg^{2+} and Li^{+}. As the magnitude of the observed ATP signals in the WaterLOGSY for the experiments carried out with ATP alone, ATP·Mg and ATP·Mg·Li were all qualitatively similar, it can be concluded that Li^{+} does not significantly inhibit ATP from binding to HSA.

Equilibrium gel filtration experiments also support the finding that ATP·Mg binds to HSA in the both presence and absence of Li^{+}. Equilibrium gel filtration measures ligand binding to protein by detecting the depletion of ligand from the ligand-equilibrated column buffer upon injection of protein into the column (see Chapter 2 for details). The

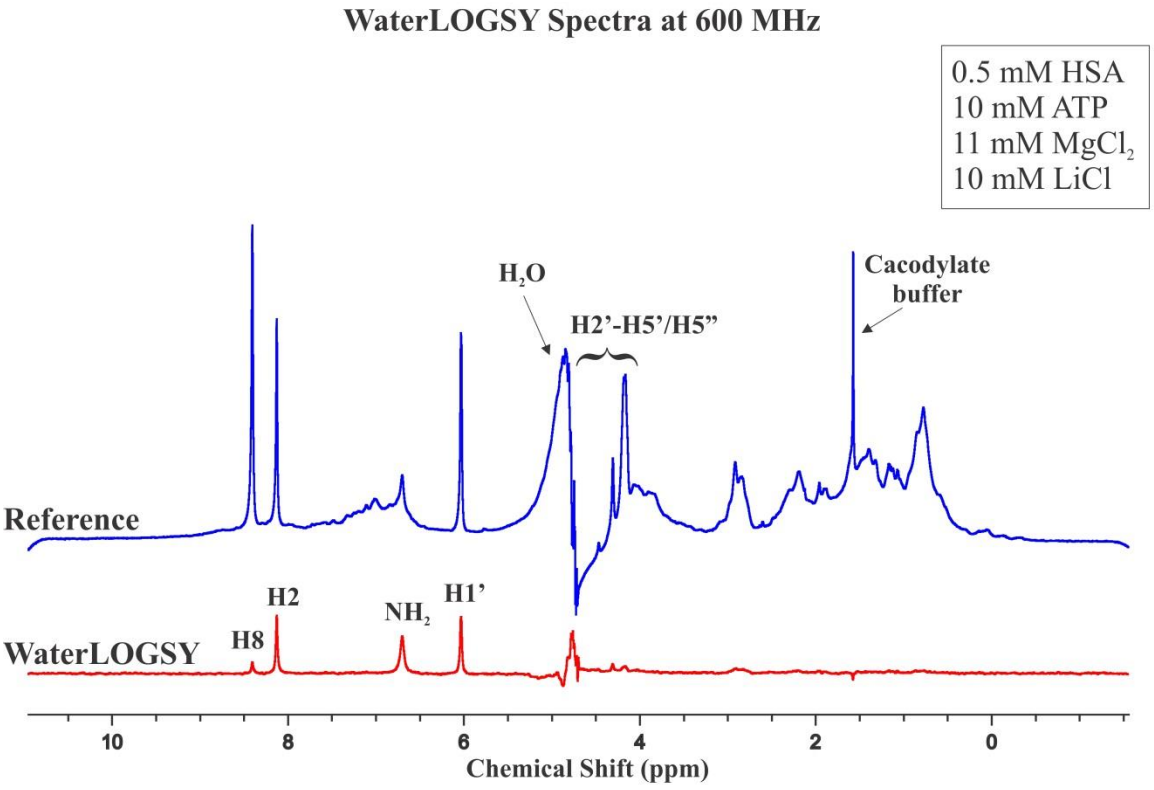

Figure 4-4. ^{1}H NMR spectra of the sample in the reference (blue) and the saturation transfer in the WaterLOGSY (red) indicating that ATP binds to the macromolecule, HSA. Experiments were taken on a 600MHz NMR Spectrometer. All of the remaining unlabeled peaks in the reference spectra can be attributed to protons on HSA.

gel filtration column was equilibrated with 1 mM ATP and 1.1 mM $MgCl_2$ (Figure 4-5). HSA was loaded on the column and eluted between 7 and 12 mL elution volume, as detected by UV absorbance at 280 nm. The high concentration of ATP in the buffer and addition of protein cause the UV detector to reach the high detection limit, noticeable at the top of the protein elution peak. Following the elution of the HSA-ligand complex, whose elution times was also between 7 and 12 mL elution volume and was overlapped and indistinguishable with the peak from HSA, the chromatogram showed a trough, at approximately 16 to 18 mL, representing the depletion of the ATP from the equilibration buffer that results due to ATP binding to HSA. The elution of ATP appears as negative signal because the concentration of ATP in the elution volume is less than the 1 mM baseline at which the column was equilibrated. The gel filtration results, therefore, clearly further confirm that ATP binds to HSA in the presence of Li^+. In addition, the gel filtration data show that the presence of Li^+ has no appreciable effect on ATP binding to HSA (Figure 4-6). While both the NMR and gel filtration data were not interpreted in a quantitative fashion, both sets of data qualitatively support the conclusion that Li^+ does not appear to significantly modulate the interaction of ATP with HSA.

Mg^{2+} Binds to ATP in the Presence of Albumin

Phosphorus nuclei can be directly detected by ^{31}P-NMR to probe the chemical environment of the triphosphates of ATP. Changes in the magnetic field of a particular nucleus due to neighboring or nearby nuclei can be detected by NMR as chemical shift perturbations (see Chapter 2 for details). The alpha (α), beta (β), and gamma (γ) phosphates of ATP are presented as stacked spectra collected under various sample conditions in Figure 4-7, that match those used in the gel filtration and WaterLOGSY

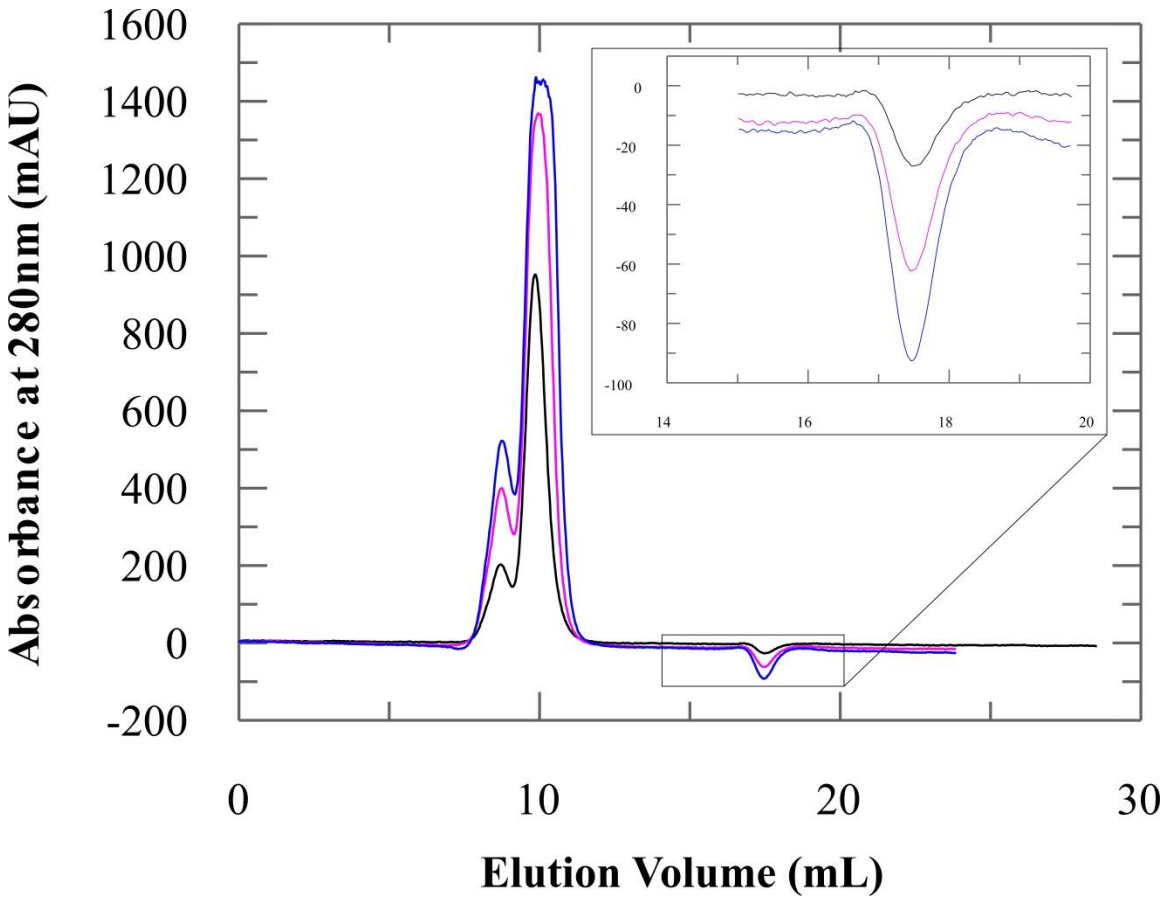

Figure 4-5. Overlay of three separate Equilibrium Gel Filtration chromatograms: 200 μM HSA (black), 400 μM HSA (pink), 600 μM HSA (blue). The HSA dimer is shown to elute at approximately 8 mL elution volume, followed by HSA monomer at approximately 10 mL, and a trough appears at the ATP elution volume of approximately 17 mL. The ATP elution (inset) appears as a trough due to ATP binding with HSA and depletion from the buffer. Equilibration buffer contained 1 mM ATP, 1.1 mM $MgCl_2$.

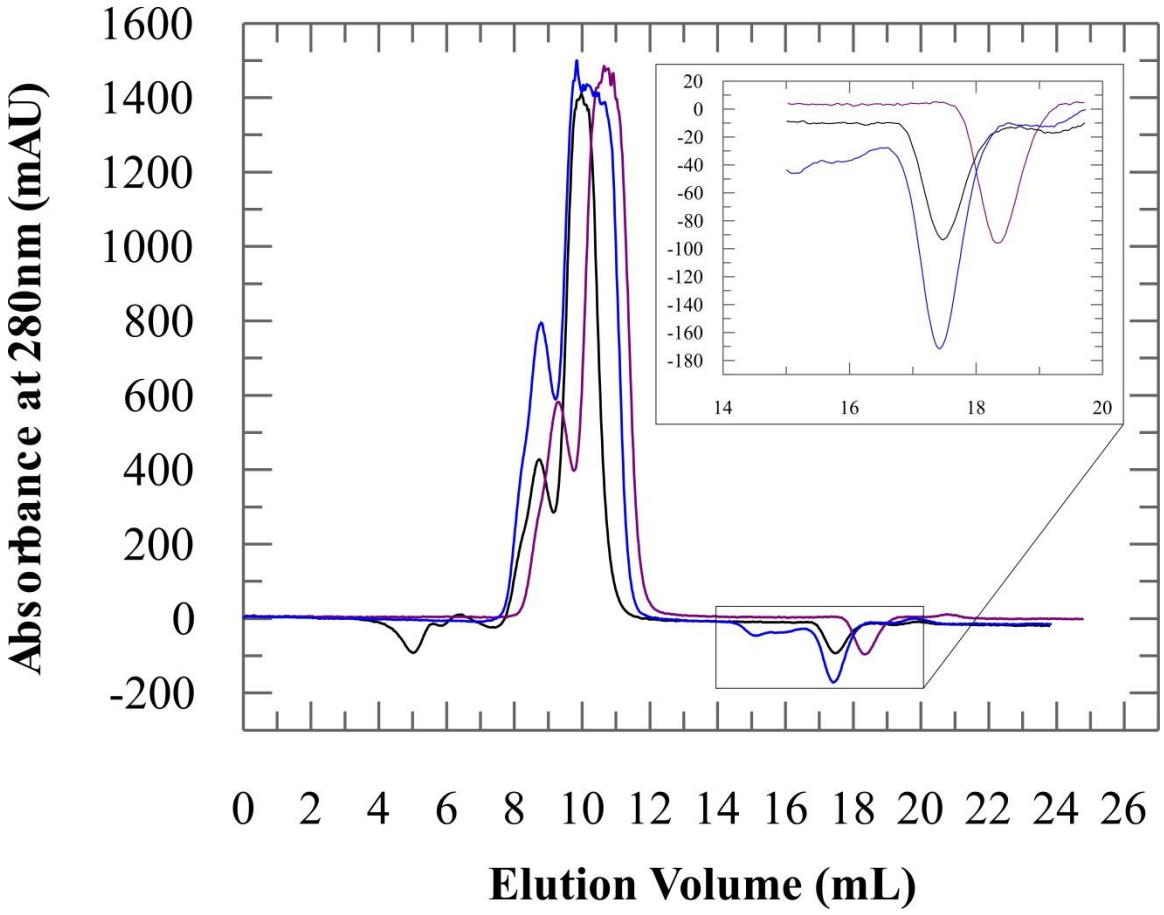

Figure 4-6. Overlay of three separate Equilibrium Gel Filtration chromatograms: 400 μM HSA (black), 600 μM HSA (purple), 800 μM HSA (blue). The HSA dimer is shown to elute at approximately 8 mL elution volume, followed by HSA monomer at approximately 10 mL, and a trough appears at the ATP elution volume of approximately 17 mL. The ATP elution (inset) appears as a trough due to ATP binding with HSA and depletion from the buffer. The equilibration buffer for all samples contained 1 mM ATP, 1.1 mM $MgCl_2$, and 1 mM LiCl. Note that the 600 μM HSA (purple) absorbance shift was a recording error rather than shifted elution profile.

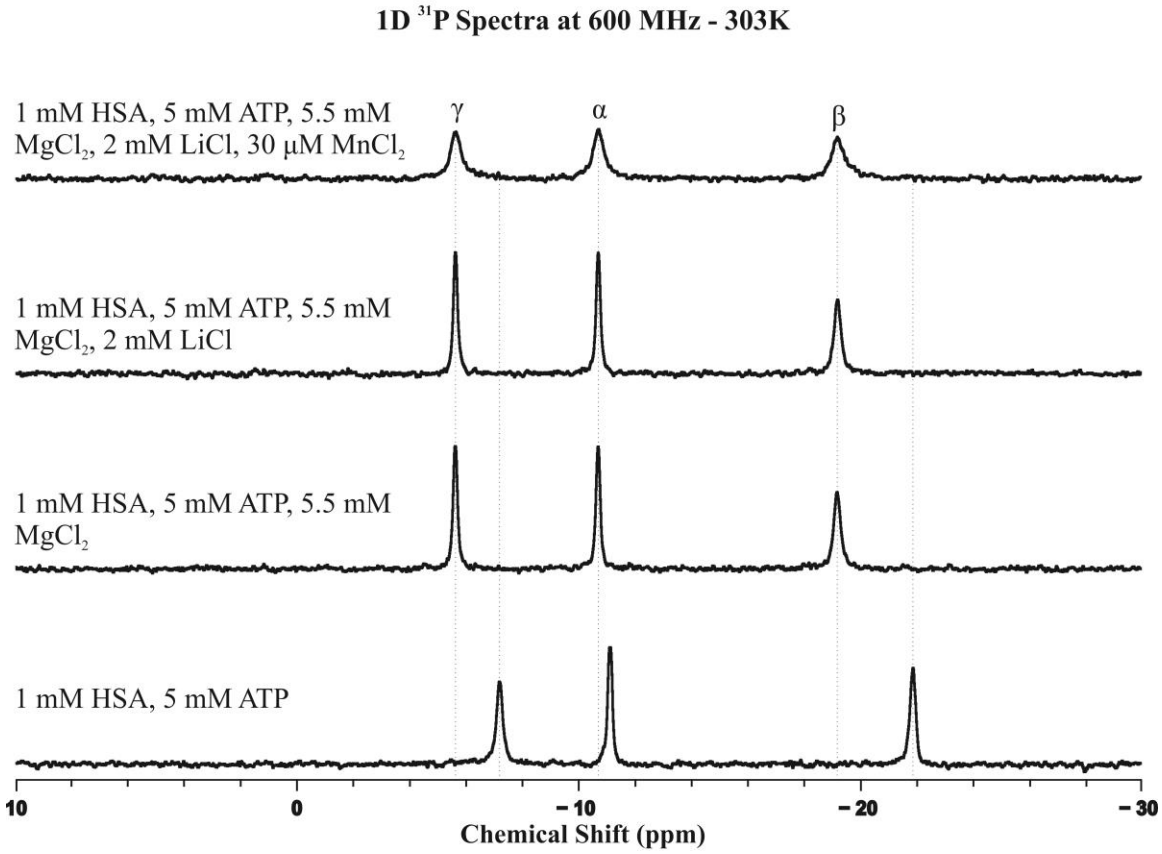

Figure 4-7. ^{31}P NMR Spectra of 5 mM ATP and 1 mM HSA alone and with the addition of $MgCl_2$, LiCl, and $MnCl_2$. The phosphates of ATP are labeled alpha, beta, and gamma in the top spectrum. Specific concentrations for each spectrum are labeled to the left of each spectrum. These spectra were collected on a 600 MHz NMR Spectrometer at 303 K.

experiments, to highlight the observed chemical shift perturbations. The bottom spectrum shows the signal positions for the three phosphates of ATP in the presence of HSA in the absence of metals. The other three phosphate spectra include the addition of metals as specified in the figure (e.g., $MgCl_2$, LiCl, and $MnCl_2$). A downfield chemical shift is observed for all phosphorus signals upon addition of $MgCl_2$ to the HSA-ATP sample. This is indicative of Mg^{2+} binding to the ATP in the presence of albumin. Further, the phosphate chemical shifts associated with ATP·Mg·Li directly aligned with the phosphate chemical shifts observed in the presence of HSA (Figure 4-8). What is clear from the spectra is that HSA, while causing a broadening of the phosphorus signals, as might be anticipated upon binding of ATP to HSA, does not significantly perturb the phosphate chemical shifts. This may suggest that the ATP binding interaction with HSA occurs via the adenosine-ribose, while the phosphates are directed outwards. Therefore the phosphates may be less affected by the HSA interaction. Nonetheless, it supports the conclusion that the ATP phosphates coordinate Mg^{2+} when ATP is bound to HSA in a manner that is similar to the way the phosphates of ATP free in solution coordinate Mg^{2+}.

As a control for all experiments involving ATP and HSA, the integrity of the ATP in the presence of HSA was also evaluated by ^{31}P-NMR. Comparison of a newly made sample and the same sample 5 days later revealed that the samples containing HSA slowly degraded over several days into ADP (Figure 4-9; Figure 4-10). The ADP peaks are difficult to see between the α and γ phosphates, but the increase in peak height of inorganic phosphate is evident. For this reason, freshly prepared samples were used for each set of NMR experiments.

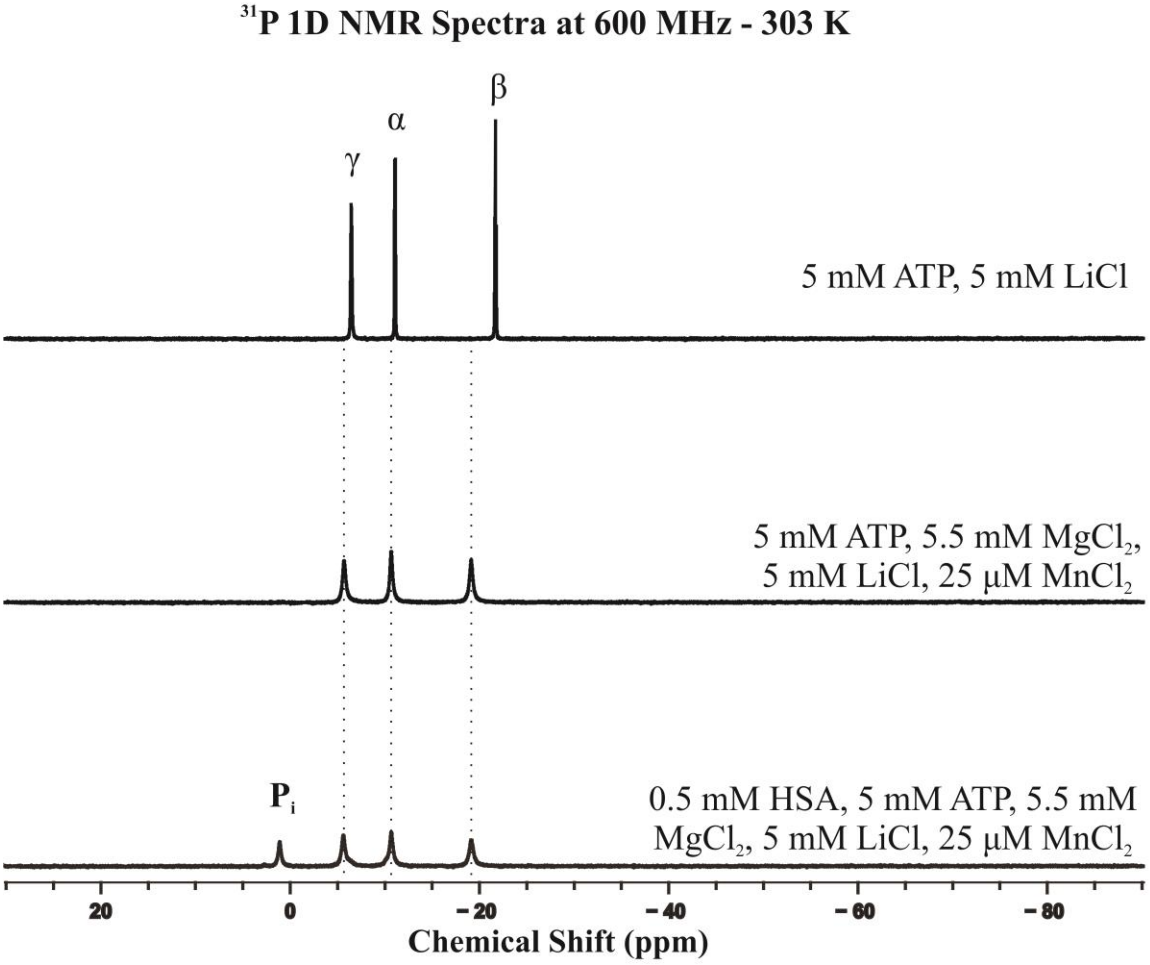

Figure 4-8. ^{31}P NMR Spectra of 5 mM ATP and 5 mM Li alone (top), with 5.5 mM Mg and 25 µM Mn (middle), and with the addition of 0.5 mM HSA (bottom). The phosphate signals of ATP are labeled as alpha, beta, and gamma on the top spectrum with the addition of inorganic phosphate labeled on the bottom spectrum. Specific concentrations for each spectrum are labeled to the right of each spectrum. These spectra were collected on a 600 MHz NMR Spectrometer at 303 K.

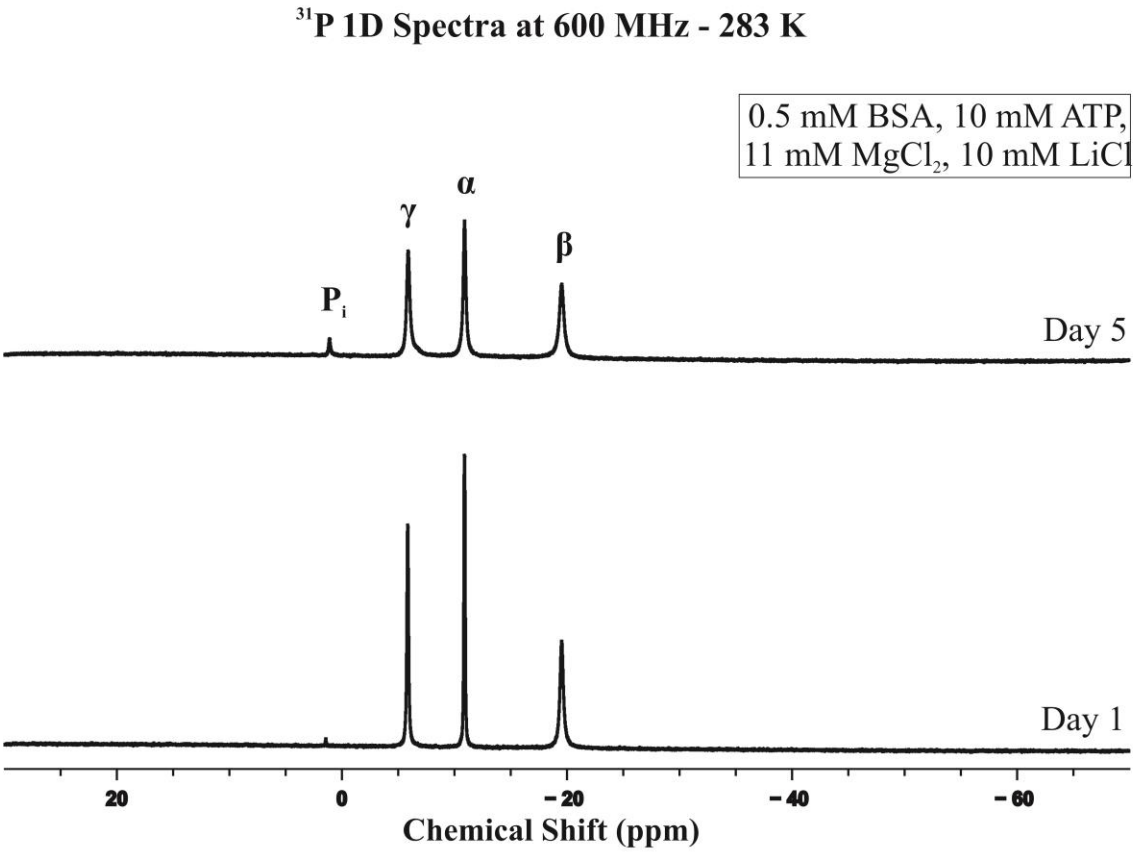

Figure 4-9. ^{31}P NMR spectra of 10 mM ATP, 11 mM $MgCl_2$, 10 mM LiCl with 0.5 mM BSA on the day the sample was prepared (bottom) and five days later (top). The phosphates of ATP (alpha, beta, and gamma) and inorganic phosphate are labeled in the top spectrum. These spectra were collected on a 600 MHz NMR Spectrometer at 283 K.

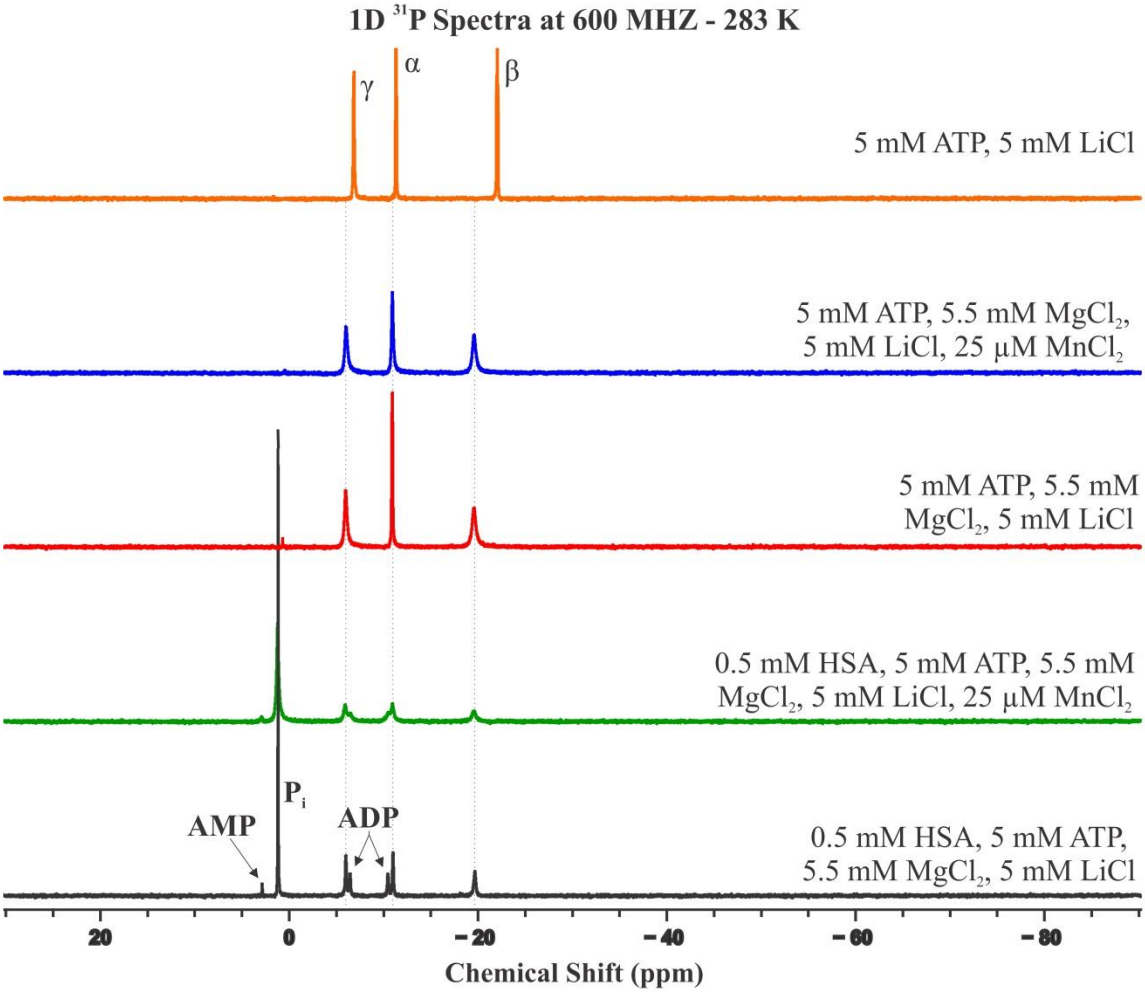

Figure 4-10. ^{31}P NMR spectra of 5 mM ATP, 5 mM LiCl (orange), with the addition of 5 mM $MgCl_2$, and 25 µM $MnCl_2$ (blue), and the addition of 0.5 mM HSA (green). Two spectra are in the absence of $MnCl_2$ (black), and in the absence of HSA and $MnCl_2$ (red). The phosphate signals of ATP are labeled as alpha, beta, and gamma on the top spectrum with the addition of inorganic phosphate, adenosine monophosphate (AMP), and adenosine diphosphate (ADP) labeled on the bottom spectrum. Specific concentrations for each spectrum are labeled to the right of each spectrum. All of these spectra were collected at on a 600 MHz NMR Spectrometer at 283 K.

ATP·Mg·Li Ternary Complex Structure in the Presence of Albumin

^{7}Li NMR can provide a direct report of Li^{+} in a molecular complex. By measuring shifts in the ensemble population of Li^{+} ions, NMR can reveal the binding behavior of Li^{+} through measurements such as T1 relaxation properties, which are expected to vary when comparing ions that are bound to molecular targets versus ions that are free in solution (see Chapter 2 for details). Li^{+} binding to ATP·Mg in the presence of HSA was therefore further probed by ^{7}Li T1 relaxation (Table 4-2). Such relaxation measurements can provide further evidence to support the conclusion that ATP binds HSA in the presence of Li^{+} and Mg^{2+} and that these two metals do not significantly inhibit ATP binding to HSA. The ^{7}Li T1 relaxation of Mg·Li in solution at 283 K is 12.80 s, while the ATP·Mg·Li has a ^{7}Li T1 of 6.70 s. The shorter T1 observed upon addition of ATP points to Li^{+} binding to a larger molecule, namely ATP·Mg. The addition of HSA to ATP·Mg·Li results in a faster ^{7}Li relaxation time of 2.985 s. Li^{+} does not bind to HSA directly, shown by ^{7}Li T1 control data of 12.702 s in the presence of 5 mM LiCl, 5.5 mM $MgCl_2$, and 0.5 mM HSA, nearly matching the ^{7}Li relaxation time of free Li^{+}. Therefore, the ^{7}Li T1 relaxation data, shown in Table 4-2, indicates that ATP is binding directly to the HSA and Li is carried onto the HSA via ATP.

Paramagnetic relaxation enhancement (PRE) is a method to probe the binding environment of the Li^{+} to discover whether Mg^{2+} is in close proximity to the detecting nucleus, in this case Li^{+}. The paramagnetic ion, Mn2+, is added to the sample in a very small quantity and rapidly exchanges with Mg^{2+}, sampling all of the Mg^{2+}-binding sites, and causing a faster relaxation of neighboring nuclei (refer to Chapter 2 for details).

^{7}Li T1 Relaxation at 600 MHz

HSA	ATP	Mg	Li	Mn	283K
-	-	+	+	-	12.80
-	-	+	+	+	12.13
				Relaxation Enhancement (%)	5.3
-	+	+	+	-	6.70
-	+	+	+	+	2.62
				Relaxation Enhancement (%)	60.9
+	+	+	+	-	2.99
+	+	+	+	+	0.48
				Relaxation Enhancement (%)	84.0
0.5 mM	**10 mM**	**11 mM**	**10 mM**	**50 µM**	

Table 4-2. ^{7}Li T1 relaxation experiments with 0.5 mM HSA, 10 mM ATP, 11 mM $MgCl_2$, 10 mM LiCl in the presence or absence of 50 µM $MnCl_2$ at 283K. Controls in the absence of HSA or HSA and ATP are also shown. Relaxation Enhancement (%) was calculated by subtracting the PRE (+ $MnCl_2$) T1 value from the initial T1, dividing the difference by the initial T1, and multiplying by 100. Experiments were collected on a 600 MHz NMR spectrometer.

Under these sample concentrations, Li^+ can be shown to bind to ATP·Mg in the presence of HSA by the observation of a PRE upon addition of Mn^{2+}. Indeed, at 283 K, the ^{7}Li T1 dropped approximately 6-fold from 2.99 s to 0.48 s. While HSA has been shown to bind zinc, copper, cadmium, and nickel metal ions, high affinity Mg binding has not been reported [132]. The ^{7}Li T1 PRE observed in the presence of HSA and ATP·Mg·Li can be attributed to Li^+ binding in close proximity to ATP·Mg on HSA rather than at a Mg^{2+} site on HSA. An interesting observation is the free ATP has a lower relaxation enhancement, 60.9 percent, than the HSA-bound, 84.0 percent (Table 4-2). This indicates that the Li local environment is slightly different in the free and albumin-bound ATP·Mg states. Perhaps the structure of the phosphate tail of ATP, while still freely accessible to Mg·Li, may change slightly when bound to albumin. The Sudlow sites of HSA, where it has been suggested that ATP may bind, are reported to bind either heterocyclic anions or aromatic carboxylates [87]. Based on the known interactions at these sites, it is reasonable to propose that the adenosine and/or ribose directly interface with HSA at one or more of these sites, leaving the phosphate tail free to be unconstrained and adopt a pseudo-free state according to the NMR observable, ^{7}Li, only slightly changing the phosphate coordination with Mg^{2+} and Li^+ at the binding pocket.

The PRE experiment reinforces that Li^+ is bound to HSA by way of the ATP nucleotide. In addition, it can be concluded that Li^+ is bound in close proximity to Mg^{2+} that is in turn bound to the albumin·ATP, shown by the ^{7}Li T1 PRE upon Mn^{2+} addition. To verify that these ^{7}Li T1 interactions are specific and not randomly diffusing into contact with Mn^{2+} to cause a PRE ^{23}Na T1 control measurements result in no change in T1 relaxation in the presence of Mn^{2+} (Table 4-3).

^{23}Na T1 Relaxation (ms) NMR Experimental Controls at 600 MHz

HSA	ATP	Mg	Li	Mn	283 K	298 K	303 K	310 K
+	+	+	+	-	37.59	51.20	55.42	61.69
+	+	+	+	+	36.70	50.28	54.51	60.66
				Relaxation Enhancement (%)	2.4	1.8	1.6	1.7
+	-	+	+	-	39.03	53.24	57.88	64.25
+	-	+	+	+	39.09	53.25	58.12	64.22
				Relaxation Enhancement (%)	-0.2	0.0	-0.4	0.0
-	+	+	+	-	37.82	52.14	56.27	63.27
-	+	+	+	+	38.18	52.65	57.27	63.86
				Relaxation Enhancement (%)	-0.1	-1.0	-1.8	-0.9
-	-	+	+	-	41.303	56.215	61.112	67.930
-	+	-	+	-	28.285	39.067	42.488	47.245
0.5mM	**5mM**	**5.5mM**	**5mM**	**25μM**				

Table 4-3. ^{23}Na (sodium) T1 relaxation control NMR experiments with 5 mM ATP were observed at 283 K, 298 K, 303 K, and 310 K. Relaxation Enhancement (%) was calculated by subtracting the PRE (+ $MnCl_2$) T1 value from the initial T1, dividing the difference by the initial T1, and multiplying by 100. Experiments were collected on a 600 MHz NMR spectrometer.

Taken together, the data in this chapter supports the model that an ATP·Mg·Li complex can remain intact upon binding to a cofactor site on a protein (e.g., the ATP binding pocket on HSA) and that the structure of this complex may be little perturbed. Based on these observations, it can be envisioned that Li^+ operates by 'piggy backing' on phosphate containing ligands, like ATP·Mg, to enable both transport within the body as well as targeting of sites on specific protein. In this sense, if Li^+ is viewed through the lens of a molecule entity, like ATP, one can begin to think about how targeting of Li^+ in the body may be achieved.

Unanticipated Differences in ATP Binding to BSA and HSA

A large difference in ^{7}Li T1 relaxation was initially observed for ATP·Mg·Li complex in the presence of HSA versus BSA (^{7}Li T1 data not shown). This observation led to the question of whether ATP bound to HSA in significantly different mode and/or with a significantly different affinity than BSA, which would cause the ^{7}Li T1 relaxation to change. However, further examination of different HSA and BSA samples by ^{7}Li T1 relaxation experiments were unable to consistently reproduce the large differences and instead showed little variability between HSA and BSA (Table 4-4). The amino acid sequence alignment of HSA and BSA shows an approximately 76% sequence identity between BSA and HSA. In addition, the highly conserved residues found specifically at the known Sudlow sites where ATP is likely to bind render it improbable, though not impossible, that there would be fundamental differences in ATP binding to HSA versus BSA (Figure 4-11). Over the course of collecting the ^{7}Li T1 relaxation of several samples, it became apparent that seemingly inconsistent variation was seen within samples of the same species, human or bovine (Table 4-5). To account for the

NMR Experiments at 298 K - 600 MHz NMR

HSA	BSA	ATP	Mg	Li	Mn	^{7}Li T1 Relaxation (sec)	Product #
-	+	+	+	+	-	8.885 ± 0.125	A6003
-	+	+	+	+	+	3.099	A6003
+	-	+	+	+	-	6.596 ± 1.23	A3782
+	-	+	+	+	+	2.618 ± 0.257	A3782
0.5 mM	**0.5 mM**	**10 mM**	**11 mM**	**10 mM**	**50 µM**		

Table 4-4. ^{7}Li T1 relaxation of samples containing either BSA or HSA. Standard deviation is shown where experiments were run in triplicate. Experiments were collected on a 600 MHz NMR spectrometer at 298K.

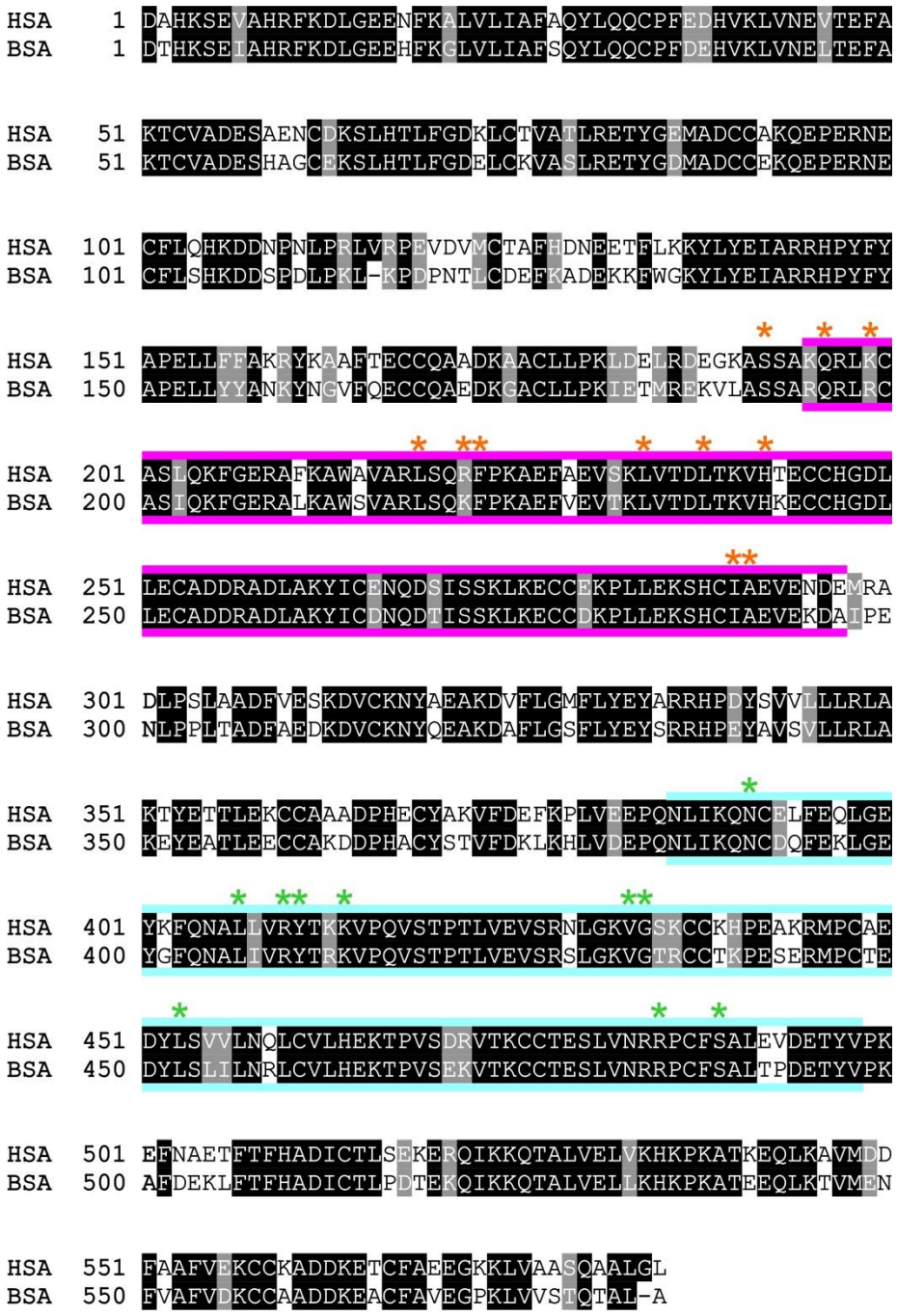

Figure 4-11. Amino acid sequence alignment of HSA (Sigma-Aldrich Product #A3782) and BSA (Sigma-Aldrich Product #A6003) using the NCBI Basic local alignment search tool (BLAST). HSA and BSA have a 76% sequence identity. Identical amino acids (black background) and similar amino acids (grey background) of HSA and BSA are shown. Subdomain IIA (pink) and subdomain IIIA (blue) are highlighted. Amino acid residues involved in Sudlow's Site I (orange asterisk) or Sudlow's Site II (green asterisk) are identified [86, 119].

^{7}Li T1 Relaxation on 600 MHz at 298 K

BSA·ATP·Mg·Li	Mn	^{7}Li T1	Cat. #	**HSA**·ATP·Mg·Li	Mn	^{7}Li T1	Cat. #
+	-	8.467	A6003	+	-	3.746	A3782
+	-	9.331	A6003	+	-	6.291	A3782
+	-	8.856	A6003	+	-	6.371	A3782
+	+	3.099	A6003	+	-	6.693	A3782
+	-	4.075	A7030	+	-	7.612	A3782
+	-	3.629	A7030	+	-	6.638	A3782
+	-	4.228	A7030	+	-	8.092	A3782
+	+	2.330	A7030	+	-	7.325	A3782
+	-	8.177	A1900	+	-	4.041	A3782
+	-	11.357	A7960	+	-	3.791	A3782
				+	+	0.651	A3782
				+	+	2.361	A3782
				+	+	2.874	A3782

Table 4-5. ^{7}Li T1 relaxation experiments of samples containing: 0.5 mM BSA (left table) or 0.5 mM HSA (right table), 10 mM ATP, 11 mM $MgCl_2$, 10 mM LiCl in the presence or absence of 50 μM $MnCl_2$ at 298 K. The units for the T1 time are in seconds. The catalog number refers to the Sigma-Aldrich product number. Experiments were collected on a 600 MHz NMR spectrometer.

differences in T1 relaxation between samples, the quality of the different albumin products that were used was assessed.

There are numerous products of albumin protein sold by Sigma-Aldrich. Differences between products in the amino acid sequences, purification procedures, and final processing and purity of the protein product were sought (Table 4-6; Table 4-7; Table 4-8; Table 4-9). From this data, it can be inferred that the differences in ^{7}Li T1 relaxation times between albumins may be due to interference from globulin, a small protein found in serum. The primary HSA that we used was globulin-free (Sigma-Aldrich Cat # A3782) and the main BSA that we used was not labeled globulin-free (Sigma-Aldrich Cat # A6003). An overlay of the HSA structure with and without fatty acids shows some significant differences in the trajectories of the helices (Figure 4-12). Such differences in structure, particularly with respect to Sudlow sites, for the different ligand bound states of HSA, highlight the likely reason why the ATP affinity for these sites may vary between albumin samples tested. Those differences in affinity would be reflected in the T1 relaxation.

Gel filtration results provided further evidence of differences in ATP binding between HSA and BSA (Figure 4-13). ATP binds to BSA with weaker affinity than ATP binds to HSA, as shown by the shallower trough of ATP at approximately 17.5 mL elution volume. Also, the elution profiles of BSA and HSA by gel filtration show that the ratio of monomer to dimer is much higher in HSA than BSA. Perhaps the ATP binding site is inaccessible or less accessible in dimer form. If this is the case, then the higher population of dimer in BSA would likely account for lower ATP binding to BSA over HSA. These differences in products may or may not cause interference in other studies,

Product #	Source of Albumin	Fatty Acid Free	Globulin Free	Protease Free	Method of Purification
A3782	Human, pooled	Y	Y	N	1. Separation of albumin from pooled human serum according to Cohn, et al. (1946)[1]. 2. Globulins removed by heat shock fractionation after addition of protein stabilizer, caprylate, which is then removed by filtration.
A1653	Human, pooled	N	N	N	Separation of albumin from pooled human serum according to Cohn, et al. (1946).
A9731	Human, recombinant	Y	Y	N	Expressed in rice.
A7030	Bovine, pooled	Y	Y	Y	Heat shock fractionation
A6003	Bovine, pooled	Y	N	N	Cold ethanol fractionation preserves native albumin structure and function
A7906	Bovine, pooled	N	N	N	Heat shock fractionation
A1900	Bovine, pooled	N	N	N	1. Cold ethanol Fractionation. 2. Monomer isolated from A4503.

Table 4-6. Serum Albumin purification processing categorized by Sigma-Aldrich product number [133].

Product #	Source of Albumin	Molecular Weight (g/mol)	Number of Amino Acids
A3782	Human, pooled	66,528	585
A1653	Human, pooled	69,363	609*
A9731	Human, recombinant	66,468	585
A7030	Bovine, pooled	66,429	583
A6003	Bovine, pooled	66,429	583
A7906	Bovine, pooled	69,289	607*
A1900	Bovine, pooled	66,429	583

Table 4-7. List of serum albumin proteins sold by Sigma-Aldrich. The proteins with an asterisk (*) contain a leader sequence that is a precursor to the mature HSA and is a localization signal directing albumin to the endoplasmic reticulum, Golgi apparatus, and ultimately secretion into the blood [134].

Amino Acid Sequences of Sigma-Aldrich Human Serum Albumin
A3782 Human, pooled DAHKSEVAHRFKDLGEENFKALVLIAFAQYLQQCPFEDHVKLVNEVTEFAKTCVADESA ENCDKSLHTLFGDKLCTVATLRETYGEMADCCAKQEPERNECFLQHKDDNPNLPRLVRP EVDVMCTAFHDNEETFLKKYLYEIARRHPYFYAPELLFFAKRYKAAFTECCQAADKAAC LLPKLDELRDEGKASSAKQRLKCASLQKFGERAFKAWAVARLSQRFPKAEFAEVSKLVT DLTKVHTECCHGDLLECADDRADLAKYICENQDSISSKLKECCEKPLLEKSHCIAEVEND EMRADLPSLAADFVESKDVCKNYAEAKDVFLGMFLYEYARRHPDYSVVLLLRLAKTYE TTLEKCCAAADPHECYAKVFDEFKPLVEEPQNLIKQNCELFEQLGEYKFQNALLVRYTK KVPQVSTPTLVEVSRNLGKVGSKCCKHPEAKRMPCAEDYLSVVLNQLCVLHEKTPVSD RVTKCCTESLVNRRPCFSALEVDETYVPKEFNAETFTFHADICTLSEKERQIKKQTALVEL VKHKPKATKEQLKAVMDDFAAFVEKCCKADDKETCFAEEGKKLVAASQAALGL
A1653 Human, pooled MKWVTFISLLFLFSSAYSRGVFRRDAHKSEVAHRFKDLGEENFKALVLIAFAQYLQQCPF EDHVKLVNEVTEFAKTCVADESAENCDKSLHTLFGDKLCTVATLRETYGEMADCCAKQ EPERNECFLQHKDDNPNLPRLVRPEVDVMCTAFHDNEETFLKKYLYEIARRHPYFYAPE LLFFAKRYKAAFTECCQAADKAACLLPKLDELRDEGKASSAKQRLKCASLQKFGERAFK AWAVARLSQRFPKAEFAEVSKLVTDLTKVHTECCHGDLLECADDRADLAKYICENQDSI SSKLKECCEKPLLEKSHCIAEVENDEMPADLPSLAADFVESKDVCKNYAEAKDVFLGMF LYEYARRHPDYSVVLLLRLAKTYETTLEKCCAAADPHECYAKVFDEFKPLVEEPQNLIK QNCELFEQLGEYKFQNALLVRYTKKVPQVSTPTLVEVSRNLGKVGSKCCKHPEAKRMP CAEDYLSVVLNQLCVLHEKTPVSDRVTKCCTESLVNRRPCFSALEVDETYVPKEFNAETF TFHADICTLSEKERQIKKQTALVELVKHKPKATKEQLKAVMDDFAAFVEKCCKADDKE TCFAEEGKKLVAASQAALGL
A9731 Human, recombinant DAHKSEVAHRFKDLGEENFKALVLIAFAQYLQQCPFEDHVKLVNEVTEFAKTCVADESA ENCDKSLHTLFGDKLCTVATLRETYGEMADCCAKQEPERNECFLQHKDDNPNLPRLVRP EVDVMCTAFHDNEETFLKKYLYEIARRHPYFYAPELLFFAKRYKAAFTECCQAADKAAC LLPKLDELRDEGKASSAKQRLKCSLQKFGERAFKAWAVARLSQRFPKAEFAESKLVTDL TKVHTECCHGDLLECADDRADLKYICENQDSISSKLKECCEKPLLEKSHCIAEVENDEMP ADLPSLAADFVESKDVCKNYAAKDVFLGMFLYEYARRHPDYSVVLLLRLAKTYETTLE KCCAAADPHECYAKVFDEFKPLVEEPQNLIKQNCELFEQLGEYKFQNALLVRYTKKVPQ VSTPTLVEVSRNLGKVGSKCCKHEAKRMPCAEDYLSVVLNQLCVLHEKTPVSDRVTKC CTESLVNRRPCFSALEVDETYVPKEFNAETFTFHADICTLSEKERQIKKQTALVELVKHKP KATKEQLKAVMDDFAAFVEKCCKDDKETCFAEEGKKLVAASQAALGL

Table 4-8. Amino acid sequences of Human Serum Albumin categorized by Sigma product number.

Amino Acid Sequences of Sigma-Aldrich Bovine Serum Albumin
A7030 Bovine, pooled DTHKSEIAHRFKDLGEEHFKGLVLIAFSQYLQQCPFDEHVKLVNELTEFAKTCVADESHA GCEKSLHTLFGDELCKVASLRETYGDMADCCEKQEPERNECFLSHKDDSPDLPKLKPDP NTLCDEFKADEKKFWGKYLYEIARRHPYFYAPELLYYANKYNGVFQECCQAEDKGACL LPKIETMREKVLASSARQRLRCASIQKFGERALKAWSVARLSQKFPKAEFVEVTKLVTDL TKVHKECCHGDLLECADDRADLAKYICDNQDTISSKLKECCDKPLLEKSHCIAEVEKDAI PENLPPLTADFAEDKDVCKNYQEAKDAFLGSFLYEYSRRHPEYAVSVLLRLAKEYEATL EECCAKDDPHACYSTVFDKLKHLVDEPQNLIKQNCDQFEKLGEYGFQNALIVRYTRKVP QVSTPTLVEVSRSLGKVGTRCCTKPESERMPCTEDYLSLILNRLCVLHEKTPVSEKVTKC CTESLVNRRPCFSALTPDETYVPKAFDEKLFTFHADICTLPDTEKQIKKQTALVELLKHKP KATEEQLKTVMENFVAFVDKCCAADDKEACFAVEGPKLVVSTQTALA
A6003 Bovine, pooled; Same sequence as A7030
A7906 Bovine, pooled MKWVTFISLLLLFSSAYSRGVFRRDTHKSEIAHRFKDLGEEHFKGLVLIAFSQYLQQCPFD EHVKLVNELTEFAKTCVADESHAGCEKSLHTLFGDELCKVASLRETYGDMADCCEKQE PERNECFLSHKDDSPDLPKLKPDPNTLCDEFKADEKKFWGKYLYEIARRHPYFYAPELLY YANKYNGVFQECCQAEDKGACLLPKIETMREKVLASSARQRLRCASIQKFGERALKAW SVARLSQKFPKAEFVEVTKLVTDLTKVHKECCHGDLLECADDRADLAKYICDNQDTISS KLKECCDKPLLEKSHCIAEVEKDAIPENLPPLTADFAEDKDVCKNYQEAKDAFLGSFLYE YSRRHPEYAVSVLLRLAKEYEATLEECCAKDDPHACYSTVFDKLKHLVDEPQNLIKQNC DQFEKLGEYGFQNALIVRYTRKVPQVSTPTLVEVSRSLGKVGTRCCTKPESERMPCTEDY LSLILNRLCVLHEKTPVSEKVTKCCTESLVNRRPCFSALTPDETYVPKAFDEKLFTFHADI CTLPDTEKQIKKQTALVELLKHKPKATEEQLKTVMENFVAFVDKCCAADDKEACFAVE GPKLVVSTQTALA
A1900 Bovine, pooled; Same sequence as A7030

Table 4-9. Amino acid sequences of Bovine Serum Albumin categorized by Sigma product number.

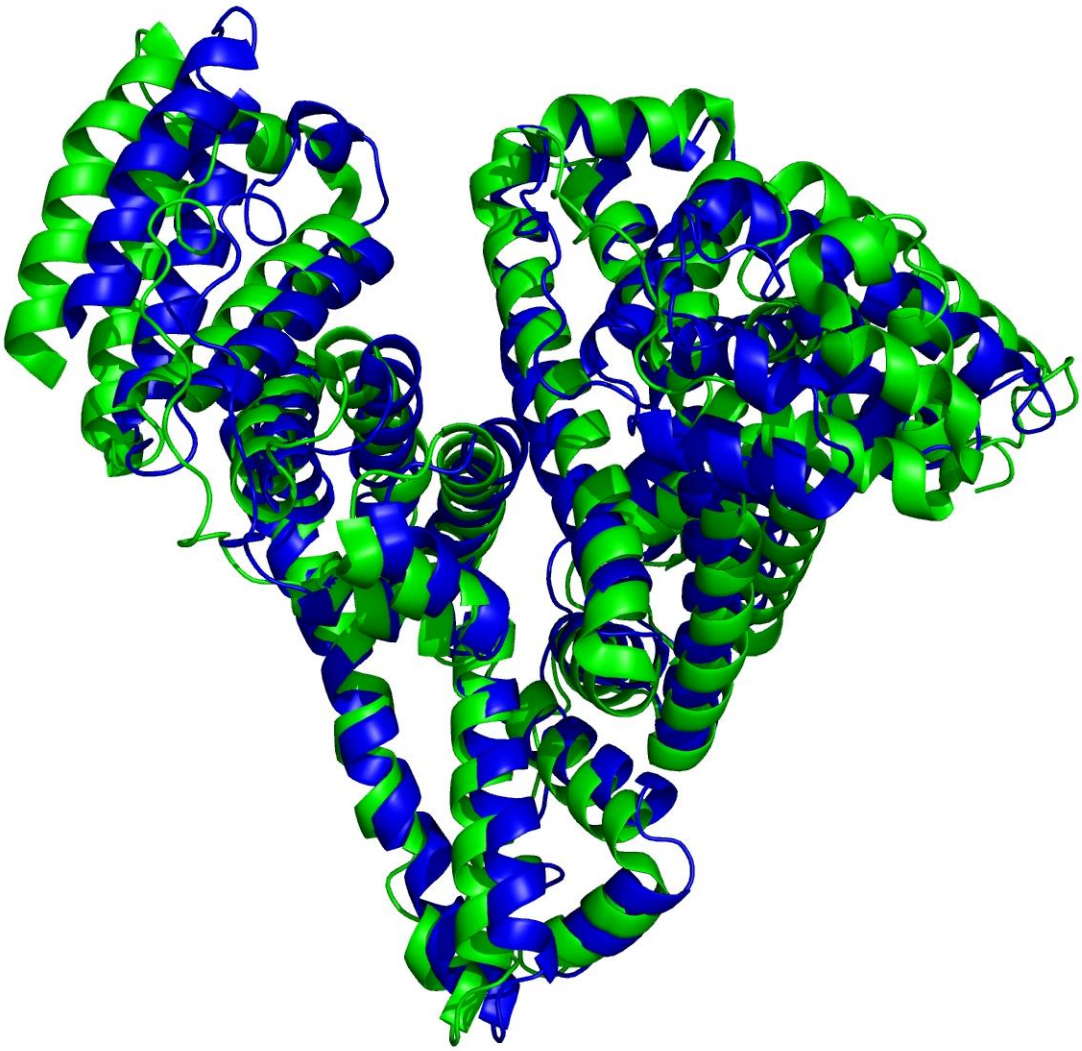

Figure 4-12. An overlay of the backbone structure of HSA bound by fatty acids (green ribbon) and HSA without any fatty acids (blue ribbon). The structures were rendered from PDB files 1E7H and 1BM0, respectively. For clarity of comparison of the protein backbone structures, the fatty acids are not shown in the rendering of the 1E7H.

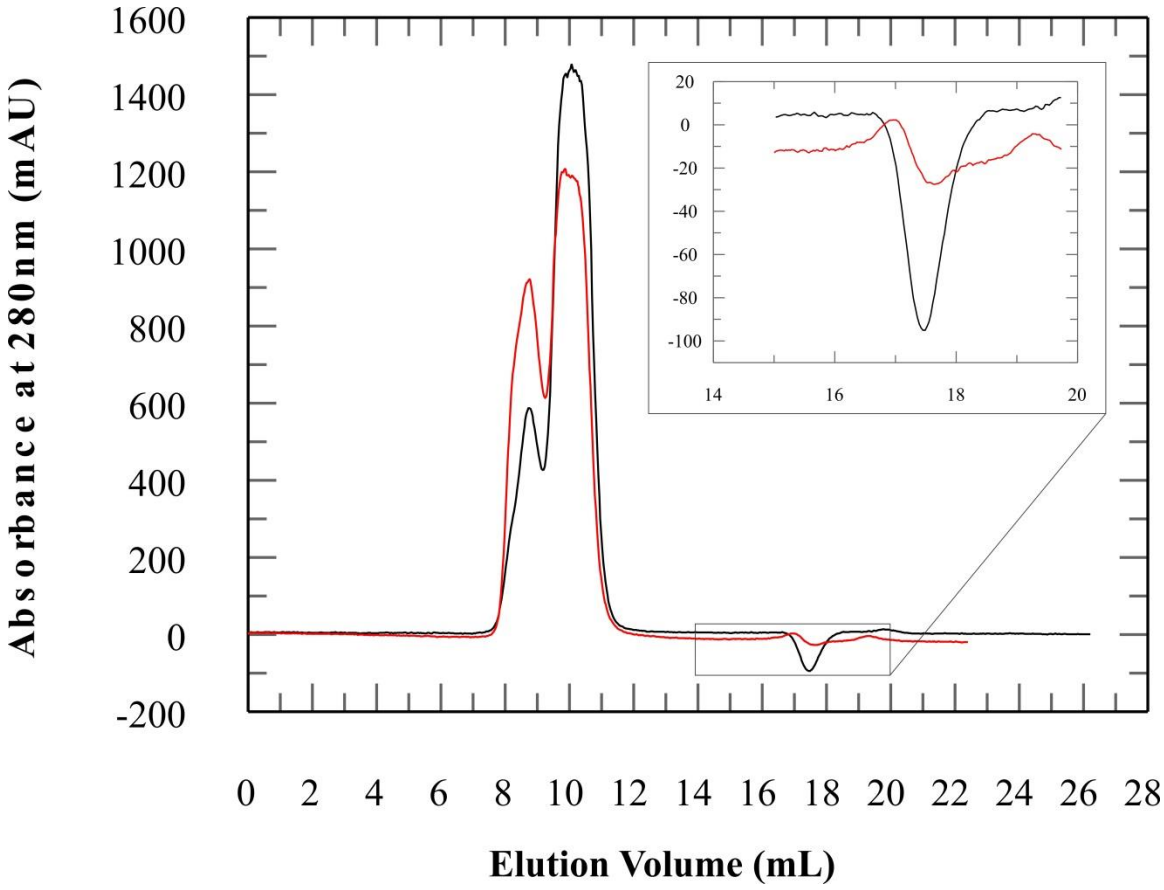

Figure 4-13. Overlay of two separate Equilibrium Gel Filtration chromatograms: 600 μM HSA (black) and 600 μM BSA (red). The HSA or BSA dimer is shown to elute at approximately 8 mL elution volume, followed by HSA or BSA monomer at approximately 10 mL, and a trough appears at the ATP elution volume of approximately 17 mL elution volume. The ATP elution (inset) appears as a trough due to ATP binding with HSA or BSA and depletion from the buffer. Equilibration buffer contained 1 mM ATP, and 1.1 mM $MgCl_2$ for both.

but it is good to be aware that there are roughly 80 types of albumin, which are commercially available.

Materials and Methods

NMR Sample Preparation

NMR samples were prepared in 5mm NMR tubes (Wilmad Labglass) with a H_2O/ D_2O (90%/10%) mixture to a final volume of 500 μL (Deuterium Oxide from Cambridge Isotope Laboratories, Inc.). Dry stocks of adenosine triphosphate, adenosine diphosphate, guanosine triphosphate, and guanosine diphosphate with sodium salts (Sigma-Aldrich) were dissolved in water, adjusted to pH 8.0 and stored at -20°C in 100 mM aliquots until ready for use. A standard pH Meter and probe were used from Beckman ϕpH Meter; Orion pH Electrode from Thermo Scientific. Samples were prepared in NMR Buffer (25 mM sodium chloride and 1 mM sodium cacodylate, pH 6.5) from a 10x stock. Sodium chloride, sodium cacodylate, lithium chloride solution (8M), magnesium chloride, 6-hydrate, manganese chloride (II) tetrahydrate were purchased from Sigma-Aldrich. Unless otherwise stated, NMR samples contained 10 mM ATP (50 μL of 100 mM stock), 11 mM $MgCl_2$ (5.5 μL of 1M $MgCl_2$ stock), 10 mM LiCl (5 μL of 1M LiCl stock), with or without 50 μM $MnCl_2$ (2.5 μL from 10 mM $MnCl_2$ stock), 50 μL D_2O, and the remaining volume up to 500 μL was NMR Buffer.

NMR Data Collection

Data were collected on either a Bruker 600 MHz AVANCE spectrometer with a Broadband Observe (BBFO) probe located at the IBBR or a Bruker 600 MHz AVANCE

spectrometer equipped with a Broadband Inverse probe located at the NIST. Datasets were collected at 283K (9.85°C), 298K (24.85°C), 300K (26.85°C), 303K (29.85°C), or 310K (36.85°C) and data are presented in the text with specific temperatures of acquisition.

Water LOGSY Experiments

One-dimensional ^{1}H NMR WaterLOGSY experiments were acquired using published methods [89]. A reference experiment was collected first, followed by the WaterLOGSY saturation transfer spectrum. Acquisition parameters for the WaterLOGSY spectra included a total digitization (TD) of 8192 points, sweep widths (sw) of 7507.507 Hz, dummy scans (DS) = 16, number of scans (NS) = 32, with a mixing time of 6.7 s. NMR spectra were processed using Bruker Topspin (version 1.3) and analyzed by electronically overlaying reference and WaterLOGSY spectra in dual display mode.

^{7}Li T1 Relaxation Measurements

One-dimensional ^{7}Li NMR inversion recovery experiments to measure T1 relaxation used the following experimental acquisition parameters unless otherwise noted in the text: pre-delay (D1) of roughly 5 times the ^{7}Li T1, which was measured at each temperature and typically exceeded 100 sec. The total digitization (TD) was 4096 points, sweep width 697.545, dummy scans (DS) = 4, number of scans (NS) = 8, with a spectrometer frequency of 233.233 MHz for lithium at 14.4 Tesla (600 MHz proton frequency spectrometer). The variable delay list was kept constant for comparable sets of

experiments but may otherwise be different depending on the expected relaxation rate (i.e. experiments at different temperatures). Spectra collected at different delay times were processed with the same zero filling to 2X the number of data points and apodized with experimental multiplication using 2.0 Hz line broadening and phase corrected based on the zero time delay of the variable delay. The lithium signal was peak picked and the peak height and integrated volume of the signal then measured and plotted for each experiment at the different variable delays. Either peak heights or volumes were then plotted and fit using a simple exponential to determine the T1 relaxation rate using Bruker Topspin 1.3 or 2.1.

^{23}Na T1 Relaxation Measurements

One-dimensional ^{23}Na NMR inversion recovery experiments to measure T1 relaxation used the following experimental acquisition parameters unless otherwise noted in the text: pre-delay (D1) of roughly 5 times the ^{23}Na T1, which was measured at each temperature. The total digitization (TD) was 2048 points, sweep width (sw) 1911.315 Hz, dummy scans (DS) = 2, number of scans (NS) = 8, with a spectrometer frequency of 232.72 MHz for lithium at 14.4 Tesla (600 MHz proton frequency spectrometer). The variable delay list was kept constant for comparable sets of experiments but may otherwise be different depending on the expected relaxation rate (i.e. experiments at different temperatures). Spectra collected at different delay times were processed with the same zero filling to 2X the number of data points and apodized with experimental multiplication using 0.30 Hz line broadening and phase corrected based on the zero time delay of the variable delay. The sodium signal was peak picked and the peak height and

integrated volume of the signal then measured and plotted for each experiment at the different variable delays. Either peak heights or volumes were then plotted and fit using a simple exponential to determine the T1 relaxation rate using Bruker Topspin 1.3 or 2.1.

^{31}P-NMR Measurements

The ^{31}P 1D experiments used a zero go pulse program with the Broadband probe tuned to 242.93 MHz for phosphorus at 14.4 Tesla (600 MHz proton frequency spectrometer), number of scans (NS) = 1024, dummy scans (DS) = 4, and total digitization (TD) = 8192. ^{31}P assignments for ATP, ADP, GTP, GDP, and triphosphate were taken from reference data in the literature.

^{1}H-NMR Measurements

The ^{1}H 1D experiments used a zero go pulse program with the Inverse probe tuned to 600.23 MHz for phosphorus at 14.4 Tesla (600 MHz proton frequency spectrometer), number of scans (NS) = 1024, dummy scans (DS) = 4, and total digitization (TD) = 8192. ^{1}H assignments for ATP were taken from reference data in the Madison Metabolomics Consortium Database [135].

Equilibrium Gel Filtration Measurements

The Equilibrium Gel Filtration technique (Hummel and Dreyer, 1962) was used to determine the dissociation constant between albumin (HSA and BSA) and ATP, in the presence of different cations (Na^+, Mg^{2+}, and/or Li^+). An FPLC HiLoad 16/60 Superdex 75 gel filtration column (GE Healthcare Life Sciences) was either equilibrated in running

buffer containing 137 mM NaCl, 2.7 mM KCl, 4.3 mM Na_2HPO_4, and 1.4 mM KH_2PO_4 and or NMR buffer, mentioned in the NMR Sample Preparation section (above), with ATP and Magnesium concentrations specified in the data figure at either 4°C or ambient temperature. Then, different concentrations of albumin were incubated in the running buffer for a minimum of 10 minutes at room temperature, but were sometimes stored at 4°C for up to 1 week. Following the incubation, the sample was loaded onto the column. The FPLC traces were followed using UV detection at 260nm and 280nm wavelength with two different detectors and the peak volumes from the traces were determined to qualitatively estimate binding affinities.

Chapter 5

Purine Receptor Explored for Functional Modulation by Interaction with ATP·Mg·Li Ternary Complex

P2X Receptor Background

The modulation of membrane receptor response by ATP·Mg·Li observed in the neuronal cell assay, discussed in Chapter 3, sparked an interest in exploring the potential therapeutic action of Li^+ with cell surface receptors. It was reasoned that if the ATP·Mg·Li model is reflective of the physiological activity of Li^+, then a receptor that requires ATP·Mg ligand binding, but not hydrolysis, for activation would be an ideal protein to test this hypothesis of lithium's mechanism of action.

ATP-activated purinergic (P2) receptors are involved in a diverse range of functions, including cardiopulmonary coordination, neuronal excitability, hearing, vision, pain, bacterial infection and cancer [136]. P2 receptors are ordered into two subclasses, P2X and P2Y, based on their structure and mechanism of signal transmission, where P2X receptors are ligand-gated ion channels and P2Y receptors are G-protein coupled receptors. P2X receptors respond to nerve damage by stimulating pain and inflammation responses [137]. In the P2X subclass, there are seven types: $P2X_1$, $P2X_2$, $P2X_3$, $P2X_4$, $P2X_5$, $P2X_6$, and $P2X_7$ (Table 5-1). All of these ion channels have a similar basic architecture: intracellular amino- and carboxy-termini, a long extracellular loop, and two transmembrane spanning domains. Within this family, the sequences are highly conserved, including ten cysteine residues in the extracellular loop, which are presumed to provide stability between subunits of P2X homo- and heterotrimers [138]. Sodium, potassium, and calcium ions flow through the ATP-activated pore opening of the P2X receptor [139].

P2X receptor activation is sensitive to the structure of the agonist and studies have been performed using ATP analogs and other nucleotides. For example, 2'- and

P2X Subclass	Monomer Length (Amino Acids)	Carboxyl-Tail Length (Amino Acids)	Pore Dilation	Channel Current Decay	EC_{50} (μM) of ATP
$P2X_1$	399	45	No	Fast (< 1 s)	0.07
$P2X_2$	472	119	Yes	Slow (> 20 s)	1.2
$P2X_3$	393	53	No	Fast (< 1 s)	0.5
$P2X_4$	389	31	Yes	Slow (> 20 s)	10
$P2X_5$	455	96	-	Slow (> 20 s)	10
$P2X_6$	379	26	-	Slow (> 20 s)	12
$P2X_7$	595	239	Yes	Slow (> 20 s)	100

Table 5-1. Properties of the seven homomeric subclasses of the P2X family of purinergic ligand-gated ion channels [140-142]. Pore dilation refers to the larger ion channel opening upon prolonged or repeated stimulation by the agonist. Channel current decay refers to the desensitization of the channel to the agonist as recorded by electrophysiology. EC_{50} is the concentration of the agonist at 50% of the maximum response or effectiveness of the receptor to the agonist, in this case ATP.

3'-O-(4-benzoyl-benzoyl)-ATP (BzATP) as a mix of isomers with an EC_{50} of 20 μM is a stronger activator than ATP with EC_{50} of >100 μM [136]. Uridine 5'-triphosphate (UTP) and α, β-methylene-adenosine 5'-triphosphate (α,β-me-ATP) are less potent agonists than ATP [143]. Furthermore, differences in P2X activation and response time for desensitization are observed across different P2X subclasses. Fully ionized, free ATP activates all P2X receptor channels to various degrees and the channels return to steady state at different rates. The addition of magnesium results in activation for some channels and does not activate other channels [144]. Given this evidence, it is plausible that the presence of lithium at the ATP site on P2X would produce a significant change in receptor activity.

Among the seven known P2X receptors, the $P2X_7$ receptor in macrophages uniquely functions through the release of pro-inflammatory cytokines, like interleukin-1β (IL-1β).[137] In this respect, it is interesting to note that bipolar disorder causes atrophy of brain tissue, which is proposed to be a result of inflammation [145]. One typical side effect of neurodegeneration or neuroinflammation is the cell's release of ATP, acting as a neurotransmitter to signal distress to neighboring cells [146]. This extracellular ATP (eATP) is known to have this important signaling role in nervous, vascular, and immune systems [147]. By regulating calcium influx, eATP-activated $P2X_7$ mediates the release of the IL-1β to respond to inflammation, thereby inducing cell lysis in neurons. Thus, $P2X_7$ is the focus of many current drug discovery efforts as a therapeutic target for neurodegenerative diseases [148].

Linkage analysis by Nicholas Barden and colleagues suggested a strong association of bipolar families with a SNP in the *P2RX7* gene which encodes $P2X_7$, resulting in a

glutamine to arginine amino acid change in the intracellular carboxy-terminus at position 460, genetically associating the $P2X_7$ receptor with bipolar disorder [47]. Although this claim was refuted by one study [149], a number of reports have confirmed the allelic association between SNPs in the *P2RX7* gene and bipolar disorder [150-153]. This genetic linkage has also been reported between *P2RX7* and major depressive disorder (MDD) [46, 154].

In addition to a genetic connection between $P2X_7$ and bipolar disorder, $P2X_7$ has a stronger sensitivity to metal binding than other P2X receptor channels. Zinc and copper have been found to completely inhibit $P2X_7$; these metals only partially inhibit other members of the P2X family. In addition, calcium and magnesium have been shown to regulate $P2X_7$ in an allosteric manner by binding to ATP [138].

The structure of $P2X_7$ has not yet been determined. However, there is a 45 percent sequence identity between $P2X_7$ and $P2X_4$ and, based on structure homology modeling, it is likely that the two proteins adopt similar structures [155]. A crystal structure of zebrafish $P2X_4$ receptor in the absence of ATP was solved at 3.1 Å resolution (Figure 5-1; Figure 5-2). This closed-channel structure, which is the resting state, is a homotrimer and forms an 'hourglass-like' shape with six transmembrane α-helices, two per monomer [156]. A different construct of the zebrafish $P2X_4$ receptor, designed with several carboxy-terminal deletions, yielded an ATP-bound crystal structure at 2.8 Å resolution. This structure revealed that three ATP molecules bind to this P2X receptor in a hydrophilic pocket located between two monomers. This unique pocket, unlike other ATP-binding motifs of proteins, binds ATP in the 'anti' conformation where it adopts a

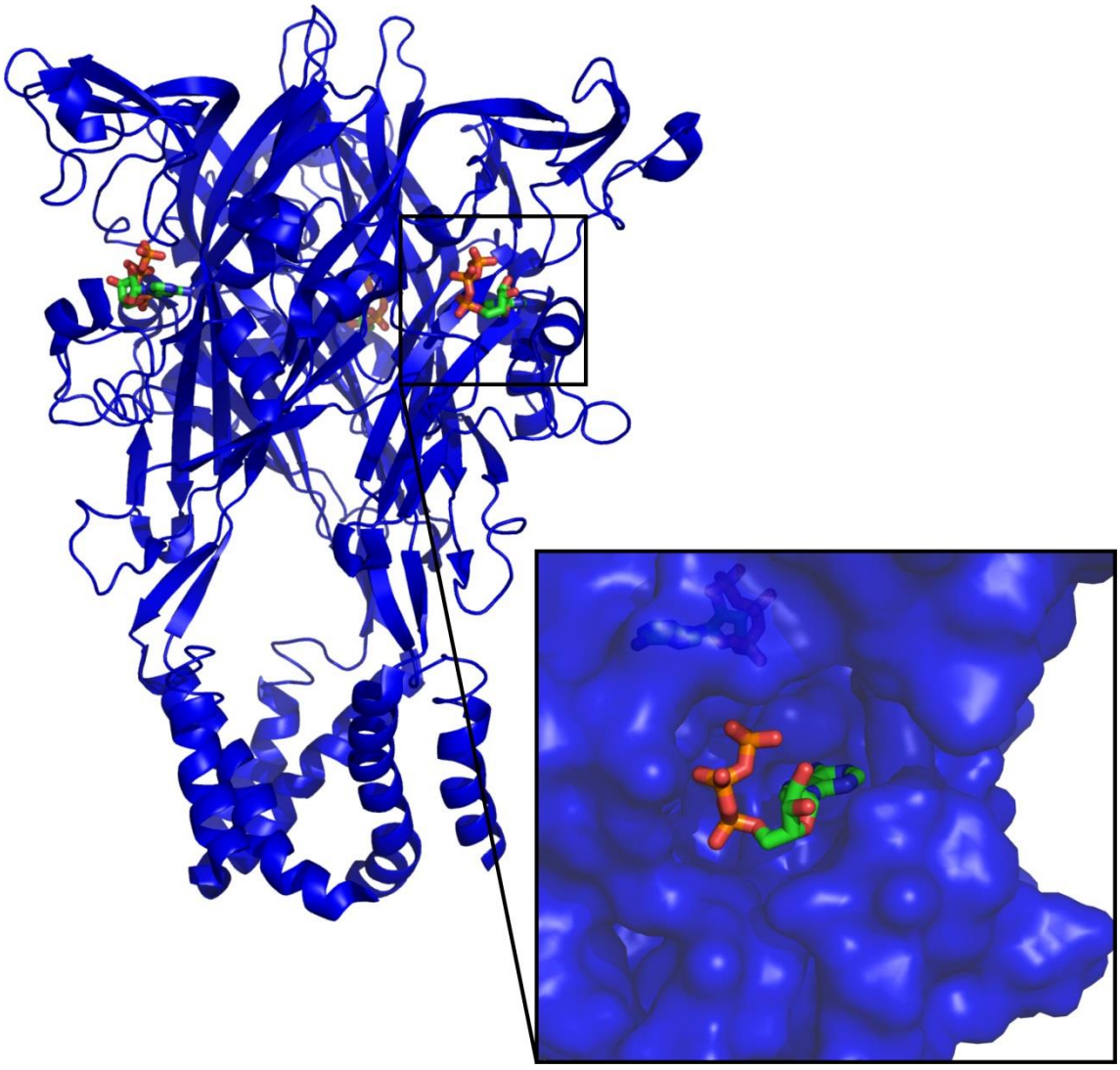

Figure 5-1. Zebrafish $P2X_4$ is shown as a ribbon diagram (blue) to highlight the three ATP molecules bound. The inset displays a closer view of ATP bound to $P2X_4$. The coordinates for this protein structure were retrieved from the PDB, entry 4DW1. The image was rendered in PyMol.

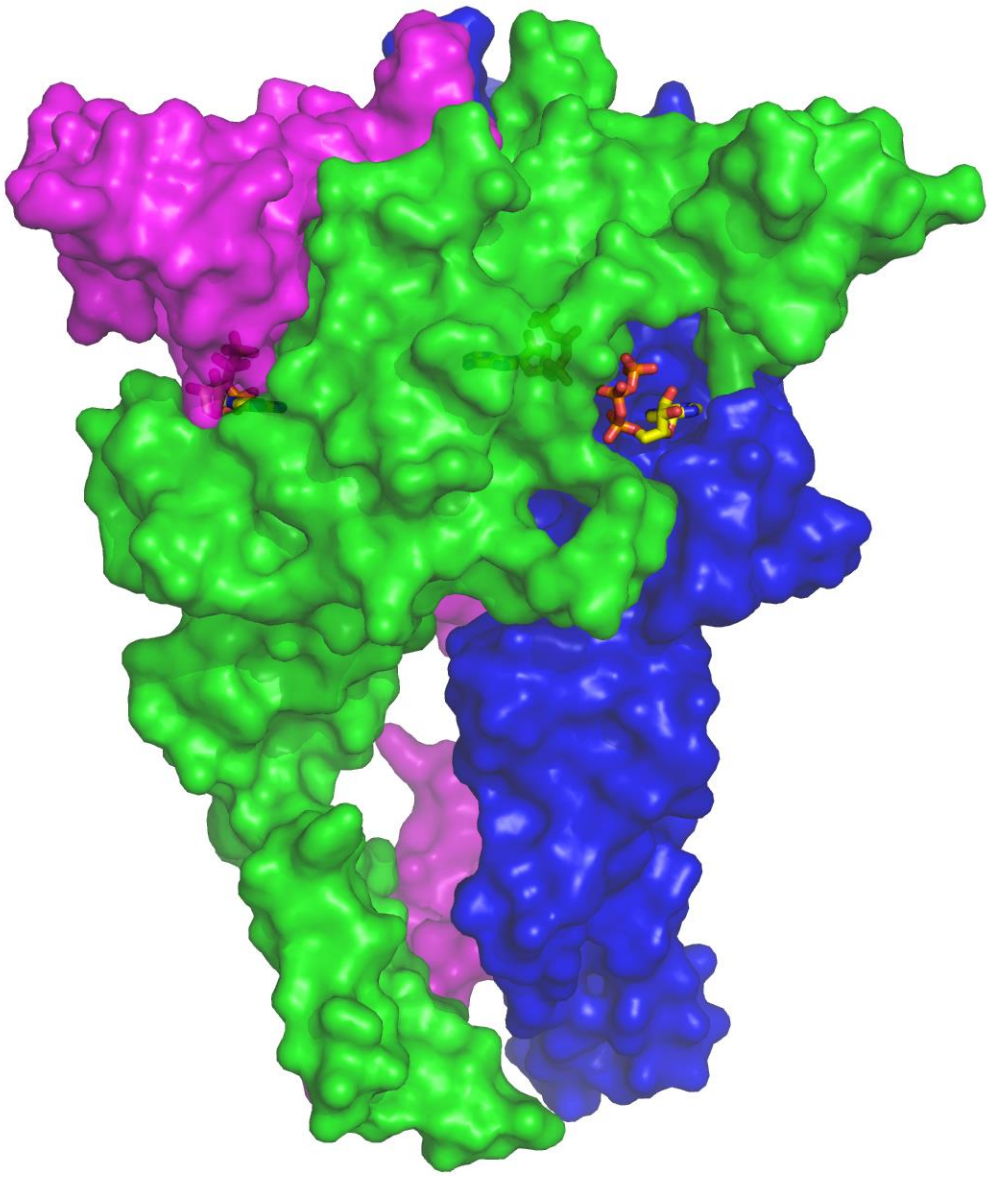

Figure 5-2. The trimer structure of the zebrafish $P2X_4$ is shown with the monomers in green, blue, and purple. An ATP is bound at the interface of two monomers, for a total of 3 ATP molecules. The coordinates for this protein structure were retrieved from the PDB entry 4DW1, and the image was rendered in PyMol.

‘scorpion-like’ shape, with the β- and γ-phosphates folded back toward the adenosine. The phosphates are still partially solvent exposed and interact with glycerol, which was present as part of the crystallization conditions. It is proposed that under physiological conditions, the glycerol would be replaced with water molecules. The phosphate oxygens interact with four lysines and one arginine [157]. The structure of ATP in this extracellular receptor pocket is ideal for the stable formation of Mg·Li binding and water coordination.

Amongst the P2X family, the $P2X_7$ receptor has the longest sequence at 595 amino acids, with the longest intracellular C-terminal tail. The $P2X_7$ receptor channel opens with short stimulation by ATP and also forms a larger membrane pore upon prolonged or repeated ATP binding. This pore activates signaling events in inflammation and cell death, as well as mitochondrial and cytoskeleton alterations. Pore formation is also reversible [138, 158].

In my work, the $P2X_7$ receptor was chosen to test the functional and structural consequences of a ternary complex of ATP·Mg·Li because of its genetic association with bipolar disorder, sensitivity to metals, and role in inflammation. However, it remains very likely that, if a similar ATP pocket exists in all the subclasses of P2X channels, the ATP·Mg·Li ternary complex may modulate to various extents all P2X receptors in a similar binding mode. If this is true, it remains possible that the lithium modulation would result in different functional outcomes for each receptor due to variation in P2X subclass receptor functions. The P2X receptor, or one of the P2X receptors, may be the primary therapeutic target of lithium. To my knowledge, this research is the first to explore the P2X receptor as a therapeutic target of lithium.

Experimental Approach

NMR and fluorescence experiments were planned for testing the ATP-Mg-Li ternary complex on both $P2X_7$ in cell membranes and detergent-solubilized $P2X_7$ protein. A plan for the expression, purification, and detergent-solubilization of the $P2X_7$ protein was developed using methods outlined in the $P2X_4$ crystal structure publication by Kawate, et al. as a guide [156]. Heterologous bacterial expression was not a practical option because of the post-translational modifications on the human $P2X_7$ protein. Instead, a protocol for protein expression in Spodoptera frugiperda 9 (Sf9) cells was designed. Sf9 cells are particularly susceptible to a virus called Autographa california Nuclear Polyhedrosis (AcNPV) baculovirus. As such, baculovirus expression systems harness the virus for expressing a recombinant protein of interest in Sf9 cells (Figure 5-3). A bacterial plasmid containing the gene of interest is inserted into viral DNA and transfects the host insect Sf9 cells. The Sf9 cells infected with the amplified virus produce the protein of interest (BD Biosciences Pharmingen™ BaculoGold Linearized Baculovirus DNA).

P2X7 Protein Production

The $P2X_7$ receptor was designed to have a terminal hexa-histidine-tag, consisting of codons for 6 histidines. At the start of these experiments, there were no commercially available $P2X_7$-specific antibodies. The histidine-tag was both to facilitate detection by His-antibody with a secondary antibody reporter on a Western blot and to purify by an immobilized metal ion affinity chromatography (IMAC). A TEV-protease site was incorporated for cleavage of the histidine tag during purification. Three different protein

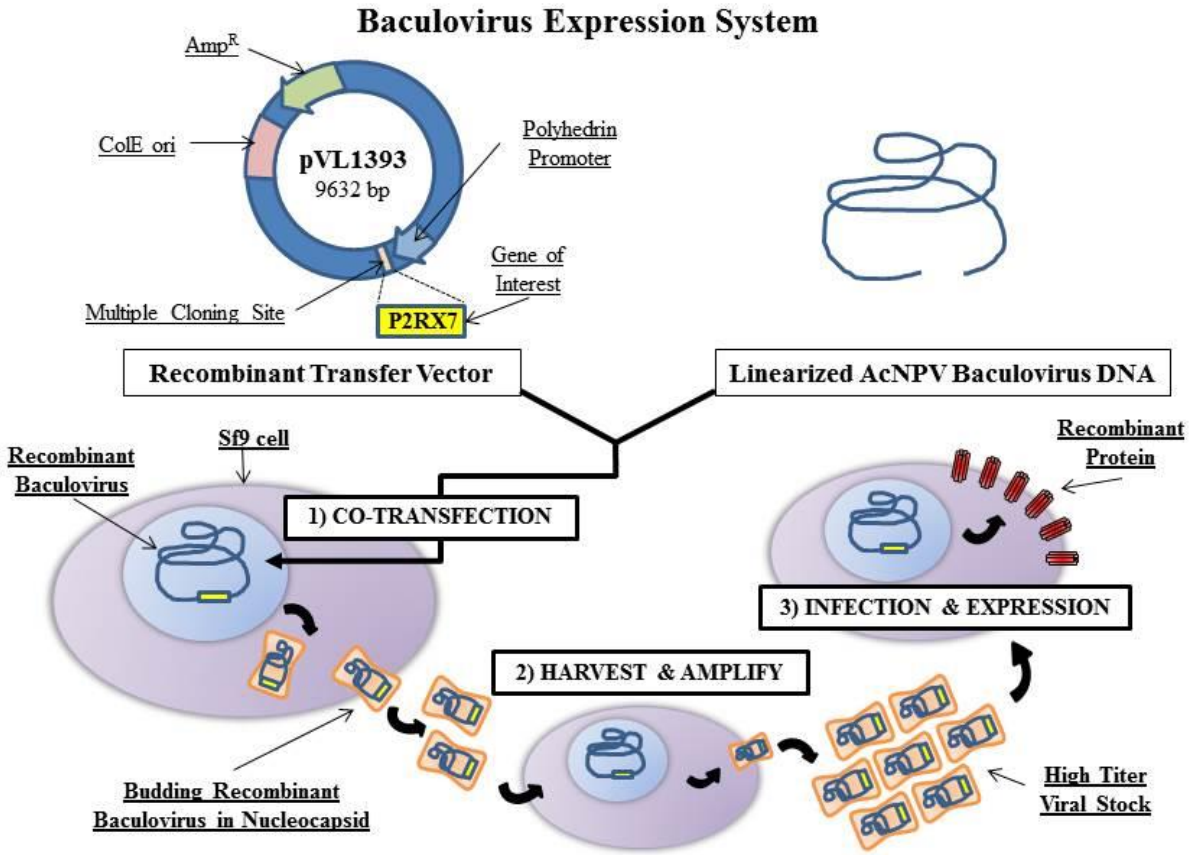

Figure 5-3. Baculovirus Expression System illustrating the three main steps towards protein expression in Sf9 cells: Co-transfection, Amplification, and Expression.

constructs were designed: full-length $P2X_7$, $P2X_7$ without the two transmembrane domains, and $P2X_7$ without the intracellular carboxy-terminus. The gene for the full-length construct was cloned into the pFastBac vector (GeneArt®, Thermo Fisher Scientific, Inc.).

The pFastBac plasmid containing the full-length *P2RX7* gene was transformed into DH5α Escherichia coli (E. coli) cells and the cells were grown in LB containing Ampicillin antibiotic. Plasmid DNA was obtained by mini prep purification (Qiagen) and the presence of the gene insert in the plasmid was confirmed by restriction enzyme digestion followed by agarose gel analysis and ethidium bromide staining.

In preparation for transfection into Sf9 cells, the *P2RX7* gene was then cloned into the pVL1393 vector, which is compatible with the BD Biosciences baculovirus expression system, BaculoGold™. PCR primers were designed to amplify the full-length construct gene contained in the pFastBac plasmid. The pVL1393 vector and PCR product were separately digested with restriction enzymes and purified, and then ligated to generate the desired recombinant plasmid. The plasmid was transformed into DH5α cells and purified plasmid was obtained as described above, and the sequence of the gene insert was confirmed by dideoxy DNA sequencing (Macrogen).

The pVL1393 plasmid containing the *P2RX7* gene of interest and was then used for protein expression in the insect cells. Sf9 cells were cultured to a cell density of approximately 0.8 million cells. Cell density was estimated using a hemacytometer under a microscope. The baculovirus expression protocol was initiated by seeding approximately 0.8 million Sf9 cells in mini petri dishes (BD Biosciences BaculoGold™). Sf9 cell adhesion to the plate surface was achieved after 10 minutes. Co-transfection of

pVL1393 transfer vector, containing the polyhedron promoter, and the linearized baculoviral DNA, lacking a gene adjacent to the polyhedron locus, provided a viable recombinant virus by homologous recombination within the host cell. The 'P1' is the result of incubating the first round of host cells with the baculovirus for a period of 5 days at 27°C. However, at that point, the cells were observed to be mostly dead. Since the cells should still be viable at this point, the plasmid was checked on an agarose gel, and transfection grade plasmid purification followed.

Co-transfection of Sf9 cells was repeated using the re-purified pVL1393 plasmid and linearized viral DNA. After 5 days, the supernatant was collected, presumably containing the amplified virus. A dilution assay with Sf9 cells was conducted to determine the potency of the virus with increasing concentration of virus in 12 wells of a 24 well plate. The first 5 wells contained increasing concentration of an empty vector control, and the second row of 5 wells contained increasing concentration of 'P1' supernatant containing *P2RX7*-inserted baculovirus. Two wells had no addition of baculoviral DNA to compare the healthy Sf9 cells with the infected cells. Wells containing lower concentrations of baculovirus resulted in a healthy appearance in shape but high density, while at higher concentration, the cell morphology changed to hexagonal shapes. To determine whether the $P2X_7$ membrane protein was expressed on the Sf9 cell surface, causing this hexagonal morphology, the cells in latter wells were collected and a Western blot was run. The Western blot was inconclusive, as neither the Sf9 cells nor the positive control produced a detectable signal. The Western blots were stripped of the antibodies and re-incubated with anti-Histidine antibody followed by the secondary antibody conjugated to horseradish peroxidase (HRP), with the same result.

SDS-PAGE for the Western blot was repeated with increased cell lysate volume, but there was no detectable signal produced by the ECL chemiluminescence system of HRP-luminol secondary antibody from either the His-tag on the $P2X_7$ or the His-tag on the control protein. Before proceeding further, the ECL chemiluminescene reagents and the primary His-antibody were tested using two control proteins containing histidine-tags (Figure 5-4). Three identical Western blots, containing the same two proteins each, tested the Histidine-tag primary antibody in the first blot, and the HRP-luminol system in the second and third blots. The controls confirmed that the Western blot detection reagents, secondary antibody conjugated with HRP reacting with luminol, function sufficiently because the two protein-specific primary antibodies produced a detectable signal by this HRP-luminol system. However, even after a long exposure period, no detectable signal was produced by HRP-luminol when the two proteins were incubated with the Histidine-tag primary antibody in the first blot. The Histidine-antibody method for detection was reassessed. Perhaps the His-antibody was a bad batch from the company, not nearly as sensitive as it claimed to be, or did not bind tightly enough to the secondary antibody. Regardless, $P2X_7$ protein expression on the Sf9 cells was not verifiable by the method engineered for detection.

It was reasoned that a large yield of protein, purified by IMAC and size exclusion chromatography (SEC), would be detectable by SDS-PAGE and NMR. Co-transfection of a new batch of Sf9 cells was initiated to advance baculovirus expression to the stages of scale-up without stopping to detect $P2X_7$ by Western blot. The supernatant containing the baculovirus from the first 1 mL of cells, ‘P1’, was used to infect the 5 mL of cells in a

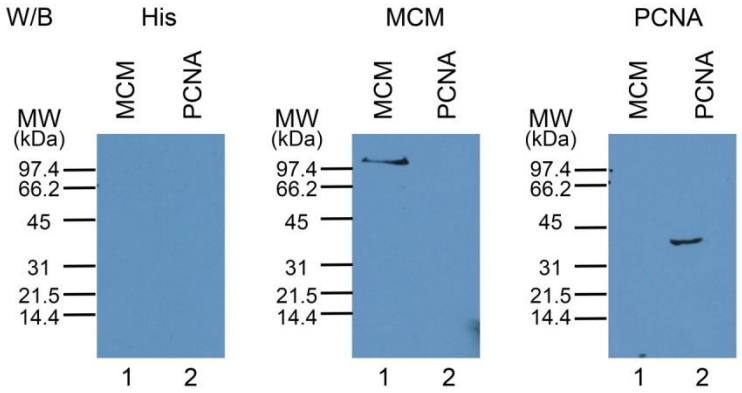

Figure 5-4. Three western blots of two proteins with His-tags, MCM and PCNA. Detection by His-tag antibody, MCM antibody, and PCNA Antibody are shown in that order (L-R).

T-25 tissue culture flask, ‘P2’. Likewise, the P2 supernatant was used to infect 30 mL of cells in a T-150 tissue culture flask, ‘P3’. Finally, the ‘P3’ infected a flask of 120 mL cells in suspension. These cells were collected, centrifuged, separated from the supernatant, and lysed. Purification of the cells continued with sonication, centrifugation, solubilization in n-dodecyl-β-o-maltoside (DDM) detergent and protein separation by nickel-charged IMAC. SDS-PAGE of the column eluent and crude cell membrane provided no obvious indication of $P2X_7$ presence.

In one final attempt, fresh Sf9 cells were cultured in a new cell culture facility equipped with a new orbital shaker, incubator, and biological safety cabinet. The sterile cell culture room was dedicated to this project in order to determine if there were other factors that may be playing a role in protein expression. After a few days of transition to the new environment, Sf9 cells were co-transfected with baculovirus DNA and *P2RX7* transfer vector. A suspension Sf9 cell culture were infected by the ‘P3’ baculovirus-containing supernatant. Following previously mentioned protocol, solubilization of these cell membranes, presumed to have expressed recombinant $P2X_7$, were purified over a nickel column. SDS-PAGE revealed no obvious dark band with the protein of interest at the molecular weight where we would expect it to appear. A second gel with the same contents as the first was blotted onto nitrocellulose and the Western blot was also inconclusive because no bands were visible.

In the time frame this work was being carried out, the $P2X_7$-antibody was made commercially available and was promptly ordered. However, $P2X_7$ expression in the Sf9 cells was still not detected by Western blot.

The recombinant baculovirus was collected to confirm that the *P2RX7* was inserted into the linearized baculovirus DNA. PCR primers were designed to anneal to the baculovirus flanking the *P2RX7* gene of interest as well as viral DNA. PCR was conducted on the Sf9 baculovirus with *P2RX7* insert, and two controls: the baculovirus without *P2RX7*, and the purified plasmid, pVL1393 containing *P2RX7* (Figure 5-5). The baculovirus with *P2RX7* in Lane 1 of the agarose gel confirmed that the baculovirus contains the *P2RX7* insert. The control, baculovirus lacking *P2RX7*, in lane 2 shows no band, as expected, while the purified plasmid, in lane 3, shows a band at approximately the same migration point as in lane 1. This also indicates that the problem with $P2X_7$ expression may not be at the phase of viral amplification.

Challenges in the expression of $P2X_7$ prevented moving forward in the research of the ternary ATP-Mg-Li complex. Several potential reasons may be given for expression difficulties with this membrane protein. Human $P2X_7$ may be synthesized by the ribosome in Sf9 cells and identified as 'foreign', triggering ubiquitinylation and degradation by proteases. It could also emerge from the ribosome misfolded, leading to degradation by the host cell. The aggregation of $P2X_7$ could form insoluble inclusion bodies within the cell. However, if this were the case, there should have been a dark band in the cell lysate. Low protein yield is also a possibility, but it would have to be very low to be below the detection of the secondary antibody-HRP, which can detect as little as 1 picogram of protein. A compounding issue may be poor translocation of $P2X_7$ to the membrane. If the protein fails to be imbedded into the cell membrane, cytoplasmic conditions may also cause $P2X_7$ to be misfolded and degraded.

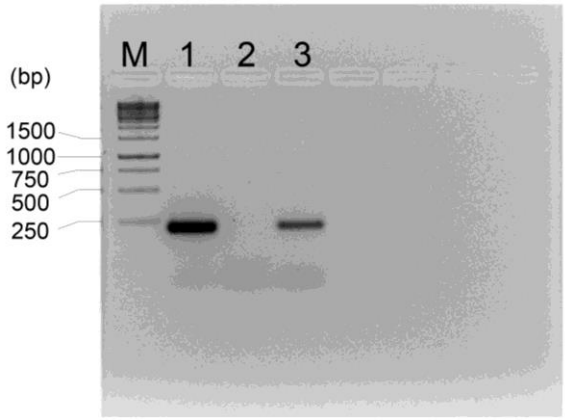

Figure 5-5. Agarose gel of digested baculovirus or recombinant plasmid; Lane 1 contains the digested baculovirus containing the *P2XR7* insert. Lane 2 contains baculovirus lacking *P2RX7*. Lane 3 shows a digestion of purified recombinant plasmid containing the *P2RX7* gene. A DNA ladder is used as a marker, labeled 'M'.

This chapter summarized the strides made in protein production and purification toward reaching the goal of NMR measurements with purified $P2X_7$. There are several ways to move this project forward. Cellular studies on $P2X_7$ have been published, but methods to purify and isolate $P2X_7$ have not yet been reported. It was reasoned that the expression of $P2X_7$ would be similar enough to the published methods of isolation of the zebrafish $P2X_4$ to yield enough protein for the purposes of this research. $P2X_7$ was preferred for this Li^+ research because of its genetic association with bipolar disorder. In hindsight, it would have been better to express $P2X_4$ because it has already been expressed and isolated, rather than $P2X_7$. The expression of membrane proteins is not trivial and the differences between members of the P2X family and possibly also between species were large enough to prevent expression of $P2X_7$. The current timeframe for developing methods for expressing purified membrane proteins for crystallography can be up to 10 years or more. Since this project is focused on measuring Li^+ interactions and not structure determination, it would be best to proceed with expressing the well characterized protein, zebrafish $P2X_4$, by closely following the published protocol from the Gouaux lab. That includes engineering a construct with an octahistidine affinity tag and mutating glycosylation sites, as well as using a cobalt IMAC column [156, 157]. Expression of zebrafish $P2X_4$ would also confirm that the Sf9 baculovirus method works in our laboratory setting. The $P2X_4$ results could be mapped through homology modeling to the $P2X_7$ receptor for comparison.

Chapter 6

A New Molecular Hypothesis for Lithium Mechanism of Action

There is a wealth of research showing cellular, biological, and clinical effects of Li^+. A recent review thoroughly summarizes the possible targets of Li^+ in BD from the clinical and cognitive levels down to the cellular levels [159]. The actions of Li^+ are diverse and seemingly unrelated to one another. Li^+ appears to be a magical drug, enabling patients afflicted with BD to maintain a life without debilitating mood changes. It is mysteriously able to balance both the highs of mania and lows of depression. Yet, Li^+'s unknown mechanism makes it difficult to understand biologically, which hinders drug discovery efforts from engineering a more effective and ideal BD drug without the dangers of toxicity, annoyance of side effects, and harm of long term tissue damage that exist with Li^+ treatment.

Evidence for a Bimetallic ATP Complex Model for Lithium's Mechanism of Action

New physiochemical evidence supports a co-binding, synergistic model of Li^+ action rather than one of direct competition with magnesium or other naturally occurring metal cation co-factors. NMR experiments which measure nuclear relaxation and employ paramagnetic relaxation enhancement techniques have provided direct physical evidence for the formation of a Nucleotide·Li·Mg ternary complex where Li^+ co-localizes with Mg^{2+} on the triphosphates of the nucleotide (refer to Chapter 3). In addition, the measured binding affinity of Li^+ to Nucleotide·Mg complexes has been found to be in the low millimolar range, which is within physiologically relevant concentrations (refer to Chapter 3). This new model is built upon an old hypothesis. Prior to this recent physical evidence, indirect evidence pointed to the possibility of the formation of such a complex. In 1976, Dr. Nicholas Birch responded to Dr. Frausto da Silva's 'conditional binding' hypothesis , which proposed the idea that Li^+ acts by challenging common biological

cations, with an assertion that one complication to the explanation for their findings had not been considered. This complication was the possibility that Li^+ forms a complex with the ATP, which was only considered by da Silva to be a benign sequestering agent for Mg^{2+} [99, 102]. Birch added that he had preliminary unpublished evidence for a ternary ADP·Mg·Li complex [102]. Further gel filtration equilibrium binding experiments carried out by Birch revealed co-incident elution peaks of ADP, Mg^{2+}, and Li^+ suggesting that Li^+ and Mg^{2+} are similar enough to interfere at sites on nucleotides, where Mg^{2+} is located, but that direct competition of Mg^{2+} by Li^+ on nucleotides was not observed [101]. It was proposed that a ternary complex might be possible, but further physical evidence was necessary [102]. Now that direct physical evidence exists for nucleotide·Mg·Li complexes, current biological and pharmacokinetic observations of Li^+ action can be reevaluated with this model as the basis for the molecular mechanism of Li^+ action. While not directly identifying the target of Li^+ in its action as a mood disorder drug, a better understanding of Li^+'s molecular mechanism of action and more accurate biological hypotheses of the therapeutic action of Li^+ could lead to a more targeted approach to new drug development for BD and give clues to the pathophysiology of BD.

Building a Unified Hypothesis of Lithium action: Biological Targets of Lithium through the Prism of the ATP·Mg·Li Model

The biological targets of Li^+ can be reexamined with the new evidence for a bimetallic ATP complex to see that Li^+ may act not only as a simple ion, but as a molecular entity (Figure 6-1). The ternary complex of ATP·Mg·Li may help to explain how Li^+ inhibits previously identified enzyme targets of the ion, such as Glycogen

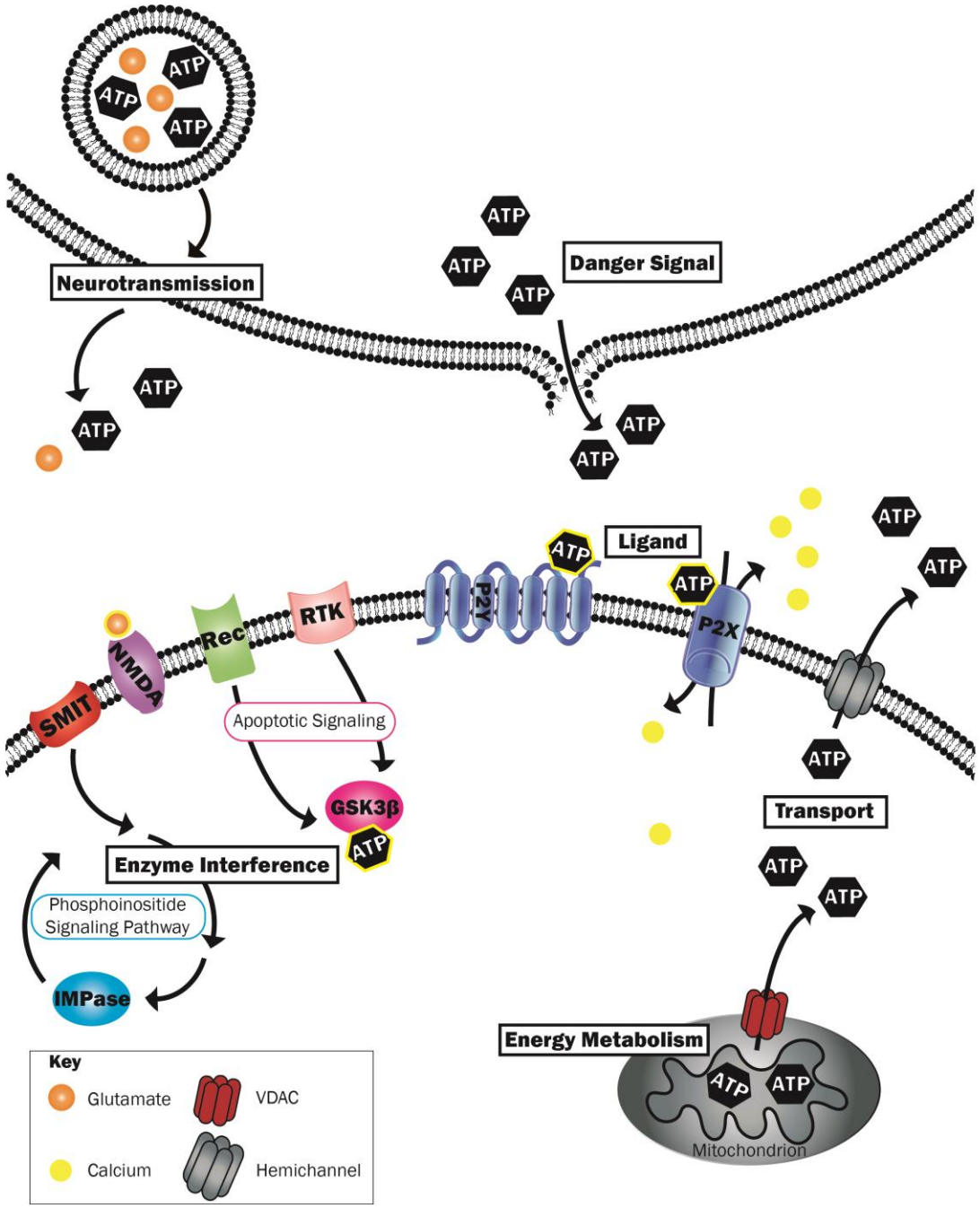

Figure 6-1. Summary of ATP functions that may play a role in the molecular mechanism of Li^+ action as an ATP·Mg·Li complex. ATP acts as a neurotransmitter, danger signal during cell death, ligand to receptors and other proteins, and transporter of metals. ATP is metabolized and provides cellular energy for enzymatic reactions. *ATP*, adenosine triphosphate; *GSK3β*, glycogen synthase kinase 3β; *IMPase*, inositol monophosphatase; *NMDA*, N-methyl-D-aspartate receptor; *P2X*, ligand-gated ion channel purine receptor; *P2Y*, G-protein coupled purine receptor; *Rec*, receptor; *RTK*, receptor tyrosine kinase; *SMIT*, sodium myo-inositol transporter; *VDAC*, voltage-dependent anion channel.

Synthase Kinase-3β (GSK-3β) [160], as well as some of the cellular and clinical neuroprotective effects observed for Li^+, as in danger signaling during cell damage and cell death and inflammation. In addition, the physiological roles of ATP also point to new biological targets such as purine receptors, neurotransmission, and mitochondria as sites for Li^+ action. The lens of the ATP·Mg·Li complex can focus where to look for Li^+ effects across a number of identified and yet to be identified targets, and guide how studies of these systems can be interpreted with the goal of better understanding Li^+'s therapeutic efficacy.

ATP as a Ligand:Receptor Activation Altered by the Mg·Li Complex with ATP

The evidence of Mg·Li co-binding on ATP prompts a reconsideration of how Li^+ might have an effect at nucleotide ligand sites. Purine ligands, ATP or ADP, bind and activate cell surface purine receptors, P2, of which there are two subtypes, P2X and P2Y, ligand-gated ion channels and G-protein coupled receptors, respectively [161]. The seven members of the P2X family each appear to serve various specific purposes, ranging from sensory signaling such as pain, taste, and bladder filling, to roles in inflammation, and are located on different types of cells. One of the functions of this receptor family, in particular the $P2X_7$ receptor found on immune cells (i.e., mast cells, macrophages, microglia, and dendritic cells), is to facilitate inflammatory signaling (see Chapter 5) [162].

Li^+ may effect changes in these receptors. In fact, long term damage or negative side effects of Li^+ treatment, such as nephrogenic diabetes insipidus (NDI), may be due to Li^+ affecting purinergic signaling. Lithium-induced NDI causes ATP-activated purine receptors, such as $P2Y_2$, to increase renal prostaglandin (PGE_2), which dampens

vasopressin, a hormone responsible for retaining water and constricting blood vessels [163]. In addition, renal P2X receptors regulate ion and water transport and are vital to maintaining physiological electrolyte balance [164].

Potassium channels are also inhibited by Li^+ [165]. ATP-sensitive potassium channels affect memory and learning in mice and Li^+ appears to improve memory [165]. These ATP-sensitive potassium channels in the pre-synaptic neuron also mediate neuromuscular transmission and muscle contraction, but are inhibited by LiCl [166].

There is an indication that these receptors are sensitive to changes in the chemical structure of ATP. Differential modulation of the $P2X_7$ receptor is seen with ATP analogs as the activating ligand. For example, ATP analogs such as BzATP, 2MeSATP, MeATP, ATPγS, and ADP activate or inactivate the receptor to varying degrees [136, 158]. More subtly, whole cell patch-clamp electrophysiology recordings reveal modulation of P2X receptors to various degrees in response to ATP and ATP analogs depending on the P2X subtype [144]. Similarly, Mg·Li may co-bind to ATP acting as a ligand to a receptor and elicit a change in cellular signaling.

ATP as a Danger Signal: Mg·Li Complexes with ATP May Alter the Signal Mediation and Induce Neuroprotection

Extracellular ATP (eATP) activates cellular receptors to signal that the cell is in distress. Though the details of processes leading to and sustaining the eATP release in local high concentrations to convey a danger signal are not well understood, purine receptors and adenosine receptors are responsible for responding to this signal, while ectonucleotidases, which cause the breakdown of ATP, help to regulate the response with

anti-inflammatory signaling [167]. In a mouse model of pulmonary fibrosis, eATP activates $P2X_7$ and Pannexin-1 membrane channels, promoting IL-1β maturation, pulmonary inflammation and eventually fibrosis, or scarring of lung tissue [168]. Inflammation is thought to play a role in the pathophysiology of BD, although it is not well understood [158]. To that point, in vitro, in vivo, and clinical studies support the notion that Li is neuroprotective and prevents cell death. ATP-induced cell death in rat hippocampal brain slices was significantly decreased upon the co-incubation with Li^+ and ATP compared to ATP alone [169]. Intracellular ATP plays a role in danger signaling as well. In particular, apoptosis requires ATP, and ATP depletion creates a bioenergetics vacuum leading to the release of cellular contents, inflammation, and necrosis [170, 171]. One could argue that the concentration and function of ATP, both extracellular and intracellular, that is normally involved in danger signaling could again be altered by forming a complex with Mg·Li, which, in turn, could dampen inflammation signaling and/or prevent apoptosis, and thereby propagate a neuroprotective effect.

ATP as an Energy Source: Mg·Li Complexes with ATP may Cause Changes in Metabolism

The cell danger response is intricately balanced to minimize unnecessary damage while responding to the immediate problem. When the response mechanisms are functioning abnormally, the cellular components, such as metabolites, that drive the danger signal are disrupted. A series of disorders and chronic illnesses are the result of abnormal maintenance of cellular metabolism resulting in aberrant cell danger signaling. These include attention deficit hyperactivity disorder (ADHD), BD, schizophrenia, post-

traumatic stress disorder (PTSD), chronic traumatic encephalopathy (CTE), epilepsy, diabetes, and Alzheimer's and Parkinson's diseases [167].

Metabolic energy is largely provided through ATP production by oxidative phosphorylation at the inner mitochondrial membrane. In the mitochondrial matrix, citric acid cycle products (reduced nicotinamide-adenine dinucleotide (NADH) and Flavin-adenine dinucleotide ($FADH_2$)) become the substrates for oxidation in the electron transport chain, resulting in a proton gradient that fuels ATP synthase through chemiosmosis to phosphorylate ADP, thus producing ATP [172]. Since ATP provides much of the cell's energy, mitochondria are essential for cell maintenance and health.

Several diseases have been associated with mitochondrial dysfunction. Recently, mitochondrial dysfunction has been proposed as a cause of BD [173-175]. This hypothesis was based on altered cellular energy metabolism measured by functional assays and by magnetic resonance spectroscopy studies in patients with BD [176]. In addition, neurons from the postmortem brains of BD patients and peripheral cells from living BD patients imaged by fluorescence microscopy displayed deviations in size and distribution of mitochondria compared to matched controls [177]. Further, polymorphisms in the mitochondrial DNA of patients with BD were discovered [174]. A specific mutation in mitochondrial DNA, affecting complex I of the electron transport chain, also appears to be associated with BD [178]. Additionally, the frontal cortex region of the brain in BD patients was analyzed by DNA microarray and revealed the differential expression of 831 genes, including several involved in the mitochondrial electron transport chain (complexes I, IV, and V). Interestingly, this report also showed

the increase in expression of complex I of the electron transport chain in lithium-treated patients compared with non-treated patients [179].

Mitochondria are not only responsible for energy metabolism through ATP production, but also generation of reactive oxygen species, regulating apoptosis, calcium signaling, and synaptic plasticity. Postmortem brains of patients with BD have higher nitrosative and oxidative stress, indicative of mitochondrial dysfunction, than controls [180]. One report, using quantitative Western blots from postmortem brains, found that hexokinase 1 (HK1), which phosphorylates glucose in the first step of glycolysis, binds to a voltage-dependent anion channel (VDAC) imbedded in the outer mitochondrial membrane, and detaches from the mitochondria in patients with mood disorders. VDAC interacts with part of the inner mitochondrial membrane protein adenine nucleotide translocase (ANT), which supports the transport of ADP and ATP [181].

The concentration of ATP within the mitochondria, roughly 8 mM, is significantly higher than in the cytoplasm, roughly 3 mM [182]. Mg^{2+} and Li^{+} may be attracted and localized to the mitochondria because of their preference to bind ATP together, so Li^{+} and Mg^{2+} may exert a reparative function on the mitochondrial enzymes and processes through the ATP·Mg·Li ternary complex. If validated as drug targets, mitochondrial enzymes may represent promising new targets for designing new BD drugs [180].

ATP in Enzyme Activity: Mg·Li Complexes with ATP may Slow or Alter Phosphorylation Events.

In addition to guiding new thinking about Li^+ targets and mechanism, the Mg·Li bimetallic ATP complex also suggests a mechanistic explanation for how Li^+ may inhibit kinases previously identified as being affected by Li^+. Li^+ is not known as a general inhibitor of kinases, but one kinase, Glycogen Synthase Kinase 3β (GSK3β), is a serine-threonine kinase that is inhibited by Li^+ at roughly therapeutic concentration (K_i= 2 mM) [160, 183-185]. GSK3β is a Mg-dependent enzyme that binds to ATP or ADP ligands. It is a constitutively active enzyme involved in several signaling pathways affecting transcription, cell structure, cell cycle, and metabolism [184, 186]. The downstream effects of phosphorylation by GSK3β affect many more cellular processes, such as synaptic plasticity, apoptosis, and the circadian cycle. Errant GSK3β activity is thought to play a role in diabetes, sleep disorders, Alzheimer's, schizophrenia, depression, and BD, among other diseases, which make it an attractive protein for drug inhibitor development [187, 188].

Another important role of GSK3β is in inflammation. In mice, GSK3 inhibitors rescued 70 percent of otherwise lethal doses of a drug that induces inflammation [185]. Most drugs are reported to bind and compete with ATP in the ATP pocket of GSK3β, which has two isoforms, α and β, differing by only one amino acid [188]. Both isoforms are inhibited by Li^+.

The active site of GSK3β requires two Mg^{2+} ions, and although the catalytic mechanism is not well understood, it is hypothesized that Li^+ inhibits via competition specifically with the Mg^{2+} that is not bound to ATP [183, 189, 190]. The ATP-bound

structure of GSK3β has not been determined, but the structure of GSK3β bound to a non-hydrolyzable ATP analog, AMP-PNP, elucidates the active site structure of GSK3β [190] (Figure 6-2). An unexplored possibility of Li^+ inhibition is the formation of an ATP·Mg·Li complex that disrupts the activity of GSK3β either directly at the active site or allosterically. Although Li^+ has a preference for the structure and coordination geometry created by ATP·Mg sites, Li^+ does not inhibit all kinases or phosphatases at therapeutic concentrations, suggesting that while the general model may apply in all cases the specific context of individual enzymes will impact the outcome of interaction [183]. It is conceivable that a smaller pocket for ATP·Mg on some kinases may be more affected by the presence of and coordination with Li^+, whereas a larger pocket in other kinases may be less affected. However, further structural elucidation of metal ATP complexes with these enzymes will be necessary to understand Li^+ inhibition more fully.

Several other enzymes are also directly inhibited by Li^+, such as Inositol monophosphatase (IMPase), Inositol polyphosphate 1-phosphatase, Bisphosphate nucleotidease, Fructose 1,6-bisphosphatase, and Phosphoglucomutase (PGM) [184, 191]. These are all Mg^{2+}-dependent phosphomonoesterases that also provide a potential structural pocket at the active site for Li^+ to form a Mg·Li complex in a phosphate environment.

IMPase has been the focus of years of BD research because it is inhibited by Li^+ at therapeutic concentrations (0.5 mM to 1.5 mM) and plays a role in the central nervous system (CNS) [184]. IMPase catalyzes the hydrolysis of myo-inositol monophosphate, giving myo-inositol and inorganic phosphate. Phosphoinositide (PI) signaling facilitates neuron excitability and responsiveness, cell division, and secretion by activating second

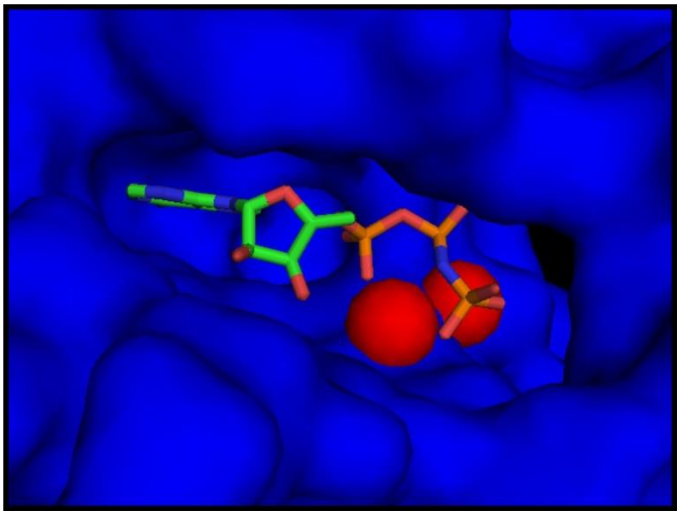

Figure 6-2. The active site of GSK3β (blue) showing AMP-PNP, a non-hydrolyzable ATP analog, bound with two Mg^{2+} ions (red). The structure of the ligand pocket was rendered from PDB file 1PYX and image created in PyMol.

messengers, like diacylglycerol (DAG) and inositol 1,4,5-triphosphate (IP_3), and regulating intracellular calcium. PI signaling can be initiated by extracellular receptors coupled to the G protein, $G_{q/11}$. This G protein then activates Phospholipase C (PLC), which, in turn, hydrolyzes the nearby cell membrane component phosphoinositide 4,5-bisphosphate (PIP_2), a phospholipid, initiating PI signaling [184]. In 1989, the 'inositol depletion hypothesis', a theory for Li^+'s mechanism of action, was first proposed by Berridge et al [192]. It states that Li^+ inhibition of IMPase interrupts the recycling of IP_3 into inositol, and decreases PIP_2 initiation of intracellular signaling [184, 193]. Although the mechanism of the Mg-dependent catalysis at the active site of these enzymes is still under investigation, biochemical, structural, and molecular dynamics experiments have assisted in elucidating its enzymatic action and Li^+ inhibition.

The mechanism of Li^+ inhibition of IMPase and aforementioned phosphatases may lie in the common sequence motif and structure at the active site of these phosphatases. The amino acid sequence for the catalytic site of IMPase is conserved with other phosphatases, IPPase and FBPase [194]. The amino acid sequence at the catalytic site of these enzymes, Asp-Pro-(Ile or Leu)-Asp-(Gly or Ser)-(Thr or Ser), also share a similar 3-dimensional core αβαβα sandwich structure among phosphomonoesterases (FBPase, IPPase, PAPase, and PIPase) [195, 196]. Li^+ and Mg^{2+} co-bind in a preferred manner over two Mg^{2+} ions with ATP (see Chapter 3). Mg·Li may be preferred over two Mg^{2+} ions in the active site of phosphatases where phosphates are present. The distinctive tetrahedral/octahedral coordination geometry of Mg·Li may be structurally and energetically favored over the native Mg·Mg octahedral/octahedral coordination geometry where six possible water molecules can bind to each Mg^{2+}.

In the case of IMPase, crystallographic and kinetic evidence as well as computer modeling have elucidated the metal-assisted catalysis at the active site of IMPase. Initially a 2-metal catalysis mechanism was proposed where a higher affinity and a lower affinity Mg^{2+} site facilitates the hydrolysis of the substrate, myo-inositol monophosphate [197, 198]. This mechanism was revised to 3-metal catalysis after a higher resolution crystal structure showed three metals bound at the active site [196, 199]. The 3-metal mechanism is currently favored due to its active site structure identity with similar enzymes and kinetic and mutagenesis research [199].

The proposed three-metal mechanism consists of two Mg^{2+} at sites 1 and 3, which coordinate the nucleophilic attack of a water hydroxyl on the phosphate of the substrate, myo-inositol-1-phosphate (Figure 6-3). The third Mg^{2+}, at site 2, coordinates with the substrate hydroxyl to facilitate a hydrogen bond with the phosphate oxygen to stabilize the transition state and accelerate the hydrolysis [199]. Indirect evidence shows that the Li^{+} binding to IMPase occurs at the Mg^{2+} site 2 location. It is thought that Li^{+} competes with Mg^{2+} at site 2 where Mg^{2+} has a lower binding affinity, and then binds to the inorganic phosphate (P_i) leaving group where it forms a tight complex, slowing the release of products [199, 200]. Direct evidence of Li^{+} binding to IMPase using ^{7}Li NMR concludes that there is only one binding site for Li^{+} on IMPase and the data is consistent with its location at site 2 [201]. Solid state NMR also confirmed that Li^{+} binds to either site 1 or site 2 but not to site 3 [202]. Site 1 is the high affinity Mg^{2+} binding site so it is thought that Li^{+} competes with Mg^{2+} at site 2, the lower affinity Mg^{2+} site [199].

Computational studies, molecular modeling, and molecular dynamics simulations have provided a glimpse at the catalytic mechanism of IMPase even in the absence of a

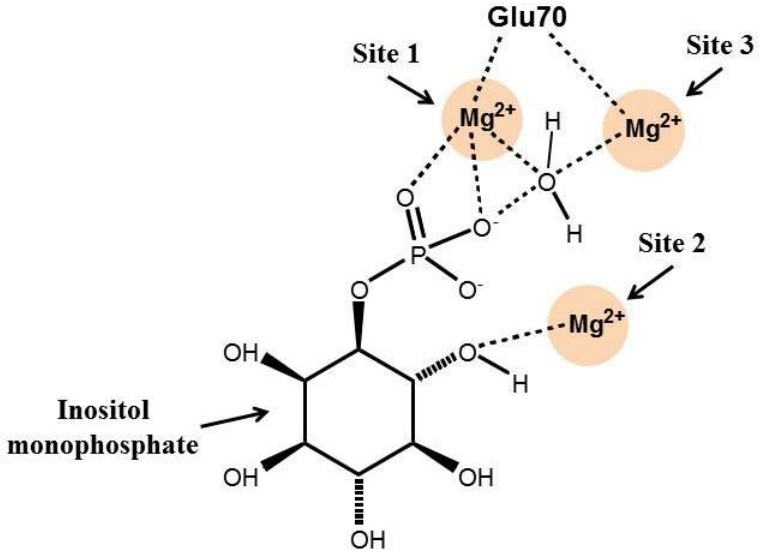

Figure 6-3. The catalytic site of Inositol monophosphatase (IMPase) is shown schematically. Two Mg^{2+} ions at sites 1 and 3 coordinate with the nucleophilic water molecule. The substrate (inositol monophosphate) 6-OH is hydrogen bonded to a third Mg^{2+} ion, which is thought to stabilize the transition state [196, 199].

crystal structure containing the substrate, inositol monophosphate. Docking of myo-inositol monophosphate to IMPase indicates how the magnesium triad works together to create a hydroxide ion that will hydrolyze the phosphate from myo-inositol monophosphate, then release the products of the reaction. Additionally, when Li^+ is substituted for Mg^{2+} at site 2, it has a coordination number of four and is not able to coordinate with a water molecule that is key for protonating the leaving groups and facilitating enzyme release of products. So, Li^+ inhibits IMPase by effectively trapping the myo-inositol and inorganic phosphate in the active site [203]. The question of what makes Li^+ attracted to the active site of this enzyme, or favored over magnesium is still not known. It seems counterintuitive that Li^+ would be preferred over magnesium, and yet, at stoichiometric concentrations of Li^+ and magnesium, Mg·Li co-binding in coordination with phosphates is preferred at specific low affinity magnesium sites. However, thinking about this interaction not as a single site for site competition, but rather as a co-binding of Li^+ and Mg^{2+} to the phosphate ligand site does provide a plausible explanation based on the idea that two metal Mg·Li binding is favored over Mg·Mg binding in the enzyme pocket.

Another protein that Li^+ inhibits is PGM, which requires Mg^{2+} and also involves phosphate binding similar to phosphomonoesterases, but is otherwise dissimilar in structure. PGM is involved in the conversion of glucose-1-phosphate to glucose 6-phosphate and is indirectly involved in inositol phosphate signaling due to a myo-inositol synthesis pathway that uses glucose 6-phosphate as the substrate [204-206]. Adenylate cyclase, guanylate cyclase, and G-proteins are also affected by Li^+ at near physiological concentrations. All of these bind to phosphate in one form or another and require Mg^{2+}

as well [207-212] creating the possibility that Mg·Li complexes could form as part of the mechanism of inhibition.

The enzymes presented in the latter half of this chapter do not bind to ATP, but interact with phosphates and Mg^{2+}. While ATP is the primary molecule for ternary complex formation explored in this chapter, the minimal components of the ternary complex are phosphates·Mg·Li and it is plausible that Li^{+} is acting as an inhibitor in these enzymes through coordination with Mg^{2+} and other phosphate containing ligands, and/or sites of amino acid phosphylation at the active sites in the absence of ATP.

Lithium Transport: ATP as Transport Vehicle for Lithium In and Out of Cells, and Around the Body

The process of exactly how Li^{+} finds its target and is transported throughout the body is not fully understood, partly because the therapeutic target(s) of Li^{+} is unknown. Lithium carbonate or lithium citrate is administered in the form of an oral tablet and it is absorbed in the small intestine for a standard formulation or the small or large intestine for a slow-release formulation. The rate of absorption varies between individuals, but nearly 100 percent of a 'standard' dose is absorbed. In approximately 1-2 hours, after a standard dose of lithium carbonate, the plasma reaches the peak concentration (3-6 hours for a slow-release tablet form). Experiments measuring gastrointestinal epithelial cells upon acute exposure to Li^{+} confirmed cellular influx to be through passive diffusion down its electrochemical gradient [74]. In erythrocytes acutely exposed to Li^{+}, most Li^{+} is absorbed by cells through passive diffusion, while approximately 30 percent of cellular Li^{+} uptake occurs by the bicarbonate-sensitive pathway, where Li^{+} replaces the hydrogen of bicarbonate to ride the anion exchange pathway into red blood cells [213]. Passive transport of Li^{+} into the cell occurs through a Na^{+} channel, sodium/proton (Na^{+}/H^{+})

exchanger, or sodium-potassium-two chloride (Na-K-2Cl) co-transporter membrane proteins [114]. The Na^+ - Li^+ countertransport mechanism is responsible for the cellular efflux of Li^+, where one intracellular Li^+ ion is exchanged for an extracellular Na^+ ion [213]. The Na^+-Li^+ countertransporter, also known as the sodium-sodium exchanger, or sodium-lithium exchanger, has a 15- to 18-fold higher affinity for Li^+ than for Na^+ [114]. The physiological concentration gradient of intracellular and extracellular Na^+ is maintained by active transport of Na^+ out of the cell by the Na^+ - K^+ pump. The maintenance of the Na^+ gradient allows for the Na^+ - Li^+ countertransport mechanism to pump Li^+ out of the cell because the intracellular Li^+ concentration is closer to the concentration of Na^+, allowing Li^+ to bind preferentially for cellular export [114, 213].

Chronic exposure to Li^+ appears to cause changes in the transport of Li^+, however. After 5 days, the efficiency of Li^+ efflux by the Na^+-Li^+ countertransport mechanism drops by 20-50 percent from non-treated cells. Two other transport pathways also change in the presence of Li^+ over time: choline transport and the Na^+ - K^+ ATPase [213].

Li^+ is filtered from the blood through the kidneys for either excretion from the body or reabsorption by the body. Li^+ enters the renal cells of the nephron passively through the Na^+/ H^+ antiporter, where it is processed like other electrolytes. During filtration of fluid in the lumen, about 60 percent of Li^+ is reabsorbed in the proximal tubule to circulate in the bloodstream, while about 25 percent is excreted in the urine [74, 114]. Li^+ export from renal cells has not been attributed to any one process and has not been well characterized. Active transport of Li^+ by the Na^+/ K^+ ATPase has not been seriously considered as a route for efflux because Li^+ does not have an affinity for this membrane protein [74].

Although the mode of Li^+ efflux from certain cells is unclear, a broadened perspective of modes of transport may provide insight into unconventional modes of Li^+ transport. With Li^+ preferentially forming a complex with ATP·Mg, ATP may act as a shuttle, or carrier, for Li^+, importing and exporting Li^+ into and out of cells and around the body. For example, Li^+ does not directly bind to serum proteins, such as human serum albumin (HSA), but ATP has been directly detected by NMR to bind to HSA (see Chapter 4). In fact, up to 10 ATP molecules can bind per HSA protein, with a measured K_D reported in a wide range from micromolar to millimolar [114, 127], though in the presence of competing molecules, like fatty acids, it is unlikely that 10 ATP bind to HSA. Still, HSA may be a shuttle for Li^+ via the ATP·Mg.

At the cellular surface and between neighboring cells, hemichannels, embedded in the membrane, facilitate the flow of ions and small molecules, such as ATP. Six protein subunits, called connexins, make up a hemichannel [214]. Specifically, connexins assist in exporting ATP [215, 216]. When two hemichannels of two neighboring cells come together, they form a gap junction channel, enabling cell to cell communication [217]. The connexin hemichannels on the surface of nodose ganglion sensory neurons, which are surrounded by sensory ganglia, or satellite glial cells, were found to participate in paracrine signaling by electrophysiology [214]. The details of the ATP involvement in paracrine signaling via connexin hemichannels are still being elucidated, but one could speculate that during signaling, the addition of Li could alter the speed, localization, or export of the ATP·Mg. Pannexins are another protein that form a hemichannel and may export ATP [218]. However, there is some controversy as to whether Pannexins release ATP [214].

ATP release has been observed in $P2X_7$ channels on astrocytes [215]. Prolonged activation of the $P2X_7$ purine receptor ion channels by eATP opens up a larger pore to allow molecules up to ~900 Da to pass through. Intracellular ATP can be released from the cell through the $P2X_7$ channel upon pore formation [218, 219].

There are also other transport mechanisms for ATP export from the cell that have not received as much attention as those mentioned above. The calcium homeostasis modulator 1 (CALHM1) is able to form a large pore in mouse neurons and is thought to be involved in ATP release [218]. Other hypotheses of ATP efflux from the cell are by way of the ATP binding cassette transporters, volume sensitive outward rectifying (VSOR) chloride channels, and plasmalemmal voltage-dependent anion channels [161, 219, 220].

In addition to transport across the phospholipid bilayer of the plasma membrane, certain organelles have mechanisms for transporting ATP. In peroxisomes, an integral membrane protein, called the ATP/ADP antiporter, specifically transfers cytoplasmic ATP across the peroxisomal membrane into the lumen of the peroxisome and swaps out ADP [221]. ATP is also exported from the mitochondria by the VDAC, mentioned earlier [181].

Transportation of ATP can also be achieved through exocytosis of vesicles of ATP that are stored in neurons and endocrine cells. ATP exocytosis has been reported in astrocytes and microglia as well [215, 222]. In humans, a protein called SLC17 is a type of vesicular nucleotide transporter (VNUT) that organizes vesicles of ATP for storage and eventually secretion [223].

In addition to passive diffusion of Li^+ by Na^+ channels, and active transport of Li^+ by the Na-K pump, a plausible mechanism of Li^+ transport may be aboard ATP·Mg in typical ATP transporting mechanisms. This expands the searchable area while offering new targets of Li's therapeutic effect.

ATP as a Neurotransmitter: Mg·Li Complexes with ATP may Interfere in Neurotransmission

Considering the therapeutic mechanism of Li^+ action for the pathophysiology of BD, an ATP·Mg·Li complex may be most relevant to focus on the central and peripheral nervous system, where ATP conveys messages as a neurotransmitter [224]. Synaptic release of ATP from the VNUT organized vesicle ranges in ATP concentration from 5 mM to 100 mM [161]. ATP can be released by itself, or in some instances, as a 'co-transmitter' released along with other neurotransmitters such as glutamate, GABA, noradrenaline and neuropeptide Y [161, 218, 225]. As previously mentioned, eATP activates P2X and P2Y purine receptors. In this way, ATP is considered a fast excitatory neurotransmitter [218]. One example of ATP acting as a co-transmitter is on the nerves surrounding blood vessels causing vasoconstriction [225]. In another, microglia, a central nervous system (CNS) sensor of pathology, are responsive to changes in eATP released from neurons. Depending on the concentration of eATP, the dynamic function of microglia may change from a 'sensing' position with extended processes, to a more mobile position, shaped like an amoeba, prepared to migrate to a site of injury and phagocytize the injured cell, and/or secrete pro-inflammatory cytokines [222]. One

hypothesis of Li^+ action is by formation of an ATP·Mg·Li complex at ATP neurotransmitters and modulation of signal transmission.

Summary

A few enzymes (e.g., GSK3β and IMPase) and other signaling molecules, such as cyclic AMP, GTP-binding proteins, and brain-derived neurotrophic factor (not discussed herein), have been studied extensively with regards to BD and have shed light on the field, but ultimately have not yet proven to be the therapeutic Li^+ target for BD. Rather, they seem to be players in a complex, multifaceted neurological disorder. A unifying theme in all of these Li^+-sensitive enzymes is that phosphates and Mg^{2+} are present and may provide a favorable binding location for Li^+. One or many of these sites that Li^+ binds may prove to be the site of BD pathology or BD therapy, but Li^+ is a monovalent cation, and has a diverse population of molecules with which to interact, both nonspecifically and specifically. Under the umbrella of this ATP·Mg·Li model, there is a place to fit most of the current hypotheses of Li^+'s therapeutic mechanism of action. In addition, this model has led to new ways of thinking about how Li^+ may act (e.g., purine receptor modulation). ATP serves numerous critical functions in the human body from signaling to providing energy for enzymatic reactions. The model of coordinated Li^+ binding to ATP·Mg can serve as a jumping point for a more focused investigation of Li^+'s therapeutic mechanism of action at locations of ATP action hopefully leading to answers of some of the bigger questions like, how does Li^+ stabilize the mood of a bipolar patient, and how does Li^+ provide neuroprotection? An interesting projection to consider with ATP·Mg·Li as a model for mechanism of therapeutic action of Li^+ in BD is that rather than a psychological disorder, BD might be a metabolic disorder. This was

first proposed in 1980 by Ehrlich, et al. [213]. Application of this ATP·Mg·Li model to future Li^+ research may indeed show that BD is primarily a somatic disorder with psychiatric symptoms, but this awaits further evidence. Nonetheless, the ATP·Mg·Li model provides a new lens through which to view the age-old question of Li^+ action and can provide some clarity as well as enable broad new insights in the field of Li^+ research.

Appendix

A. Non-dissertation Publications

1. Cohen HB, **Briggs KT**, Marino JP, Ravid K, Robson SC, Mosser DM. TLR stimulation initiates a CD39-based autoregulatory mechanism that limits macrophage inflammatory responses. *Blood*. 2013 Sept 12; 122 (11): 1935-45.

2. Aduri R, **Briggs KT**, Gorelick RJ, Marino JP. Molecular Determinants of HIV-1 NCp7 chaperone activity in maturation of the HIV-1 dimerization initiation site. *Nucleic Acids Res*. 2013 Feb 01; 41 (4): 2565-80.

3. Lee HW, **Briggs KT**, Marino JP. Dissecting structural transitions in the HIV-1 dimerization initiation site RNA using 2-aminopurine fluorescence. *Methods*. 2009 Oct; 49 (2): 118-27.

References

1. *Diagnostic and statistical manual of mental disorders : DSM-5*. 2013, Diagnostic and Statistical Manual Task Force; Washington, D.C.: American Psychiatric Association.
2. Goodwin, F.K. and K.R. Jamison, *Manic-depressive illness bipolar disorders and recurrent depression*. 2007, New York ; Oxford: Oxford University Press.
3. *Bipolar Disorder*, in *National Institute of Mental Health*. 2008, U.S. Department of Health and Human Services: National Institutes of Health.
4. Swann, A.C., et al., *Bipolar mixed states: an international society for bipolar disorders task force report of symptom structure, course of illness, and diagnosis.* Am J Psychiatry, 2013. **170**(1): p. 31-42.
5. Ormel, J., et al., *Disability and treatment of specific mental and physical disorders across the world.* Br J Psychiatry, 2008. **192**(5): p. 368-75.
6. Kessler, R.C., et al., *Prevalence, severity, and comorbidity of 12-month DSM-IV disorders in the National Comorbidity Survey Replication.* Arch Gen Psychiatry, 2005. **62**(6): p. 617-27.
7. Wier LM (Thomson Reuters), P.A.T.R., Maeda J (Thomson Reuters), Stranges E (Thomson Reuters), Ryan K (Thomson Reuters), Jagadish P (AHRQ), Collins Sharp B (AHRQ), Elixhauser A (AHRQ). *Facts and Figures: Statistics on Hospital-based Care in the United States, 2009*. 2009, Healthcare Cost and Utilization Project: Agency for Healthcare Research and Quality, 2011: Rockville, MD.
8. Marmol, F., *Lithium: bipolar disorder and neurodegenerative diseases Possible cellular mechanisms of the therapeutic effects of lithium.* Prog Neuropsychopharmacol Biol Psychiatry, 2008. **32**(8): p. 1761-71.
9. Altshuler, L.L., et al., *Gender and depressive symptoms in 711 patients with bipolar disorder evaluated prospectively in the Stanley Foundation bipolar treatment outcome network.* Am J Psychiatry, 2010. **167**(6): p. 708-15.
10. Suppes, T., et al., *Mixed hypomania in 908 patients with bipolar disorder evaluated prospectively in the Stanley Foundation Bipolar Treatment Network: a sex-specific phenomenon.* Arch Gen Psychiatry, 2005. **62**(10): p. 1089-96.
11. McElroy, S.L., et al., *Prevalence and correlates of eating disorders in 875 patients with bipolar disorder.* J Affect Disord, 2011. **128**(3): p. 191-8.
12. Frye, M.A., et al., *Gender differences in prevalence, risk, and clinical correlates of alcoholism comorbidity in bipolar disorder.* Am J Psychiatry, 2003. **160**(5): p. 883-9.
13. *Leading Causes of Death Reports, 2009.* Web-based Injury Statistics Query and Reporting System (WISQARS).
14. Cipriani, A., et al., *Lithium in the prevention of suicide in mood disorders: updated systematic review and meta-analysis.* BMJ, 2013. **346**: p. f3646.
15. Goodwin, F.K., et al., *Suicide risk in bipolar disorder during treatment with lithium and divalproex.* JAMA, 2003. **290**(11): p. 1467-73.
16. Tondo, L., G. Isacsson, and R. Baldessarini, *Suicidal behaviour in bipolar disorder: risk and prevention.* CNS Drugs, 2003. **17**(7): p. 491-511.

17. Baldessarini, R.J. and L. Tondo, *Suicide risk and treatments for patients with bipolar disorder.* JAMA, 2003. **290**(11): p. 1517-9.
18. Yerevanian, B.I., R.J. Koek, and J. Mintz, *Bipolar pharmacotherapy and suicidal behavior. Part I: Lithium, divalproex and carbamazepine.* J Affect Disord, 2007. **103**(1-3): p. 5-11.
19. Cipriani, A., et al., *Lithium in the prevention of suicidal behavior and all-cause mortality in patients with mood disorders: a systematic review of randomized trials.* Am J Psychiatry, 2005. **162**(10): p. 1805-19.
20. Antypa, N., M. Antonioli, and A. Serretti, *Clinical, psychological and environmental predictors of prospective suicide events in patients with Bipolar Disorder.* J Psychiatr Res, 2013. **47**(11): p. 1800-8.
21. Hauser, M., B. Galling, and C.U. Correll, *Suicidal ideation and suicide attempts in children and adolescents with bipolar disorder: a systematic review of prevalence and incidence rates, correlates, and targeted interventions.* Bipolar Disord, 2013. **15**(5): p. 507-23.
22. Kemp, J.a.B., Robert, *Suicide Data Report*, M.H.S. U.S. Department of Veterans Affairs, Suicide Prevention Program, Editor. 2012.
23. Ahearn, E.P., et al., *Suicide attempts in veterans with bipolar disorder during treatment with lithium, divalproex, and atypical antipsychotics.* J Affect Disord, 2013. **145**(1): p. 77-82.
24. Merikangas, K.R., et al., *Lifetime Prevalence of Mental Disorders in US Adolescents: Results from the National Comorbidity Study-Adolescent Supplement (NCS-A).* Journal of the American Academy of Child and Adolescent Psychiatry, 2010. **49**(10): p. 980-989.
25. Jette, N., et al., *Comorbidity of migraine and psychiatric disorders--a national population-based study.* Headache, 2008. **48**(4): p. 501-16.
26. Ortiz, A., et al., *Cross-prevalence of migraine and bipolar disorder.* Bipolar Disord, 2010. **12**(4): p. 397-403.
27. Sicras, A., et al., *Metabolic syndrome in bipolar disorder: a cross-sectional assessment of a Health Management Organization database.* Bipolar Disord, 2008. **10**(5): p. 607-16.
28. Teive, H.A., L. Paola, and R.P. Munhoz, *Edgar Allan Poe and neurology.* Arq Neuropsiquiatr, 2014. **72**(6): p. 466-8.
29. Blumer, D., *The illness of Vincent van Gogh.* Am J Psychiatry, 2002. **159**(4): p. 519-26.
30. Guu, T.W. and K.P. Su, *Musical creativity and mood bipolarity in Robert Schumann: a tribute on the 200th anniversary of the composer's birth.* Psychiatry Clin Neurosci, 2011. **65**(1): p. 113-4.
31. Koutsantoni, K., *Manic depression in literature: the case of Virginia Woolf.* Med Humanit, 2012. **38**(1): p. 7-14.
32. Schou, M., *Artistic productivity and lithium prophylaxis in manic-depressive illness.* Br J Psychiatry, 1979. **135**: p. 97-103.
33. Jamison, K.R., *Mood disorders and patterns of creativity in British writers and artists.* Psychiatry, 1989. **52**(2): p. 125-34.

34. Dieguez, S., *'A man can be destroyed but not defeated': Ernest Hemingway's near-death experience and declining health.* Front Neurol Neurosci, 2010. **27**: p. 174-206.
35. Potash, J.B. and J.R. DePaulo, Jr., *Searching high and low: a review of the genetics of bipolar disorder.* Bipolar Disord, 2000. **2**(1): p. 8-26.
36. Lapalme, M., S. Hodgins, and C. LaRoche, *Children of parents with bipolar disorder: a metaanalysis of risk for mental disorders.* Can J Psychiatry, 1997. **42**(6): p. 623-31.
37. Mesman, E., et al., *The Dutch bipolar offspring study: 12-year follow-up.* Am J Psychiatry, 2013. **170**(5): p. 542-9.
38. *Genome-wide association study of 14,000 cases of seven common diseases and 3,000 shared controls.* Nature, 2007. **447**(7145): p. 661-678.
39. Baum, A.E., et al., *A genome-wide association study implicates diacylglycerol kinase eta (DGKH) and several other genes in the etiology of bipolar disorder.* Mol Psychiatry, 2008. **13**(2): p. 197-207.
40. Green, E.K., et al., *Replication of bipolar disorder susceptibility alleles and identification of two novel genome-wide significant associations in a new bipolar disorder case-control sample.* Mol Psychiatry, 2013. **18**(12): p. 1302-7.
41. Green, E.K., et al., *Association at SYNE1 in both bipolar disorder and recurrent major depression.* Mol Psychiatry, 2013. **18**(5): p. 614-7.
42. *Large-scale genome-wide association analysis of bipolar disorder identifies a new susceptibility locus near ODZ4.* Nat Genet, 2011. **43**(10): p. 977-83.
43. Shinozaki, G. and J.B. Potash, *New developments in the genetics of bipolar disorder.* Curr Psychiatry Rep, 2014. **16**(11): p. 493.
44. Cichon, S., et al., *Genome-wide Association Study Identifies Genetic Variation in Neurocan as a Susceptibility Factor for Bipolar Disorder.* The American Journal of Human Genetics, 2011. **88**(3): p. 372-381.
45. Kalsi, G., et al., *Identification of the Slynar gene (AY070435) and related brain expressed sequences as a candidate gene for susceptibility to affective disorders through allelic and haplotypic association with bipolar disorder on chromosome 12q24.* Am J Psychiatry, 2006. **163**(10): p. 1767-76.
46. Lucae, S., et al., *P2RX7, a gene coding for a purinergic ligand-gated ion channel, is associated with major depressive disorder.* Hum Mol Genet, 2006. **15**(16): p. 2438-45.
47. Barden, N., et al., *Analysis of single nucleotide polymorphisms in genes in the chromosome 12Q24.31 region points to P2RX7 as a susceptibility gene to bipolar affective disorder.* Am J Med Genet B Neuropsychiatr Genet, 2006. **141B**(4): p. 374-82.
48. Knight, H.M., et al., *A cytogenetic abnormality and rare coding variants identify ABCA13 as a candidate gene in schizophrenia, bipolar disorder, and depression.* Am J Hum Genet, 2009. **85**(6): p. 833-46.
49. Curran, G. and A. Ravindran, *Lithium for bipolar disorder: a review of the recent literature.* Expert Rev Neurother, 2014. **14**(9): p. 1079-98.
50. *FDA Online Label Repository*. Available from: labels.FDA.gov.
51. Cade, J.F.J., *Lithium Salts In The Treatment Of Psychotic Excitement.* The Medical Journal of Australia, 1949: p. 349-352.

52. Schou, M., *Lithium treatment at 52.* Journal of Affective Disorders, 2001. **67**(1-3): p. 21-32.
53. Johnson, G. and S. Gershon, *Early North American research on lithium.* Aust N Z J Psychiatry, 1999. **33 Suppl**: p. S48-53.
54. Cipriani, A., et al., *Comparative efficacy and acceptability of antimanic drugs in acute mania: a multiple-treatments meta-analysis.* Lancet, 2011. **378**(9799): p. 1306-15.
55. Yildiz, A., et al., *Efficacy of antimanic treatments: meta-analysis of randomized, controlled trials.* Neuropsychopharmacology, 2011. **36**(2): p. 375-89.
56. Okusa, M.D. and L.J. Crystal, *Clinical manifestations and management of acute lithium intoxication.* Am J Med, 1994. **97**(4): p. 383-9.
57. Johnson, G., *Lithium--early development, toxicity, and renal function.* Neuropsychopharmacology, 1998. **19**(3): p. 200-5.
58. Freeman, M.P., *Bipolar disorder and pregnancy: risks revealed.* Am J Psychiatry, 2007. **164**(12): p. 1771-3.
59. McKnight, R.F., et al., *Lithium toxicity profile: a systematic review and meta-analysis.* Lancet, 2012. **379**(9817): p. 721-8.
60. Chiu, C.T. and D.M. Chuang, *Molecular actions and therapeutic potential of lithium in preclinical and clinical studies of CNS disorders.* Pharmacol Ther, 2010. **128**(2): p. 281-304.
61. Chuang, D.M. and H.K. Manji, *In search of the Holy Grail for the treatment of neurodegenerative disorders: has a simple cation been overlooked?* Biol Psychiatry, 2007. **62**(1): p. 4-6.
62. Contestabile, A., et al., *Lithium rescues synaptic plasticity and memory in Down syndrome mice.* J Clin Invest, 2013. **123**(1): p. 348-61.
63. Fornai, F., et al., *Lithium delays progression of amyotrophic lateral sclerosis.* Proc Natl Acad Sci U S A, 2008. **105**(6): p. 2052-7.
64. Su, Y., et al., *Lithium, a common drug for bipolar disorder treatment, regulates amyloid-beta precursor protein processing.* Biochemistry, 2004. **43**(22): p. 6899-908.
65. Forlenza, O.V., et al., *Disease-modifying properties of long-term lithium treatment for amnestic mild cognitive impairment: randomised controlled trial.* Br J Psychiatry, 2011. **198**(5): p. 351-6.
66. Macdonald, A., et al., *A feasibility and tolerability study of lithium in Alzheimer's disease.* Int J Geriatr Psychiatry, 2008. **23**(7): p. 704-11.
67. Hampel, H., et al., *Lithium trial in Alzheimer's disease: a randomized, single-blind, placebo-controlled, multicenter 10-week study.* J Clin Psychiatry, 2009. **70**(6): p. 922-31.
68. Nunes, P.V., O.V. Forlenza, and W.F. Gattaz, *Lithium and risk for Alzheimer's disease in elderly patients with bipolar disorder.* Br J Psychiatry, 2007. **190**: p. 359-60.
69. Abraha, A., et al., *Competition between Li+ and Mg2+ for ATP and ADP in aqueous solution: A multinuclear NMR study.* Journal of Inorganic Biochemistry, 1991. **42**(3): p. 191-198.
70. Mota de Freitas, D., M.M. Castro, and C.F. Geraldes, *Is competition between Li+ and Mg2+ the underlying theme in the proposed mechanisms for the*

pharmacological action of lithium salts in bipolar disorder? Acc Chem Res, 2006. **39**(4): p. 283-91.
71. Kara, N.Z. and H. Einat, *Rodent models for mania: practical approaches.* Cell Tissue Res, 2013. **354**(1): p. 191-201.
72. Nestler, E.J. and S.E. Hyman, *Animal models of neuropsychiatric disorders.* Nat Neurosci, 2010. **13**(10): p. 1161-9.
73. Einat, H. and H.K. Manji, *Cellular Plasticity Cascades: Genes-To-Behavior Pathways in Animal Models of Bipolar Disorder.* Biological Psychiatry, 2006. **59**(12): p. 1160-1171.
74. Birch, N.J., *Lithium and the cell : pharmacology and biochemistry*. 1991, London; Boston: Academic Press.
75. Berridge, M.J., C.P. Downes, and M.R. Hanley, *Lithium amplifies agonist-dependent phosphatidylinositol responses in brain and salivary glands.* Biochem J, 1982. **206**(3): p. 587-95.
76. Holdgate, G.A. and W.H. Ward, *Measurements of binding thermodynamics in drug discovery.* Drug Discov Today, 2005. **10**(22): p. 1543-50.
77. Perozzo, R., G. Folkers, and L. Scapozza, *Thermodynamics of protein-ligand interactions: history, presence, and future aspects.* J Recept Signal Transduct Res, 2004. **24**(1-2): p. 1-52.
78. Sanders, C.R. *Biomolecular Ligand-Receptor Binding Studies: Theory, Practice, and Analysis*. 2010; Available from: http://structbio.vanderbilt.edu/sanders/Binding_Principles_2010.pdf.
79. Winzor, D.J. and W.H. Sawyer, *Quantitative characterization of ligand binding*. 1995, New York: Wiley-Liss.
80. Beeckmans, S., *Chromatographic methods to study protein-protein interactions.* Methods, 1999. **19**(2): p. 278-305.
81. Jacobsen, N.E., *NMR Spectroscopy Explained: Simplified Theory, Applications and Examples for Organic Chemistry and Structural Biology*. 2007, Hoboken, NJ: Wiley-Interscience.
82. Clore, G.M., C. Tang, and J. Iwahara, *Elucidating transient macromolecular interactions using paramagnetic relaxation enhancement.* Current Opinion in Structural Biology, 2007. **17**(5): p. 603-616.
83. Bakhmutov, V.I., *Practical NMR relaxation for chemists*. 2004, Chichester, West Sussex, England; Hoboken, NJ: Wiley.
84. Niccolai, N., E. Tiezzi, and G. Valensin, *Manganese(II) as magnetic relaxation probe in the study of biomechanisms and of biomacromolecules.* Chemical Reviews, 1982. **82**(4): p. 359-384.
85. Hoesch, R.E., et al., *Coexistence of Functional IP3 and Ryanodine Receptors in Vagal Sensory Neurons and Their Activation by ATP*. Journal of Neurophysiology, 2002. **88**(3): p. 1212-1219.
86. Ascenzi, P. and M. Fasano, *Allostery in a monomeric protein: The case of human serum albumin.* Biophysical Chemistry, 2010. **148**(1-3): p. 16-22.
87. Fasano, M., et al., *The extraordinary ligand binding properties of human serum albumin.* International Union of Biochemistry and Molecular Biology Life, 2005. **57**(12): p. 787-796.

88. Dalvit, C., et al., *Identification of compounds with binding affinity to proteins via magnetization transfer from bulk water.* J Biomol NMR, 2000. **18**(1): p. 65-8.
89. Dalvit, C., et al., *WaterLOGSY as a method for primary NMR screening: practical aspects and range of applicability.* J Biomol NMR, 2001. **21**(4): p. 349-59.
90. Lumsden, M. *Using Bulk Water to Detect Ligand Binding: Introducing the WaterLOGSY Experiment*. 2014 May 29, 2014; Available from: http://www.dal.ca/content/dam/dalhousie/pdf/Diff/nmr3/NMR%20Experiments/WaterLogsy.pdf.
91. Hummel, J.P. and W.J. Dreyer, *Measurement of protein-binding phenomena by gel filtration.* Biochim Biophys Acta, 1962. **63**: p. 530-2.
92. Cooper, P.F. and G.C. Wood, *Protein-binding of small molecules: new gel filtration method.* J Pharm Pharmacol, 1968. **20**: p. Suppl:150S+.
93. Pollard, T.D., *A guide to simple and informative binding assays.* Mol Biol Cell, 2010. **21**(23): p. 4061-7.
94. Birch, N.J., *Effects of lithium on plasma magnesium.* Br J Psychiatry, 1970. **116**(533): p. 461.
95. Birch, N.J., *Letter: The role of magnesium and calcium in the pharmacology of lithium.* Biol Psychiatry, 1973. **7**(3): p. 269-72.
96. Housecroft, C.E. and A.G. Sharpe, *Inorganic chemistry*. 2008, Harlow, England; New York: Pearson Prentice Hall.
97. Marcus, Y., *Effect of ions on the structure of water: structure making and breaking.* Chem Rev, 2009. **109**(3): p. 1346-70.
98. Bock, C., et al., *The Arrangement of First- and Second-shell Water Molecules Around Metal Ions: Effects of Charge and Size.* Theoretical Chemistry Accounts, 2006. **115**(2-3): p. 100-112.
99. Frausto da Silva, J.J. and R.J. Williams, *Possible mechanism for the biological action of lithium.* Nature, 1976. **263**(5574): p. 237-9.
100. Frausto Da Silva, J.J.R. and R.J.P. Williams, *Possible mechanism for the biological action of lithium.* Nature, 1976. **263**(5574): p. 237-239.
101. Birch, N.J. and I. Goulding, *Lithium-nucleotide interactions investigated by gel filtration.* Analytical Biochemistry, 1975. **66**(1): p. 293-297.
102. Birch, N.J., *Possible mechanism for biological action of lithium.* Nature, 1976. **264**(5587): p. 681-681.
103. Brown, S.G., R.M. Hawk, and R.A. Komoroski, *Competition of Li(I) and Mg(II) for ATP binding: A 31P NMR study.* Journal of Inorganic Biochemistry, 1993. **49**(1): p. 1-8.
104. Wilson, J.E. and A. Chin, *Chelation of divalent cations by ATP, studied by titration calorimetry.* Anal Biochem, 1991. **193**(1): p. 16-9.
105. Cowan, J.A., *Metallobiochemistry of magnesium. Coordination complexes with biological substrates: site specificity, kinetics and thermodynamics of binding, and implications for activity.* Inorganic Chemistry, 1991. **30**(13): p. 2740-2747.
106. Sari, J.C. and J.P. Belaich, *Microcalorimetric studies on the formation of magnesium complexes with 5'-ribonucleotides of guanine, uracil, and hypoxanthine.* Journal of the American Chemical Society, 1973. **95**(22): p. 7491-7496.

107. Benesch, R. and R.E. Benesch, *The effect of organic phosphates from the human erythrocyte on the allosteric properties of hemoglobin.* Biochem Biophys Res Commun, 1967. **26**(2): p. 162-7.
108. Gonzatti, M.I. and J.A. Traugh, *2,3-Bisphosphoglycerate inhibits hemoglobin synthesis and phosphorylation of initiation factor 2 by casein kinase II in reticulocyte lysates.* Biochemical and Biophysical Research Communications, 1988. **157**(1): p. 134-139.
109. Gunther, T., *Total and free Mg2+ contents in erythrocytes: a simple but still undisclosed cell model.* Magnes Res, 2007. **20**(3): p. 161-7.
110. Waters, R.S., et al., *EDTA chelation effects on urinary losses of cadmium, calcium, chromium, cobalt, copper, lead, magnesium, and zinc.* Biol Trace Elem Res, 2001. **83**(3): p. 207-21.
111. Leal-Cardoso, H., et al., *Electrophysiological properties and chemosensitivity of acutely isolated nodose ganglion neurons of the rabbit.* J Auton Nerv Syst, 1993. **45**(1): p. 29-39.
112. *Table 2: Annual Estimates of the Population by Selected Age Groups and Sex for the United States: April 1, 2000 to July 1, 2004*. U.S. Census Bureau Population Estimates by Demographic Characteristics Release Date: June 9, 2005; Available from: http://www.census.gov/popest/national/asrh/.
113. Wang, P.S., et al., *Twelve-Month Use of Mental Health Services in the United States: Results From the National Comorbidity Survey Replication.* Arch Gen Psychiatry, 2005. **62**(6): p. 629-640.
114. Timmer, R.T. and J.M. Sands, *Lithium intoxication.* J Am Soc Nephrol, 1999. **10**(3): p. 666-74.
115. Ryan, A.J., et al., *Structural basis of binding of fluorescent, site-specific dansylated amino acids to human serum albumin.* J Struct Biol, 2011. **174**(1): p. 84-91.
116. Evans, T.W., *Review article: albumin as a drug--biological effects of albumin unrelated to oncotic pressure.* Aliment Pharmacol Ther, 2002. **16 Suppl 5**: p. 6-11.
117. Quinlan, G.J., G.S. Martin, and T.W. Evans, *Albumin: biochemical properties and therapeutic potential.* Hepatology, 2005. **41**(6): p. 1211-9.
118. Fanali, G., et al., *Human serum albumin: From bench to bedside.* Molecular Aspects of Medicine, 2012. **33**(3): p. 209-290.
119. Ghuman, J., et al., *Structural basis of the drug-binding specificity of human serum albumin.* J Mol Biol, 2005. **353**(1): p. 38-52.
120. Sudlow, G., D.J. Birkett, and D.N. Wade, *Further characterization of specific drug binding sites on human serum albumin.* Mol Pharmacol, 1976. **12**(6): p. 1052-61.
121. Sudlow, G., D.J. Birkett, and D.N. Wade, *The characterization of two specific drug binding sites on human serum albumin.* Mol Pharmacol, 1975. **11**(6): p. 824-32.
122. Simard, J.R., et al., *Location of high and low affinity fatty acid binding sites on human serum albumin revealed by NMR drug-competition analysis.* J Mol Biol, 2006. **361**(2): p. 336-51.

123. Drabikowski, W., *Binding of ATP by human serum albumin in solution.* Acta Biochim Pol, 1961. **8**: p. 289-99.
124. Bauer, M., J. Baumann, and W.E. Trommer, *ATP binding to bovine serum albumin.* FEBS Letters, 1992. **313**(3): p. 288-290.
125. Takeda, S., et al., *Adenosine 5'-triphosphate binding to bovine serum albumin.* Biophysical Chemistry, 1997. **69**(2–3): p. 175-183.
126. Maity, H.a.J., GK, *Conformation of ATPMg(II) bound at the specific site on bovine serum albumin: 1H-nuclear magnetic resonance study.* Current Science, 1996. **71**(10): p. 9.
127. Song, Z., et al., *Characterizing the binding of nucleotide ATP on serum albumin by 31P NMR diffusion.* Canadian Journal of Chemistry, 2012. **90**(5): p. 411-418.
128. He, X.M. and D.C. Carter, *Atomic structure and chemistry of human serum albumin.* Nature, 1992. **358**(6383): p. 209-15.
129. Curry, S., et al., *Crystal structure of human serum albumin complexed with fatty acid reveals an asymmetric distribution of binding sites.* Nat Struct Biol, 1998. **5**(9): p. 827-35.
130. Bujacz, A., *Structures of bovine, equine and leporine serum albumin.* Acta Crystallogr D Biol Crystallogr, 2012. **68**(Pt 10): p. 1278-89.
131. Majorek, K.A., et al., *Structural and immunologic characterization of bovine, horse, and rabbit serum albumins.* Mol Immunol, 2012. **52**(3-4): p. 174-82.
132. Lu, J., et al., *Albumin as a zinc carrier: properties of its high-affinity zinc-binding site.* Biochem Soc Trans, 2008. **36**(Pt 6): p. 1317-21.
133. Cohn, E.J., et al., *Preparation and Properties of Serum and Plasma Proteins. IV. A System for the Separation into Fractions of the Protein and Lipoprotein Components of Biological Tissues and Fluids1a,b,c,d.* Journal of the American Chemical Society, 1946. **68**(3): p. 459-475.
134. Saunders, C.W., et al., *Secretion of human serum albumin from Bacillus subtilis.* J Bacteriol, 1987. **169**(7): p. 2917-25.
135. *Madison-Quingdao Metabolomics Consortium Database*. mmcd.nmrfam.wisc.edu: University of Wisconsin-Madison.
136. Jacobson, K.A., M.F. Jarvis, and M. Williams, *Purine and Pyrimidine (P2) Receptors as Drug Targets.* Journal of Medicinal Chemistry, 2002. **45**(19): p. 4057-4093.
137. Young, M.T., *P2X receptors: dawn of the post-structure era.* Trends in Biochemical Sciences, 2010. **35**(2): p. 83-90.
138. Jiang, L.-H., *Inhibition of P2X7 receptors by divalent cations: old action and new insight.* European Biophysics Journal, 2009. **38**(3): p. 339-346.
139. Silberberg, S.D. and K.J. Swartz, *Structural biology: Trimeric ion-channel design.* Nature, 2009. **460**(7255): p. 580-1.
140. Jarvis, M.F. and B.S. Khakh, *ATP-gated P2X cation-channels.* Neuropharmacology, 2009. **56**(1): p. 208-15.
141. Roberts, J.A., et al., *Molecular properties of P2X receptors.* Pflugers Arch, 2006. **452**(5): p. 486-500.
142. Jones, C.A., et al., *Functional regulation of P2X6 receptors by N-linked glycosylation: identification of a novel alpha beta-methylene ATP-sensitive phenotype.* Mol Pharmacol, 2004. **65**(4): p. 979-85.

143. Donnelly-Roberts, D.L. and M.F. Jarvis, *Discovery of P2X7 receptor-selective antagonists offers new insights into P2X7 receptor function and indicates a role in chronic pain states.* Br J Pharmacol, 2007. **151**(5): p. 571-9.
144. Li, M., S.D. Silberberg, and K.J. Swartz, *Subtype-specific control of P2X receptor channel signaling by ATP and Mg2+.* Proc Natl Acad Sci U S A, 2013. **110**(36): p. E3455-63.
145. Rapoport, S.I., et al., *Bipolar disorder and mechanisms of action of mood stabilizers.* Brain Research Reviews, 2009. **61**(2): p. 185-209.
146. Apolloni, S., et al., *Membrane compartments and purinergic signalling: P2X receptors in neurodegenerative and neuroinflammatory events.* FEBS Journal, 2009. **276**(2): p. 354-364.
147. Trautmann, A., *Extracellular ATP in the Immune System: More Than Just a "Danger Signal".* Sci. Signal., 2009. **2**(56): p. pe6-.
148. Sun, S., *Roles of P2X7 Receptor in Glial and Neuroblastoma Cells: The Therapeutic Potential of P2X7 Receptor Antagonists.* Molecular Neurobiology, 2010. **41**(2): p. 351-355.
149. Grigoroiu-Serbanescu, M., et al., *Variation in P2RX7 candidate gene (rs2230912) is not associated with bipolar I disorder and unipolar major depression in four European samples.* Am J Med Genet B Neuropsychiatr Genet, 2009. **150B**(7): p. 1017-21.
150. McQuillin, A., et al., *Case-control studies show that a non-conservative amino-acid change from a glutamine to arginine in the P2RX7 purinergic receptor protein is associated with both bipolar- and unipolar-affective disorders.* Mol Psychiatry, 2009. **14**(6): p. 614-20.
151. Roger, S., et al., *Single nucleotide polymorphisms that were identified in affective mood disorders affect ATP-activated P2X7 receptor functions.* J Psychiatr Res, 2010. **44**(6): p. 347-55.
152. Soronen, P., et al., *P2RX7 gene is associated consistently with mood disorders and predicts clinical outcome in three clinical cohorts.* Am J Med Genet B Neuropsychiatr Genet, 2011. **156B**(4): p. 435-47.
153. Backlund, L., et al., *Cognitive manic symptoms associated with the P2RX7 gene in bipolar disorder.* Bipolar Disord, 2011. **13**(5-6): p. 500-8.
154. Harvey, M., P. Belleau, and N. Barden, *Gene interactions in depression: pathways out of darkness.* Trends in Genetics, 2007. **23**(11): p. 547-556.
155. Jiang, L.H., et al., *Insights into the Molecular Mechanisms Underlying Mammalian P2X7 Receptor Functions and Contributions in Diseases, Revealed by Structural Modeling and Single Nucleotide Polymorphisms.* Front Pharmacol, 2013. **4**: p. 55.
156. Kawate, T., et al., *Crystal structure of the ATP-gated P2X4 ion channel in the closed state.* Nature, 2009. **460**(7255): p. 592-598.
157. Hattori, M. and E. Gouaux, *Molecular mechanism of ATP binding and ion channel activation in P2X receptors.* Nature, 2012. **485**(7397): p. 207-12.
158. Bartlett, R., L. Stokes, and R. Sluyter, *The P2X7 receptor channel: recent developments and the use of P2X7 antagonists in models of disease.* Pharmacol Rev, 2014. **66**(3): p. 638-75.

159. Malhi, G.S., et al., *Potential mechanisms of action of lithium in bipolar disorder. Current understanding.* CNS Drugs, 2013. **27**(2): p. 135-53.
160. Klein, P.S. and D.A. Melton, *A molecular mechanism for the effect of lithium on development.* Proc Natl Acad Sci U S A, 1996. **93**(16): p. 8455-9.
161. Burnstock, G., B.B. Fredholm, and A. Verkhratsky, *Adenosine and ATP receptors in the brain.* Curr Top Med Chem, 2011. **11**(8): p. 973-1011.
162. Idzko, M., D. Ferrari, and H.K. Eltzschig, *Nucleotide signalling during inflammation.* Nature, 2014. **509**(7500): p. 310-317.
163. Zhang, Y., et al., *Potential role of purinergic signaling in lithium-induced nephrogenic diabetes insipidus.* Am J Physiol Renal Physiol, 2009. **296**(5): p. F1194-201.
164. Wildman, S.S. and B.F. King, *P2X receptors: epithelial ion channels and regulators of salt and water transport.* Nephron Physiol, 2008. **108**(3): p. p60-7.
165. Zarrindast, M.R., M. Ebrahimi, and A. Khalilzadeh, *Influence of ATP-sensitive potassium channels on lithium state-dependent memory of passive avoidance in mice.* Eur J Pharmacol, 2006. **550**(1-3): p. 107-11.
166. Abdel-Zaher, A.O., *The myoneural effects of lithium chloride on the nerve-muscle preparations of rats. Role of adenosine triphosphate-sensitive potassium channels.* Pharmacol Res, 2000. **41**(2): p. 163-78.
167. Naviaux, R.K., *Metabolic features of the cell danger response.* Mitochondrion, 2014. **16**: p. 7-17.
168. Riteau, N., et al., *Extracellular ATP is a danger signal activating P2X7 receptor in lung inflammation and fibrosis.* Am J Respir Crit Care Med, 2010. **182**(6): p. 774-83.
169. Wilot, L., et al., *Lithium and Valproate Protect Hippocampal Slices Against ATP-induced Cell Death.* Neurochemical Research, 2007. **32**(9): p. 1539-1546.
170. Tsujimoto, Y., *Apoptosis and necrosis: Intracellular ATP level as a determinant for cell death modes.* Cell Death & Differentiation, 1997. **4**(6): p. 429.
171. Edinger, A.L. and C.B. Thompson, *Death by design: apoptosis, necrosis and autophagy.* Curr Opin Cell Biol, 2004. **16**(6): p. 663-9.
172. Krauss, S., *Mitochondria: Structure and Role in Respiration*, in *eLS*. 2001, John Wiley & Sons, Ltd.
173. Young, L.T., *Is bipolar disorder a mitochondrial disease?* J Psychiatry Neurosci, 2007. **32**(3): p. 160-1.
174. Kato, T., *Mitochondrial dysfunction as the molecular basis of bipolar disorder: therapeutic implications.* CNS Drugs, 2007. **21**(1): p. 1-11.
175. Rezin, G.T., et al., *Mitochondrial dysfunction and psychiatric disorders.* Neurochem Res, 2009. **34**(6): p. 1021-9.
176. Clay, H.B., S. Sillivan, and C. Konradi, *Mitochondrial dysfunction and pathology in bipolar disorder and schizophrenia.* Int J Dev Neurosci, 2011. **29**(3): p. 311-24.
177. Cataldo, A.M., et al., *Abnormalities in mitochondrial structure in cells from patients with bipolar disorder.* Am J Pathol, 2010. **177**(2): p. 575-85.
178. Munakata, K., et al., *Mitochondrial DNA 3644T-->C mutation associated with bipolar disorder.* Genomics, 2004. **84**(6): p. 1041-50.

179. Sun, X., et al., *Downregulation in components of the mitochondrial electron transport chain in the postmortem frontal cortex of subjects with bipolar disorder.* J Psychiatry Neurosci, 2006. **31**(3): p. 189-96.
180. de Sousa, R.T., et al., *Targeting mitochondrially mediated plasticity to develop improved therapeutics for bipolar disorder.* Expert Opin Ther Targets, 2014. **18**(10): p. 1131-47.
181. Regenold, W.T., et al., *Mitochondrial detachment of hexokinase 1 in mood and psychotic disorders: implications for brain energy metabolism and neurotrophic signaling.* J Psychiatr Res, 2012. **46**(1): p. 95-104.
182. Traut, T.W., *Physiological concentrations of purines and pyrimidines.* Mol Cell Biochem, 1994. **140**(1): p. 1-22.
183. Ryves, W.J., et al., *Glycogen synthase kinase-3 inhibition by lithium and beryllium suggests the presence of two magnesium binding sites.* Biochem Biophys Res Commun, 2002. **290**(3): p. 967-72.
184. Quiroz, J.A., T.D. Gould, and H.K. Manji, *Molecular effects of lithium.* Mol Interv, 2004. **4**(5): p. 259-72.
185. Li, X. and R.S. Jope, *Is Glycogen Synthase Kinase-3 a Central Modulator in Mood Regulation[quest]*. Neuropsychopharmacology, 2010. **35**(11): p. 2143-2154.
186. Gould, T.D., *Targeting glycogen synthase kinase-3 as an approach to develop novel mood-stabilising medications.* Expert Opinion on Therapeutic Targets, 2006. **10**(3): p. 377-392.
187. Medina, M. and F. Wandosell, *Deconstructing GSK-3: The Fine Regulation of Its Activity.* Int J Alzheimers Dis, 2011. **2011**: p. 479249.
188. Bhat, R.V., S.L. Budd Haeberlein, and J. Avila, *Glycogen synthase kinase 3: a drug target for CNS therapies.* Journal of Neurochemistry, 2004. **89**(6): p. 1313-1317.
189. Aoki, M., et al., *Structural insight into nucleotide recognition in tau-protein kinase I/glycogen synthase kinase 3 beta.* Acta Crystallogr D Biol Crystallogr, 2004. **60**(Pt 3): p. 439-46.
190. Bertrand, J.A., et al., *Structural Characterization of the GSK-3β Active Site Using Selective and Non-selective ATP-mimetic Inhibitors.* Journal of Molecular Biology, 2003. **333**(2): p. 393-407.
191. Gould, T.D., C.A. Zarate, and H.K. Manji, *Glycogen synthase kinase-3: a target for novel bipolar disorder treatments.* J Clin Psychiatry, 2004. **65**(1): p. 10-21.
192. Berridge, M.J., C.P. Downes, and M.R. Hanley, *Neural and developmental actions of lithium: a unifying hypothesis.* Cell, 1989. **59**(3): p. 411-9.
193. Atack, J.R., *Inositol monophosphatase inhibitors: A novel treatment for bipolar disorder?* Biological Psychiatry, 1995. **37**(11): p. 761-763.
194. York, J.D. and P.W. Majerus, *Isolation and heterologous expression of a cDNA encoding bovine inositol polyphosphate 1-phosphatase.* Proc Natl Acad Sci U S A, 1990. **87**(24): p. 9548-52.
195. York, J.D., J.W. Ponder, and P.W. Majerus, *Definition of a metal-dependent/Li(+)-inhibited phosphomonoesterase protein family based upon a conserved three-dimensional core structure.* Proc Natl Acad Sci U S A, 1995. **92**(11): p. 5149-53.

196. Gill, R., et al., *High-resolution structure of myo-inositol monophosphatase, the putative target of lithium therapy.* Acta Crystallographica Section D, 2005. **61**(5): p. 545-555.
197. Pollack, S.J., et al., *Mechanism of inositol monophosphatase, the putative target of lithium therapy.* Proc Natl Acad Sci U S A, 1994. **91**(13): p. 5766-70.
198. Bone, R., et al., *Structural studies of metal binding by inositol monophosphatase: evidence for two-metal ion catalysis.* Biochemistry, 1994. **33**(32): p. 9468-76.
199. Miller, D.J. and R.K. Allemann, *myo-Inositol monophosphatase: a challenging target for mood stabilising drugs.* Mini Rev Med Chem, 2007. **7**(2): p. 107-13.
200. Leech, A.P., et al., *Chemical and kinetic mechanism of the inositol monophosphatase reaction and its inhibition by Li+.* Eur J Biochem, 1993. **212**(3): p. 693-704.
201. Saudek, V., et al., *7Li nuclear-magnetic-resonance study of lithium binding to myo-inositolmonophosphatase.* Eur J Biochem, 1996. **240**(1): p. 288-91.
202. Haimovich, A., U. Eliav, and A. Goldbourt, *Determination of the lithium binding site in inositol monophosphatase, the putative target for lithium therapy, by magic-angle-spinning solid-state NMR.* J Am Chem Soc, 2012. **134**(12): p. 5647-51.
203. Lu, S., et al., *Insights into the role of magnesium triad in myo-inositol monophosphatase: metal mechanism, substrate binding, and lithium therapy.* J Chem Inf Model, 2012. **52**(9): p. 2398-409.
204. Ray, W.J., Jr., C.B. Post, and J.M. Puvathingal, *Comparison of rate constants for (PO3-) transfer by the Mg(II), Cd(II), and Li(I) forms of phosphoglucomutase.* Biochemistry, 1989. **28**(2): p. 559-69.
205. Masuda, C.A., et al., *Phosphoglucomutase is an in vivo lithium target in yeast.* Journal of Biological Chemistry, 2001.
206. Harwood, A.J., *Lithium and bipolar mood disorder: the inositol-depletion hypothesis revisited.* Mol Psychiatry, 2005. **10**(1): p. 117-26.
207. Nahorski, S.R., C.I. Ragan, and R.A. Challiss, *Lithium and the phosphoinositide cycle: an example of uncompetitive inhibition and its pharmacological consequences.* Trends Pharmacol Sci, 1991. **12**(8): p. 297-303.
208. Avissar, S., et al., *Lithium inhibits adrenergic and cholinergic increases in GTP binding in rat cortex.* Nature, 1988. **331**(6155): p. 440-2.
209. Minadeo, N., et al., *Effect of Li+ upon the Mg2+-dependent activation of recombinant Gialpha1.* Arch Biochem Biophys, 2001. **388**(1): p. 7-12.
210. Tesmer, J.J., et al., *Two-metal-Ion catalysis in adenylyl cyclase.* Science, 1999. **285**(5428): p. 756-60.
211. Srinivasan, C., et al., *Competition between lithium and magnesium ions for the G-protein transducin in the guanosine 5'-diphosphate bound conformation.* J Inorg Biochem, 2004. **98**(5): p. 691-701.
212. Husseini, M.K., et al., *Bipolar Medications: Mechanisms of Action.* Journal of nervous and mental disease., 2001. **189**(1): p. 64.
213. Ehrlich, B.E. and J.M. Diamond, *Lithium, membranes, and manic-depressive illness.* J Membr Biol, 1980. **52**(3): p. 187-200.

214. Retamal, M.A., et al., *Opening of pannexin and connexin based-channels increases the excitability of nodose ganglion sensory neurons.* Frontiers in Cellular Neuroscience, 2014. **8**.
215. Orellana, J.A. and J. Stehberg, *Hemichannels: new roles in astroglial function.* Front Physiol, 2014. **5**: p. 193.
216. Patel, D., X. Zhang, and R.D. Veenstra, *Connexin hemichannel and pannexin channel electrophysiology: how do they differ?* FEBS Lett, 2014. **588**(8): p. 1372-8.
217. Scemes, E., et al., *Connexin and pannexin mediated cell–cell communication.* Neuron Glia Biology, 2007. **3**(03): p. 199-208.
218. Cisneros-Mejorado, A., et al., *ATP signaling in brain: release, excitotoxicity and potential therapeutic targets.* Cell Mol Neurobiol, 2015. **35**(1): p. 1-6.
219. Bonan, C.D., *Ectonucleotidases and nucleotide/nucleoside transporters as pharmacological targets for neurological disorders.* CNS Neurol Disord Drug Targets, 2012. **11**(6): p. 739-50.
220. Higgins, C.F. and K.J. Linton, *The ATP switch model for ABC transporters.* Nat Struct Mol Biol, 2004. **11**(10): p. 918-26.
221. Antonenkov, V.D. and J.K. Hiltunen, *Transfer of metabolites across the peroxisomal membrane.* Biochim Biophys Acta, 2012. **1822**(9): p. 1374-86.
222. Domercq, M., N. Vazquez-Villoldo, and C. Matute, *Neurotransmitter signaling in the pathophysiology of microglia.* Front Cell Neurosci, 2013. **7**: p. 49.
223. Sawada, K., et al., *Identification of a vesicular nucleotide transporter.* Proc Natl Acad Sci U S A, 2008. **105**(15): p. 5683-6.
224. Agteresch, H.J., et al., *Adenosine Triphosphate: Established and Potential Clinical Applications.* Drugs, 1999. **58**(2): p. 211-232.
225. Ralevic, V., *Purines as neurotransmitters and neuromodulators in blood vessels.* Curr Vasc Pharmacol, 2009. **7**(1): p. 3-14.